Late Quaternary Seismicity and Climate in the Western Nepal : Himalaya

Zakaria Ghazoui

Communauté
UNIVERSITÉ Grenoble Alpes

UNIVERSITEIT GENT

THÈSE

Pour obtenir le grade de

DOCTEUR DE LA COMMUNAUTE UNIVERSITE GRENOBLE ALPES et DOCTOR OF SCIENCE: GEOLOGY FROM GHENT UNIVERSITY

préparée dans le cadre d'une cotutelle *entre la Communauté Université Grenoble Alpes et Universiteit Gent*

Spécialité : **Sciences de la Terre et Univers, Environnement**

Arrêté ministériel : le 6 janvier 2005 – 25 mai 2016

Présentée par

Zakaria Ghazoui

Thèse dirigée par **Peter van der Beek** et **Sebastien Bertrand**

préparée au sein de **l'Institut des Sciences de la Terre** (UGA) et du **Department of Geology** (UGent)

dans les écoles doctorales **Terre Univers Environnement** (UGA) et **Doctoral School Natural Sciences** (UGent)

Late Quaternary Seismicity and Climate in the western Nepal Himalaya

Thèse soutenue publiquement le **29 octobre 2018**,
devant le jury composé de :

Jean-Robert Grasso
Physicien du globe, Université Grenoble Alpes, France, Président
Flavio Anselmetti
Professeur, Universität Bern, Suisse, Rapporteur
Rodolphe Cattin
Professeur, Université de Montpellier, France, Rapporteur
Peter van der Beek
Professeur, Université Grenoble Alpes, France, Directeur de thèse
Sebastien Bertrand
Professeur, Universiteit Gent, Belgique, co-Directeur de thèse
Monique Fort
Professeure émérite, Université Paris Diderot, France, Examinatrice
Marc De Batist
Professeur, Universiteit Gent, Belgique, Examinateur

Résumé

L'Himalaya résultant de la collision indo-asiatique, dans laquelle l'Inde plonge sous le Tibet, initie régulièrement des tremblements de terre destructeurs dont la plupart sont mortel pour les communautés népalaises et limitrophes. Telle une muraille séparant les plaines d'Inde et le haut plateau du Tibet, l'Himalaya façonne la circulation atmosphérique, affectant tant le climat régional que global. Cette thèse vise à se pencher sur l'histoire et l'évolution peu connue du climat et de la sismicité de l'Himalaya, dans une des régions les moins peuplées et les plus reculées du Népal occidental.

Dans le contexte de changements climatiques et environnementaux, l'un des aspects les moins bien élucidés de l'histoire de l'Himalaya au cours du Quaternaire supérieur est celui de l'extension des glaciers ainsi que leurs impacts sur l'évolution du paysage. En nous appuyant sur des observations de terrain, sur des datations par nucléides cosmogéniques (^{10}Be) ainsi que des observations satellitaires, nous avons pu estimer l'étendue maximale des glaciers durant le dernier maximum glaciaire. Soutenant ainsi l'hypothèse suivant laquelle la présence de glacier fut relativement plus étendue à l'échelle du Népal occidental mais pas de l'ordre d'une calotte glaciaire. Par ailleurs, nos résultats suggèrent que les glaciers ont eu un effet durable sur le paysage, à la fois de façon directe et possiblement indirecte par la génération d'éboulements et glissement rocheux. Nous montrons également que le développement de deux des plus grands lacs du Népal, les lacs Rara et Phoksundo, semble être directement contrôlé par l'activité glaciaire.

Sur le plan sismologique, l'enjeu à la fois sociale, économique et politique de l'occurrence d'un séisme de magnitude plus élevée que le récent séisme de 2015 dont l'épicentre se situe près de la ville de Gorkha constitue une préoccupation majeure et motive en grande partie cette thèse. Le dernier séisme majeur ayant rompu le Main Frontal Thrust de magnitude supérieure à 8 (M_b) s'est déroulé le 6 juin 1505 et a considérablement impacté la population népalaise et environnante. Le caractère singulier du Népal occidental s'exprimant ainsi par l'hypothèse de la présence d'un hiatus sismique s'étendant sur plus de 500 ans sur base d'archives historiques et d'études paléosismologiques. Dans cette perspective, cette thèse se penche sur deux questions majeures relatives au comportement sismique de l'Himalaya : d'une part, l'hypothèse d'une lacune sismique dans l'Himalaya central et, d'autre part, de la distribution temporelle des séismes au cours de la fin du Quaternaire. A cette fin, une nouvelle approche de recherche, indépendamment du recours aux tranchées paléosismiques, a été mise en œuvre en Himalaya. En utilisant les lacs comme paleoseismomètre, au travers de la collecte de carottes sédimentaires, nous avons pu affiner la résolution temporelle et déceler des séismes à ce jours non répertorié dans les basses de données accessible et ce sur une échelle de ~700 ans. La mise en évidence de séismes important ($M_w \geq \sim 6.5$) non répertorié indique que le Népal occidental connait une activité sismique comparable au centre du Népal et remet en question l'hypothèse d'un gap sismique au centre de l'Himalaya.

Sur base d'une carotte sédimentaire plus longue provenant du même lac, nous avons étudié la distribution temporelle des séismes sur une période de 6000 ans, permettant ainsi de mettre en évidence le caractère aléatoire de l'occurrence des séismes constituant un changement de paradigme là où notion de cycle sismique est encore prépondérante. La mise en évidence du

caractère aléatoire de l'occurrence des séismes tant à courte échelle de temps (instrumentale) qu'à l'échelle du Quaternaire infirme l'hypothèse du gap sismique au centre de l'Himalaya et mets en évidence le risque permanent pour le million de personnes concernées.

Cette thèse s'achève en se penchant sur une possible relation à l'échelle globale entre la variation de taux de séismicité et les changements climatiques au cours de l'Holocène. Nous constatons ainsi que la sismicité globale connu des périodes de séismes accrue sur 7000 ans. Ces périodes de plus fortes activités semblent être synchrone avec la somme des avancées glaciaires de l'Holocène moyen et supérieur. Cette dernière est étayée par une analyse des diverses variables climatiques et physiques qui peuvent contribuer à la nucléation et à l'occurrence des séismes sous la contrainte de phénomènes climatiques extrêmes de forte intensité et de faible amplitude.

Abstract

The Himalayan collision, in which India underthrusts below Tibet, regularly produces major destructive earthquakes in Nepal and its neighboring countries, most of which are fatal to nearby communities. As a wall dividing the Indian plains and the Tibetan plateau, the Himalaya also significantly modifies the atmospheric circulation, affecting both the local and global climate. This thesis explores the poorly known Quaternary history and evolution of Himalayan climate and seismicity, more particularly in the least populated and most remote region of Western Nepal.

In terms of climate and environmental change, one of the least understood aspects of Himalayan history during the late Quaternary is the extension of glaciers and their impacts on landscape evolution. Based on field observations, cosmogenic nuclide dating (^{10}Be) and satellite observations, we estimated the maximum extent of glaciers during the Last Glacial Maximum, which supports the hypothesis of a relatively large glacier cover, but not of an extended ice cap, at the scale of Western Nepal. In addition, our results suggest that the glaciers had a lasting effect on the landscape, both directly and possibly indirectly via the generation of rockslides. We also show that the development of two of Nepal's largest lakes, Lakes Rara and Phoksundo, appears to be directly controlled by glacial activity.

In terms of seismology, the social, economic and political implications of the occurrence of an earthquake of higher magnitude than the recent earthquake of 2015, whose epicenter is located near the city of Gorkha, is a major concern and largely motivates this thesis. The last major earthquake of magnitude greater than 8 (M_b) took place on 6 June 1505 and had a profound impact on the Nepalese population and the surrounding area. In Western Nepal the 1505 event was the last earthquake that ruptured the Main Frontal Thrust according to historical archives and paleoseismological studies, which gave rise to the concept of a seismic gap in western Nepal and adjacent areas in northern India. With this in mind, this thesis addresses two major issues on the Himalayan seismic behavior: on the first hand is the hypothesis of a seismic gap in the central Himalaya and on the second the temporal distribution of earthquakes during the late Quaternary. For this purpose, a new research approach independent of paleoseismic trenches was applied in the Himalaya. By using lakes as paleoseismometers, we were able to refine the temporal resolution and identify earthquakes that had not yet been documented in the accessible databases on a ~700-year scale. Our results from Lake Rara highlight significant previously-unknown earthquakes ($M_w \geq \sim 6.5$) and they reveal that Western Nepal is seismically as active as central Nepal. Furthermore, they call into question the hypothesis of a seismic gap in the central Himalaya.

Based on a longer sediment core from the same lake, we studied the temporal distribution of earthquakes over a period of 6000 years, which has highlighted the random nature of the occurrence of earthquakes, constituting a paradigm shift where the notion of seismic cycle is still prevalent. The random nature of the occurrence of earthquakes both on short (instrumental) and Quaternary time scales disproves the hypothesis of the seismic gap in the central Himalaya and underlines the permanent risk for the million people of concern.

The final part of this thesis addresses the possible global relationship between seismic rate fluctuations and climate change during the Holocene. Our results show that the global

seismicity clustered over 7000 years and appears to be synchronous with the sum of glacial advances through the Mid and Late Holocene. The latter is supported by an analysis of the various climatic and physical variables that can contribute to the nucleation and occurrence of earthquakes under the constraint of extreme climatic phenomena of high intensity and low amplitude.

Samenvatting

De botsing van continentale platen in de Himalaya, waarbij India onder Tibet schuift, veroorzaakt regelmatig grote destructieve aardbevingen in Nepal en de buurlanden, waarvan de meeste fataal zijn voor de nabijgelegen gemeenschappen. Als een muur die de Indische vlaktes en het Tibetaanse plateau scheidt, wijzigt de Himalaya ook aanzienlijk de atmosferische circulatie, wat zowel het lokale als het globale klimaat beïnvloedt. Deze thesis verkent de weinig bekende geschiedenis en evolutie van het klimaat en de seismiciteit gedurende het Quartair in de Himalaya, meer bepaald in de minst bevolkte en meest afgelegen regio van West-Nepal.

Een van de minst begrepen aspecten van de klimatologische geschiedenis van de Himalaya tijdens het late Quartair is de uitbreiding van gletsjers en hun impact op de evolutie van het landschap. Op basis van veldwaarnemingen, kosmogene nuclide-datering (^{10}Be) en satellietwaarnemingen schatten we de maximale omvang van gletsjers tijdens het Laatste Glaciale Maximum, dat de hypothese van een relatief grote gletsjerbedekking, maar niet van een uitgebreide ijskap, op de schaal van West-Nepal ondersteunt. Daarnaast suggereren onze resultaten dat de gletsjers een blijvend effect hebben gehad op het landschap, zowel direct als mogelijk indirect via het ontstaan van rotslawines. We tonen ook aan dat de ontwikkeling van de twee grootste meren van Nepal, Rara en Phoksundo, direct door glaciale activiteit gecontroleerd lijkt te worden.

Op het gebied van seismologie zijn de sociale, economische en politieke implicaties van het optreden van een aardbeving van grotere omvang dan de recente aardbeving van 2015, waarvan het epicentrum in de buurt van Gorkha ligt, een belangrijk aandachtspunt en een belangrijke drijfveer voor deze thesis. De laatste grote aardbeving van omvang groter dan 8 (M_b) vond plaats op 6 juni 1505 en had een diepgaande impact op de Nepalese bevolking en het omliggende gebied. In West-Nepal was de aardbeving van 1505 de laatste aardbeving die volgens historische archieven en paleoseismologische studies de Main Frontal Thrust deed breken, wat leidde tot het concept van een seismische kloof in West-Nepal en aangrenzende gebieden in Noord-India. Met dit in gedachten behandelt deze thesis twee belangrijke kwesties met betrekking tot het seismisch gedrag in de Himalaya: enerzijds de hypothese van een seismische kloof in het centrale deel van de Himalaya en anderzijds de temporele verdeling van aardbevingen tijdens het late Quartair. Hiervoor werd in de Himalaya een nieuwe onderzoek aanpak toegepast, onafhankelijk van de paleoseismische greppels. Door gebruik te maken van meren als paleoseismometers konden we de temporele resolutie verfijnen en aardbevingen identificeren die nog niet op een schaal van ~700 jaar waren gedocumenteerd in de toegankelijke databases. Onze resultaten van Lake Rara belichten belangrijke, tot dan toe onbekende aardbevingen ($M_w \geq \sim 6.5$) en laten zien dat West-Nepal even actief is als centraal Nepal. Bovendien stellen ze de hypothese van een seismische kloof in het centrale deel van de Himalaya ter discussie.

Op basis van een langere sedimentkern uit hetzelfde meer hebben we de temporele verdeling van aardbevingen over een periode van 6000 jaar bestudeerd, wat de nadruk heeft gelegd op de willekeurige aard van het optreden van aardbevingen, wat een paradigmaverschuiving vormt waar de notie van seismische cyclus nog steeds gangbaar is. Het

willekeurige karakter van het optreden van aardbevingen, zowel op korte (instrumentele) als op quartaire tijdschalen, weerlegt de hypothese van de seismische kloof in het centrale deel van de Himalaya en onderstreept het permanente risico voor de miljoen mensen in kwestie.

Het laatste deel van deze thesis gaat over de mogelijke wereldwijde relatie tussen fluctuaties in seismische activiteit en klimaatverandering tijdens het Holoceen. Onze resultaten tonen aan dat de wereldwijde seismiciteit zich over een periode van 7000 jaar heeft geclusterd en synchroon lijkt te lopen met de som van de glaciale aangroeiingen in het midden en late Holoceen. Dit laatste wordt ondersteund door een analyse van de verschillende klimatologische en fysische variabelen die kunnen bijdragen tot de nucleatie en het optreden van aardbevingen onder de beperkingen van extreme klimatologische fenomenen van hoge intensiteit en lage amplitude.

Contents

Chapter 1

Introduction

1.1 Context

The Himalayan chain is one of the most seismically active regions in the world, inhabited by millions of economically and socially highly vulnerable people who are under the constant threat of the next earthquake. The seismic history of the Himalaya is punctuated by large to major earthquakes (i.e., the 1505 AD western Nepal earthquake (Ms ~8.2), 1905 Kangra earthquake (Mw 7.8), 1934 Bihar–Nepal earthquake (Mw 8.2), 1950 Assam earthquake (Mw 8.4), 2005 Kashmir earthquake (Mw 7.6), and 2015 Gorkha earthquake (Mw 7.8)) that are vivid expressions of the collisional process in which India underthrusts below the Tibetan plateau and the Himalayan range (Fig. 1.1; Bilham et al., 2001; Avouac, 2003; Feldl and Bilham, 2006; Mugnier et al., 2013). Convergence across the Himalayan arc at a rate increasing from ~14 to ~21 mm/yr from west to east (e.g. Stevens and Avouac, 2015) leads the Main Himalayan Thrust (the plate interface between India and Tibet) to be considered the largest and most rapidly slipping continental megathrust worldwide (e.g. Cattin and Avouac, 2000).

The possible occurrence of major earthquakes poses a significant threat to the densely populated Himalayan region and its foreland (Fig. 1.1); therefore, constraining the time distribution of large to great earthquakes remains both a socio-economic necessity and a scientific challenge. In the last two decades, the Himalayan arc has been the centre of many studies aimed at deciphering and understanding the patterns of earthquake occurrence, size, extent, and time distribution. To assess seismic hazard in the Himalaya, many studies have relied on comparison of geodetic deformation rates to the level of seismic moment release, measured by instrumental seismicity and derived from paleoseismology (Fig. 1.1; Bilham et al., 2001; Avouac, 2003; Feldl and Bilham, 2006; Mugnier et al., 2013; Avouac et al., 2015; Hayes et al., 2015; Stevens and Avouac, 2016).

Most paleo-seismological studies have focused on traditional techniques (e.g., trenches) to assess recurrence times of large to great earthquakes (see Bollinger et al., 2014 for a review). However, along most segments of the Main Frontal Thrust (MFT), paleo-seismic trenches site have generally revealed only few events over the past millennium (e.g. Bollinger et al., 2014). The lack of earthquakes within the catalogues of parts of the Himalaya has led to the concepts of seismic gaps and slip deficit along the Himalayan arc, which could potentially trigger great

earthquakes in the future (Bilham et al., 2001; Rajendran and Rajendran., 2015; Stevens and Avouac, 2016; Arora and Malik, 2017). Moreover, in the absence of long paleo-seismological time series (> 1000 years), the temporal distribution of large to great earthquakes cannot be robustly ascertained, preventing us from identifying the most adequate model (e.g. cyclic to random; Bollinger et al., 2014; Arora and Malik, 2017). The presence of seismic gaps and the behaviour of earthquakes through time are two sensitive and prominent current questions (e.g. Arora and Malik, 2017).

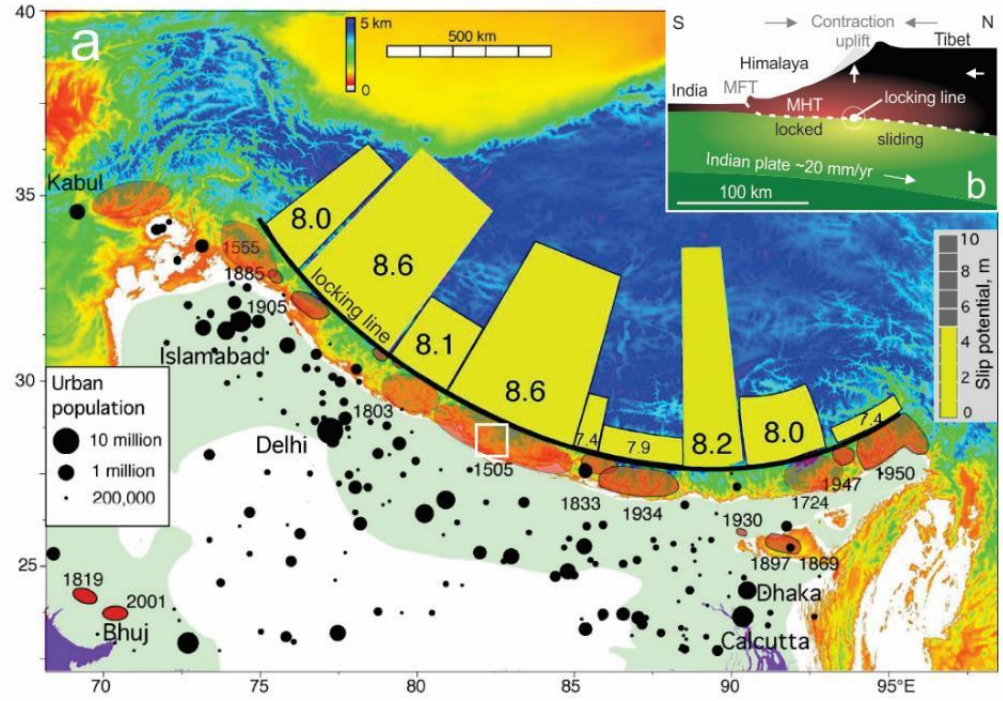

Figure 1.1. Seismic gaps and slip potential of the Himalayan arc. (**a**) Highlights the estimated slip potential along the arc (yellow trapezoids) on a scale of 1 to 10 meters, and the urban population (black dots). The height of each trapezoid is proportional to the current slip potential in meters, and the numbers refer to the potential magnitude (Mw). These trapezoids thus represent how much energy is stored based on the last earthquake that occurred and highlight in how much earthquakes are "overdue". The white box illustrates the western districts of Nepal. (**b**) Simplified cross section through the Himalayan arc highlighting the transition between the locked, shallow portions of the fault that rupture in great earthquakes and the deeper zone where India slides beneath southern Tibet without earthquakes. The Main Frontal Thrust (MFT) and the Main Himalayan Thrust (MHT) are also represented. Vertical movement, horizontal contraction, and micro-earthquake activity are currently concentrated above the locking line (i.e. the transition from the locked to the slipping portion of the MHT); modified after Bilham et al. (2001) and Bilham and Wallace (2005).

On a broader spatial and temporal scale, it is considered that tectonics and climate are interdependent, both having an impact on erosion, topography and weathering. Topography, as a result of uplift and erosion, affects precipitation patterns and therefore causes regional variations in climate (e.g. Bookhagen and Burbank, 2010). The growth of a single mountain range can affect the global atmospheric circulation pattern (e.g. Molnar et al., 2010). On the other hand, climate may moderate tectonics through erosion and weathering (e.g. Willett, 1999; Whipple, 2009). The lithosphere is far from an isolated entity but interacts with other components of the Earth system, such as the hydrosphere and the atmosphere in complex and

often unexpected ways. Over the last decades, numerous studies have been aimed at deciphering the potential interplay between climatic and lithospheric processes in the present and the past (e.g., Last Glacial Maximum; Gao et al., 2000; Heki, 2003; Hampel et al., 2010; Godard and Burbank, 2011; Ader and Avouac, 2013; Bollinger et al., 2014; Scafetta et al., 2015; Johnson et al., 2018) but none have addressed the climatic variations during the Holocene. The response of thrusts and faults to climate-driven changes in ice and water volumes on Earth's surface poses a challenging and unique question: is it possible for climate to modulate regional to global seismicity through the Late Quaternary?

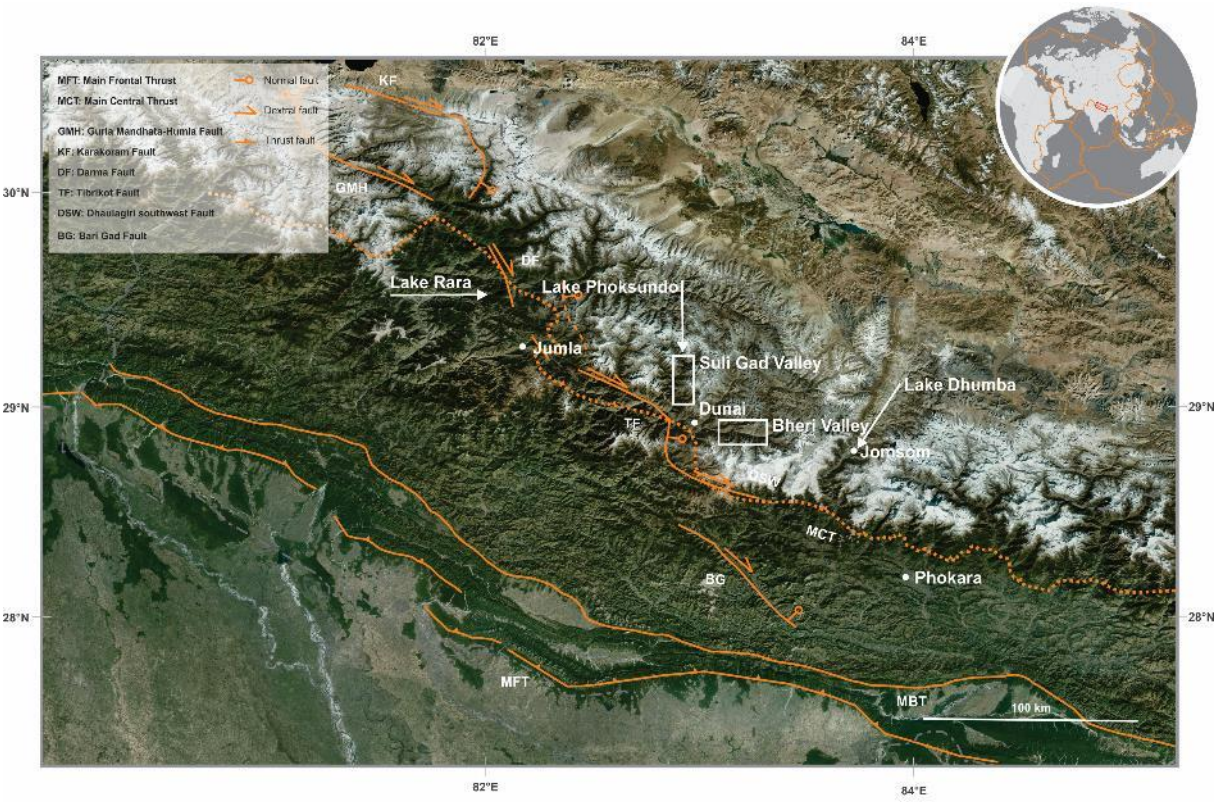

Figure 1.2. Satellite image of Western Nepal outlining the areas investigated and the active faults. The main faults are the Main Frontal Thrust (MFT), Main Boundary Thrust (MBT), Bari Gad Fault (BG), Main Central Thrust (MCT), Tibrikot Fault (TF), Dharma Fault (DF), Gurla Mandhata-Humla Fault (GMH) and the Karakoram Fault (KF).

1.2 Aim

The present thesis focuses on western Nepal in the central Himalaya as a case study and has four primary goals (Fig. 1.2). Having been only partially studied and arguably being the locus of a significant 500-year seismic gap, western Nepal constitutes a privileged target. Our first two goals are closely related. First, we aim to elucidate if the notion of a seismic gap is justified and linked to geological processes or whether it represents a recording bias in historical and geological archives. To do so a fresh approach is necessary. We use, for the first time in the Himalaya, lake-sediment cores that may provide a complementary and more continuous paleoseismic record in comparison to trenches, as earthquake-triggered slope failures and surficial sediment remobilization form turbidite deposits (e.g. Monecke et al., 2004; Howarth et al., 2014; Moernaut et al., 2014; Gomez et al., 2015). Three lakes are studied using a multiproxy approach: Lake Rara, Lake Phoksundo and Lake Dhumba (Fig. 1.2). The second

goal, directly related to the first one, is to characterize the time distribution of a long time series inferred from a long sediment core retrieved from Lake Rara (Fig 1.2). The third goal is to understand the glacial dynamics and their impacts on the landscape of western Nepal through the Late Quaternary. As the final goal, we aim to decipher the response of the lithosphere and therefore the seismicity to climate variability through the Holocene on a global scale.

1.3 Thesis outline

This thesis is composed of four chapters. The second chapter introduces the geomorphological, geological and climatic context of the Himalaya and western Nepal throughout the Quaternary. We present and complement the sparse knowledge on the glacial history and postglacial landscape evolution in western Nepal and we discuss the glacial evolution at the scale of the Himalaya.

The third chapter is dedicated to a discussion of the western Nepal seismic gap and the apparent discrepancy in seismicity between central and western Nepal. Our discussion is based on the analysis of short sediment cores collected in Lake Rara. A thorough discussion of the potential triggering sources of the turbidites observed in the cores is presented and a new earthquake record for western Nepal is proposed, containing several previously unrecognized earthquakes. In chapter four, we use a long sediment core drilled in Lake Rara by a Japanese team who shared the logs with us, to perform a statistical analysis on the earthquake-time distribution. We calibrate our results with the instrumental USGS earthquake catalogue. Based on our analysis we discuss a possible shift of paradigm in the concept of earthquake temporal distributions from cyclic to Poissonian (~random). In the fifth and last chapter, we compare the earthquake time distribution from several records around the world to Holocene climate variability. We explore the different climatic drivers that could influence/promote earthquake nucleation/occurrences. Before concluding, I also present an outlook on future research projects that could substantially support and enhance the conclusions drawn in this thesis. Finally, in the appendices, I provide some detrital apatite fission-track results obtained from the Dolpo area, which were the initial project focus. These data can be used as a base for future detrital thermochronology projects in the area. Also present is the raw dataset from the other sediment core taken in Lakes Rara, Phoksundo and Dhumba.

Chapter two will be submitted to *Geomorphology*. Chapter three is under final revision at *Nature Communications*. Chapter four will be submitted to *Science* before the defense of the thesis. Chapter five is likewise written in paper style and will be submitted after some final adjustments.

Chapter 2

Glacial and landslide controls on the geomorphology of Lakes Rara and Phoksundo, western Nepal

Zakaria Ghazoui [1, 2], Lorenzo Gemignani [3, 4], Julien Carcaillet [1], Monique Fort [4], Rodolfo Carosi [5], and Peter van der Beek [1]

[1] ISTerre, Institut des Sciences de la Terre, Université Grenoble Alpes, Grenoble, France.

[2] RCMG, Renard Centre of Marine Geology, Ghent University, Ghent, Belgium.

[3] Faculty of Earth and Life Science, Vrije Universiteit, Amsterdam, The Netherlands.

[4] Dipartimento di Scienze della Terra, University of Torino, Torino, Italy.

[5] Département de Géographie, Université Paris Diderot - SPC, Paris, France.

In preparation for *Geomorphology*

The Himalaya, due to its climatic and topographic variability, constitutes a genuine open-air laboratory to attempt to comprehend and investigate the character, evolution and dynamics of landscape development in an orogenic context. However, reconstructing paleoenvironmental changes from geological records in the Himalaya remains logistically challenging, in particular in remote regions such as western Nepal. This chapter will attempt to illustrate the variability in processes, landforms and sediment types by studying the Quaternary depositional environments, landforms and sediments of glacial lakes Rara and Phoksundo, as well as the adjacent Bheri and Suli Gad valleys, in the Mugu and Dolpo districts of western Nepal. An attempt is being made to reappraise the extent of glaciers during the Last Glacial Maximum (LGM) as well as to assess the impact of glacier retreat on the landscape of western Nepal.

2.1 Introduction

The Late Quaternary glacial history of the Nepal Himalaya remains incompletely understood. Several factors contribute to this relatively sparse knowledge: first, access to much of the region is arduous, because of challenging relief and poor infrastructure. Second, high relief and abundant precipitation on the southern slopes of the High Himalaya result in poor preservation of depositional landforms (e.g. Fort, 2004): glacial moraines, fluvial terraces, and landslide deposits are easily eroded. Moreover, frequent large landslides complicate glacial records, because discrimination between glacial and gravitational deposits may be difficult and contentious (Hewitt, 2009). Finally, age control for most of the preserved deposits is still lacking (Owen and Dortch, 2014), because material for radiocarbon dating is scarce and more expensive and time-consuming luminescence and surface-exposure dating techniques must be applied to establish event chronologies (Owen and Dortch, 2014).

Early studies of the Himalayan-Tibetan orogen were initiated in the late 19th and early 20th centuries, when Western naturalist-explorers travelled the region and documented its cultural and environmental peculiarities (e.g., Shaw 1871; Drew 1875). Klute (1930) provided the first comprehensive map of the extent of glaciation for the entire Himalayan–Tibetan region during the Last Glacial Maximum (LGM; ~20 ka). Glaciological studies in the early 20th century were motivated by the desire to link Himalayan glacial successions to those identified in Europe. Penck and Brunkner's (1909) pioneering work in the Alps suggested that four glaciations characterized the Quaternary; thus, many authors have inferred four glaciations in regions of Tibet and the Himalaya from their glacial-geological observations (Owen and Dortch, 2014and references therein).

The first modern studies of glaciations in Tibet and the Himalaya were conducted by von Wissmann (1959) and Frenzel (1960), who used early explorers' observations to reconstruct a regional overview of glaciations (Owen, 2010). They both hypothesized that, during the Ice Age, ice caps had expanded and valley-glacier systems developed over most of the Himalaya, Pamir, Kunlun and Qilian Shan. Such a view was disputed by Kuhle (1985, 1995) who advocated for a single vast ice sheet covering most of the Tibetan plateau during the LGM (Owen and Dortch, 2014). However, numerous studies have refuted the existence of an extensive ice sheet over Tibet (Derbyshire1987; Schäfer et al. 2002; Owen et al. 2003; Owen and Dortch, 2014). In particular, Owen et al. (2008) and Seong et al. (2008) emphasized that

the differences in interpretation between Kuhle (1985, 1995) and other studies are the direct consequence of diverging interpretations of landforms and deposits, improper use of Equilibrium Line Altitudes (ELA) to determine the past ice extension, and poor chronological control. Nowadays it is commonly assumed that a large ice cap has never covered the Tibetan plateau, at least during the last 500 kyr (Owen, 2010; Owen and Dortch, 2014). Figure 2.1 illustrates the evolving and contrasting reconstructions of the extent of the last glaciation across the Himalaya and Tibet from Klute (1930) to Shi et al. (1992), the latter now being generally recognized as the prevailing view of the former extent of glaciation (Owen, 2010).

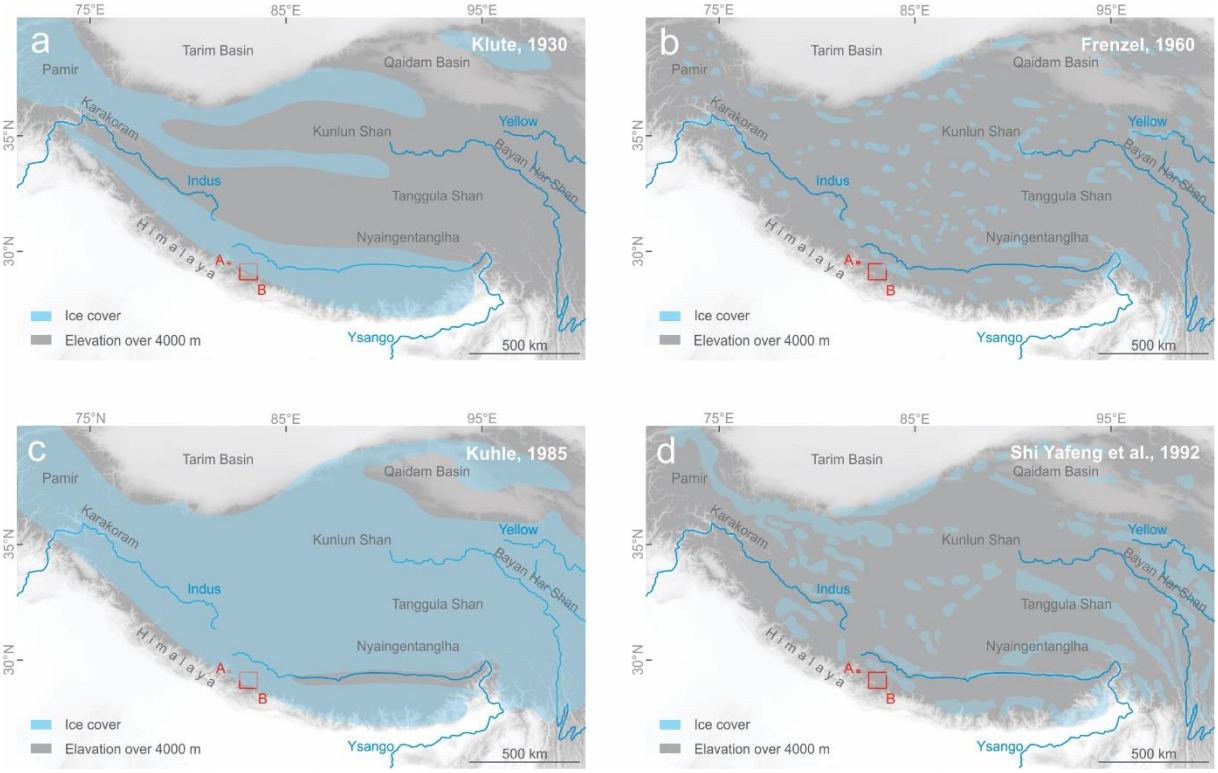

Figure 2.1. Reconstructions of maximum glacial extents across the Himalaya, Tibet and adjacent mountains during the Last Glacial Maximum (modified from Owen et al., 2008). Dark grey: elevation over 4000 m; light blue: areas considered to have been covered by ice. (**a**) Reconstruction of Klute (1930). (**b**) Frenzel's (1960) reconstruction, based on Wissmann's (1959) work on observations of early explorers. (**c**) The field-based reconstruction of Kuhle (1985) who extrapolated large ELA depressions (>1000 m) from the margins of Tibet towards the interior regions. (**d**) Reconstruction of Shi et al. (1992) from detailed field mapping of glacial landforms and sediments. Dot A indicates location of Lake Rara; red square B shows study area around Lake Phoksundo and the Bheri and Suli Gad valleys.

As the marine oxygen-isotope stratigraphy for the Quaternary developed through the 1970s and 1980s, the complexity of the glaciation history in the Himalaya and Tibet, with considerably more than four glaciations occurring during the Quaternary, began to be assessed by researchers. However, the definition of the timing of glacial advances in the Himalayan-Tibetan orogen has been hampered by the lack of quantitative ages on the moraines and landforms associated with them (Owen and Dortch, 2014).

Modern glaciation theories for the Himalaya-Tibet attribute the scale of glacial expansion and climate forcing as both a regional and global cause-and-effect phenomenon (Owen and Dortch, 2014). By addressing the spatio-temporal correlation of glacial chronologies, several studies

(Zech et al., 2009; Kirkbride and Winkler, 2012; Ali et al., 2013; Owen and Dortch, 2014; Bisht et al., 2015) assess the inherent regulating drivers due to differential topography, precipitation, temperature and help in the conceptualization of glacial mechanisms in the Himalaya. While evidence of the Last Glacial Maximum (LGM; ~18-24 ka) preserved in different Himalayan valleys challenges the hypothesis of climatic fluctuations through space and time (Zech et al., 2009; Scherler et al., 2011; Bali et al., 2013; Ali et al., 2013; Eugster et al., 2014; Mehta et al., 2014), an overall possible explanation of the inferred differences is proposed in terms of climate variables (e.g. temperature and precipitation; Zech et al., 2009). For instance, it has been shown that glacier extension through arid Himalayan regions are more sensitive to precipitation, in wetter regions they are more sensitive to temperature, whereas in climate transition zones they show a sensitivity to both precipitation and temperature changes (Scherler et al., 2011; Dortch et al., 2013; Murari et al., 2014; Bisht et al., 2015; Kumar et al., 2017; Shukla et al., 2018). Nonetheless, an accurate mechanism establishing glacier sensitivity to the Himalayan climate system is still lacking (Scherler et al., 2011; Owen and Dortch, 2014).

At a broader scale, two major climate systems affect the Himalaya: the Indian Summer Monsoon (ISM) and the mid-latitude westerlies (Benn and Owen, 1998). Monsoon air masses coming from the south collide with orographic barriers, causing convection and heavy precipitation on the southern margin of the central Himalaya (Bookhagen et al., 2005). The Himalayan topography is thus characterized by a strong rainfall gradient on its southern front (Fig. 3; Barros and Lettenmaier, 1994; Bookhagen et al., 2005; Srivastava et al., 2017). Temperature and pressure gradients bring moisture from the Arabian Sea and the Bay of Bengal to the Himalaya, which imposes a pattern of increasing precipitation from west to east (Fig. 2; Bookhagen and Burbank, 2010). The mid-latitude westerlies cause prevailing winter precipitation in the extreme west of the Himalaya, Trans-Himalaya and Tibet, while in summer, they migrate south of the Himalaya (Benn and Owen, 1998; Owen and Dortch, 2014).

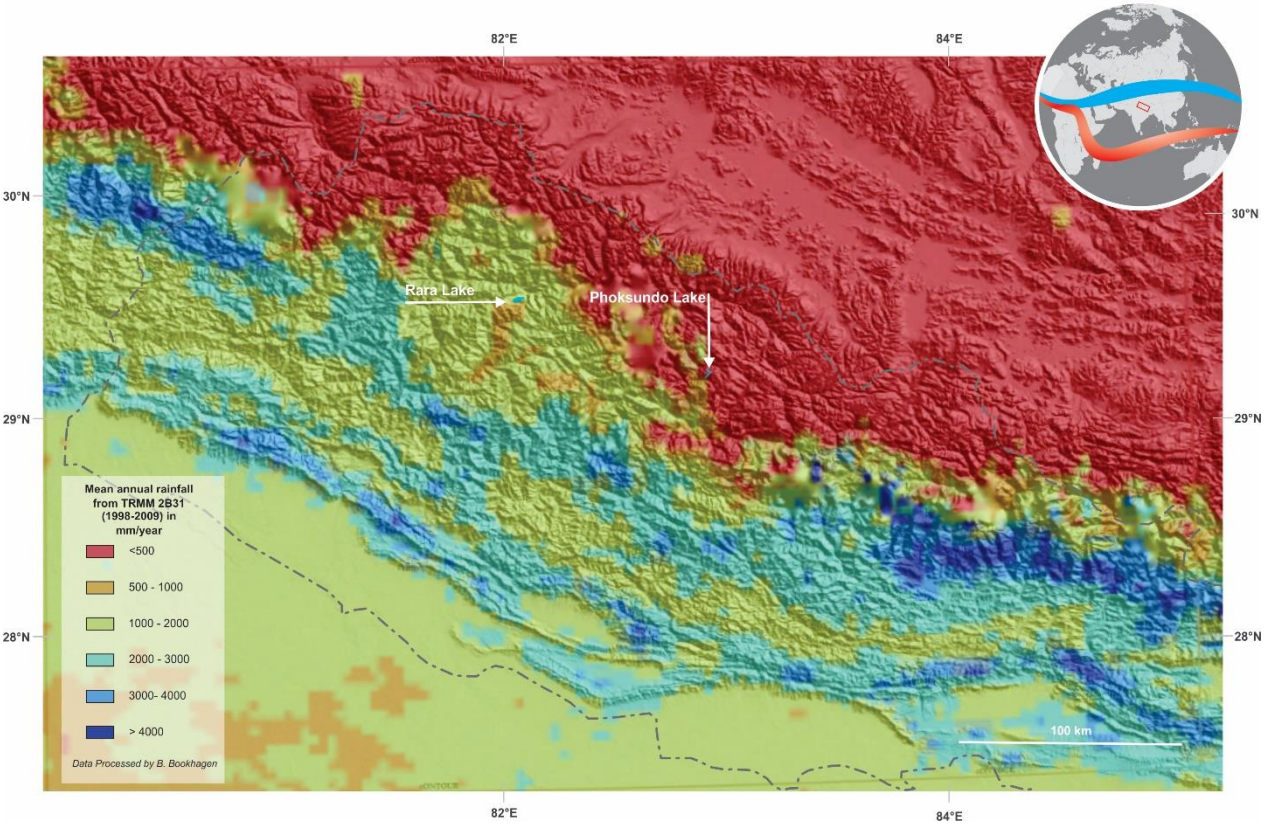

Figure 2.2. Precipitation map of Western Nepal. Mean annual rainfall (mm/yr) between 1998 and 2009 derived from TRMM 2B31 dataset (Bookhagen and Burbank, 2010). Inset map shows locaton within Eurasia; red and blue curves illustrate the summer and winter location of the Intertropical Convergence Zone (ITCZ), respectively.

The glacial response to climate change is expressed by a change in the mass balance related to fluctuation in the precipitation influx and melting outflux (e.g. Dyurgerov and Meier, 2005). The larger and flatter the glacier (leading to slower flow velocity), the longer its response time under equivalent climatic conditions will be (Bolch et al., 2012). Therefore, changes in length and surface are more challenging to interpret in a climatic perspective than the changes in the mass balance (Bolch et al., 2012).

A further important implication of glacier recession is the exposure of steeply glaciated bedrock walls. The melting and removal of ice modifies the state of stress that exists in the rock mass and may trigger collapse of the rock walls following three possible response modes (e.g. Johnson, 1984; Ballantyne 2002): (1) catastrophic large-scale failure of a rock slope, through major rock slides or avalanches; (2) large-scale deformation of a rock mass, through slow, progressive movements that can result in catastrophic failure; and (3) rapid adjustment of walls by frequent, discrete rock falls, resulting in accumulation of slope debris at the foot of the slope. As illustrated by a series of recent studies (Weidinger and Ibetsberger, 2000; Hewitt, 2009; Korup et al., 2010), we are still in the early stages of identifying and grasping these phenomena within the Himalayan context.

In order to complement the still sparse knowledge on the glacial history and postglacial landscape evolution in the western Nepal Himalaya, we present here reconnaissance field data

and preliminary ^{10}Be exposure ages from glacial and gravitational deposits surrounding lakes Rara and Phoksundo. These regions are particularly interesting for several reasons. So far, very few studies focused on Quaternary geomorphology have been conducted in this region characterised by a significant climatic (e.g. precipitation; Fig. 2.2) gradient. The Mugu region is partly affected by the monsoon, while the Dolpo is protected by the barrier formed by the peaks of the Dhaulagiri massif and is relatively arid. Using a limited amount of samples and in combination with our field observations we attempted a preliminary reconstruction of Quaternary landscape evolution, by discussing (1) the role of climate in influencing glacial extent in the central Himalaya, and (2) the role of rockslides and landslides in landscape evolution.

2.2 Tectonic and climatic context

The collision of India and Eurasia results in the underthrusting of India and a southward-propagating system of thrusts in the overlying Himalayan wedge (Fig. 2.3; e.g., Le Fort, 1975; Hodges, 2000). The Main Central Thrust (MCT) marks the transition from the high-grade metamorphic Higher Himalayan Sequence in the north to the lower-grade Lesser Himalayan Sequence in the south. The MCT is mostly inactive today; tectonic convergence is inferred to occur mainly along the Main Frontal Thrust (Fig. 2.2), which currently separates the Himalaya from its foreland (e.g., DeCelles et al., 2001).

Millennial timescale erosion rates derived from ^{10}Be data in central Nepal have been interpreted to indicate persistent erosion and active faulting at the foot of the High Himalaya just south of the MCT, where monsoonal precipitation is high (Wobus et al., 2005). However, this view has been contested; the spatial variations in erosion/exhumation rates are better explained by movement over a major mid-crustal ramp in the underlying Main Himalayan Thrust, possibly associated with tectonic underplating (Robert et al., 2009; Herman et al., 2010; Godard et al., 2014; van der Beek et al., 2016). Strong dynamic feedbacks between climate, erosion, and tectonics have been inferred for other regions along the Himalayan front (Bookhagen et al., 2005; Thiede et al., 2005; Grujic et al., 2006). The observed coincidence of high precipitation and tectonics, however, does not prove causality, apart from the recently confirmed notion that orographic precipitation and related erosion are strongly controlled by topography (Bookhagen and Burbank, 2006; Gabet et al., 2008; Scherler et al., 2014).

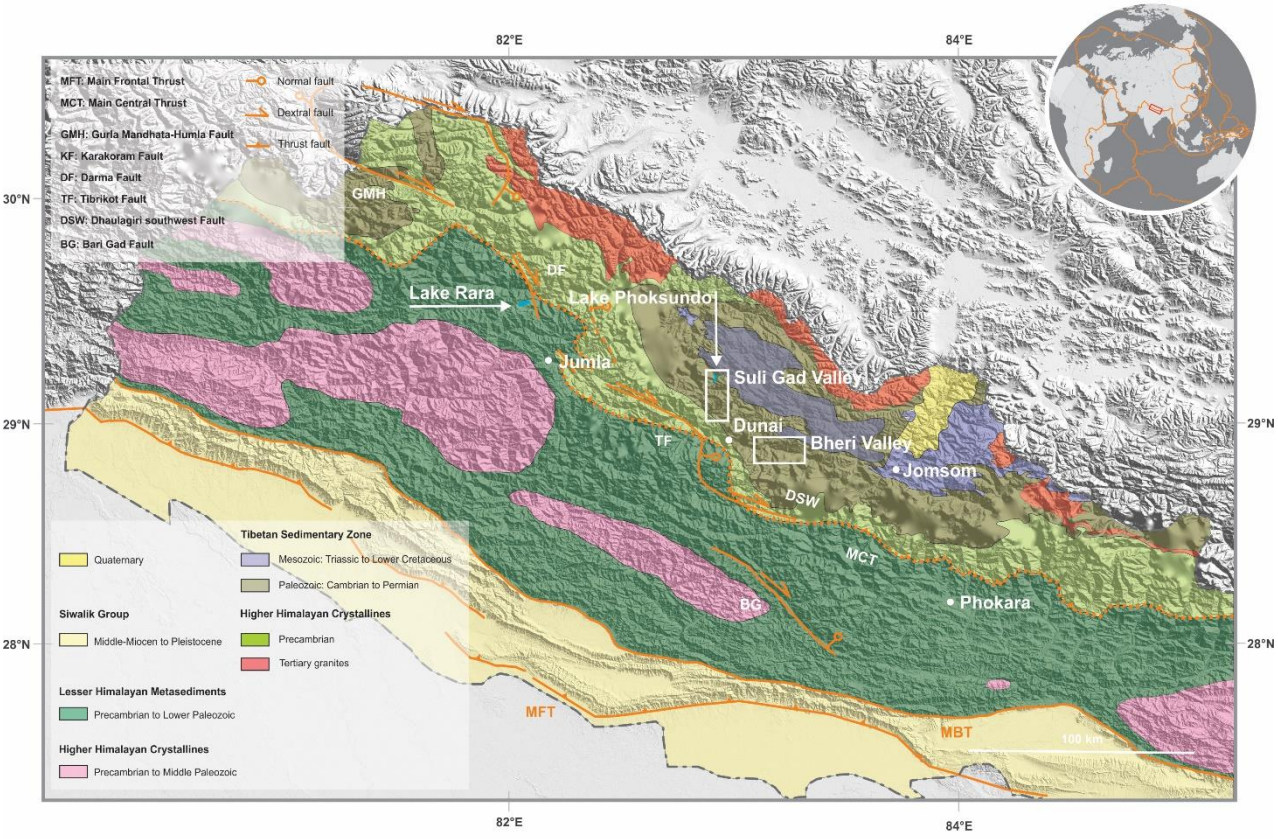

Figure 2.3. Simplified geological map of Western Nepal (modified after Upreti, 1999). Active faults are shown in continuous orange lines and inactive major thrusts in dashed lines. White arrows (lakes Rara and Phoksundo) and white boxes (Bheri and Suli Gad valleys) show the location of the studied areas.

Through topographic analyses in central and western Nepal, Harvey et al. (2015) delineated a clear discontinuity west of 82.5°E, where the prominent, central Himalayan mountain front bifurcates into two, less abrupt topographic steps that continue north-westward for about 100 km before merging again into a single band in northern India (Fig. 3). While the observed topography can be generated in a variety of ways, the spatial distribution of micro-seismicity together with morphologic evidence for spatial variations in rock-uplift rates suggest that the discontinuity in topography has a tectonic origin (Harvey et al., 2015; van der Beek et al., 2016). These authors suggest that the Main Himalayan Thrust (MHT) ramp makes an ~50° northward bend in western Nepal, while recent duplexing accommodates some of the convergence over a younger mid-crustal ramp beneath the southern topographic step.

Climatically, past glacial advances in the central Himalaya as reconstructed based on glacial landform dating appear asynchronous (Murari et al., 2014). Some authors (Kaser and Osmaston, 2002; Kull et al., 2008; Rupper and Roe, 2008) have suggested that this variability is due to variations in landscape and temperature, precipitation and cloud cover. As such, the glacial extension during Marine Isotopic Stage (MIS) 3 (30–60 ka) seems to be the result of increased Asian monsoon precipitation and cloudiness (Finkel et al., 2003; Owen et al., 2003, 2005, 2006, 2009; Rupper et al., 2009). Conversely, the LGM and Younger Dryas advances are believed to be influenced by the westerlies (Owen and Dortch, 2014). The western Himalaya and drier interior parts of Tibet appear to be little influenced by the Indian Summer Monsoon, but the

central Himalayan glaciations seem to be influenced by strong monsoon variations linked to rapid Northern-Hemisphere climate fluctuations (Zech et al., 2009; Dortch et al., 2013; Murari et al., 2014).

One of the main debates in Nepal is to which MIS (2, 3 or 4?) the regional LGM should be attributed. In this context, Nepal is located in an interesting and important climatic transitional position, between regions mainly under the influence of the westerlies and those impacted by the Indian Summer Monsoon (ISM; Fort, 2004). The eastern half of Nepal is mainly affected by the ISM, bringing abundant precipitation and high-altitude snowfall in summer. In contrast, western Nepal is exposed to winter precipitation originating from the westerlies, during which the monsoon air flux cools down the massive barrier formed by the Annapurna and Dhaulagiri ranges resulting in a rain shadow effect (Fort, 2004). As a result, paleoclimatology in the western and eastern Himalayan ranges cannot be treated in the same way (Fort, 2004). In central Nepal, the transition, enhanced by a narrow range with limited glacial catchment basins, renders inter-stage glacial correlations more elusive (Fort, 2004).

In her review on the Quaternary glaciations of central and eastern Nepal, Fort (2004) suggested that the LGM in Nepal occurred not during MIS 2 but rather during MIS 3. The reconstructed length of glacial tongues appears on the order of 15–20 km, indicating that glaciers were never very extensive (Fort, 2004). The explanation for the fairly limited glacier extension given by Fort (2004) involves three main factors: First, the topographic steepness and climate gradients along the mountain slopes appear to prevent the accumulation and advance of ice, which thaws before it is able to flow further down the valleys. Secondly, Nepal is located far enough to the east and south of the westerlies to have been affected by the abundance and seasonality of high-altitude precipitation throughout the Quaternary. Where the snow supply is mostly driven by the ISM air flux, with an accumulation peak generally in summer and freezing period only from the beginning of autumn, such climatic conditions result in a reduced ice volume. Moreover, the Himalayan range is narrowest in its central (i.e. Nepalese) part, and the highest-altitude massifs (>6000 m) appear to have been less favourable to feed extended glacial tongues (Fort, 2004), the air at such high elevations only containing reduced amounts of water vapour. In contrast, to the south of the highest Nepal ranges, at altitudes ranging from 4000 to 5500 m, relatively small massifs with their gentle slopes were extensively glaciated by small ice caps (Fort, 2004).

2.3 Study area

Fuchs (1970, 1977) first investigated the geology of western Nepal, more specifically the Jumla and Dolpo districts. For our field reconnaissance in 2013 and 2014, we first made a traverse from Jumla to Jomsom (Fig. 3.3).

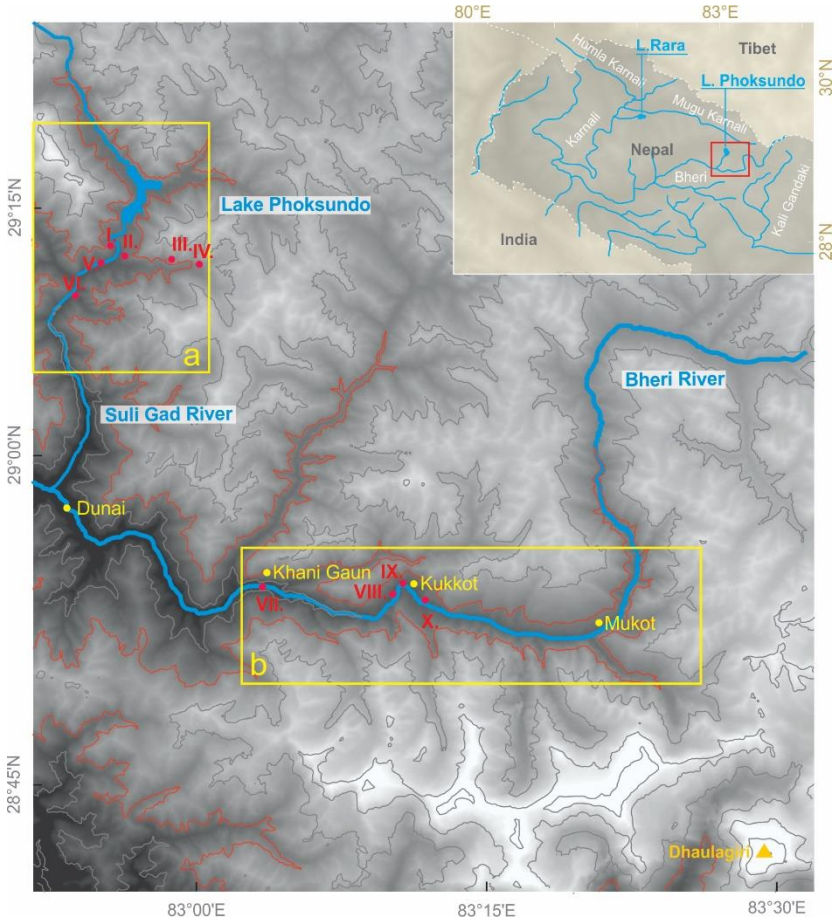

Figure 3.4. ASTER digital terrain model of the Suli Gad valley, Lake Phoksundo and the Bheri valley. Boxes indicate (**a**) Suli Gad valley and Lake Phoksundo, (**b**) Bheri valley. The red dots with roman numbers I to X indicate the location of the field photos shown in Figures 9–12 to illustrate the principal glacial landforms. Yellow dots indicate the main villages of the area. Grey lines are 1000-m topographic contours; the red contour marks 4000 m elevation.

The second expedition led us to work on Lakes Rara and Phoksundo. Although the main objective of these two expeditions was not to make a study of the glacial landforms, we observed and described the landforms and deposits in passing and collected some samples for dating. This work is therefore reconnaissance in nature and shows the potential of this region for more thorough and rigorous geomorphological studies in the future. In this chapter, we focus on three areas with remarkable glacial features: first, Lake Rara in the Jumla District, which features well-preserved frontal and lateral moraines; second, the Suli Gad Valley between Dunai and Lake Phoksundo (Fig. 3.4; Dolpo District), which preserves remnants of glacial and fluvial-glacial deposits and the giant rockslide of Lake Phoksundo (Yagi, 1977; Weidinger and Ibetsberger, 2000); finally, the Bheri valley (between Kauni Gaun and Kukkot, Dolpo District; Fig. 3.4), which preserves a record of ancient lakes that may be either glacial or landslide-induced.

2.3.1 Lake Rara

Lake Rara, located in the Mugu district (Western Nepal), occupies a small plateau surrounded by three valleys, including that of the Mugu Karnali to the north. The lake-level elevation is approximately 2980 m, while the surrounding mountains rise up to 3200 m in the south and

3700–3900 m in the north and southwest. The unusual setting of Lake Rara raises many questions on its origin. The bathymetry of the western half of Lake Rara is box-shaped with a flat bottom more than 160 meters below the lake level (Fig. 3.5). The present-day outlet is situated at the northwestern corner of the lake, from where a shallow stream flows down to the Karnali main trunk ~30 km to the west. The bedrock surrounding the lake consists of greenschist-facies metasediments of the Lesser Himalaya series (Fig. 3.3; Fuch, 1970). The lowest, eastern bank of the lake is surrounded by low-relief hills that rise less than 50 m above the lake level. This bank looks like a natural dam, which is 500 m wide and 1.3 km long (Fig. 5). The narrow embankment is composed of sediments that are >100 m thick, and consist of metre-sized quarzitic boulders enclosed in a fine matrix. The lack of landslide-related features (i.e. clusters of mounds and hollows) in the bathymetry of the eastern part of the lake, together with the absence of arcuate landslide scarps on surrounding mountain slopes, suggests that these deposits are not gravitational in origin. We interpret these as glacial deposits, i.e. the frontal and lateral moraines of a small glacier that flowed north-eastward and carved out lake Rara.

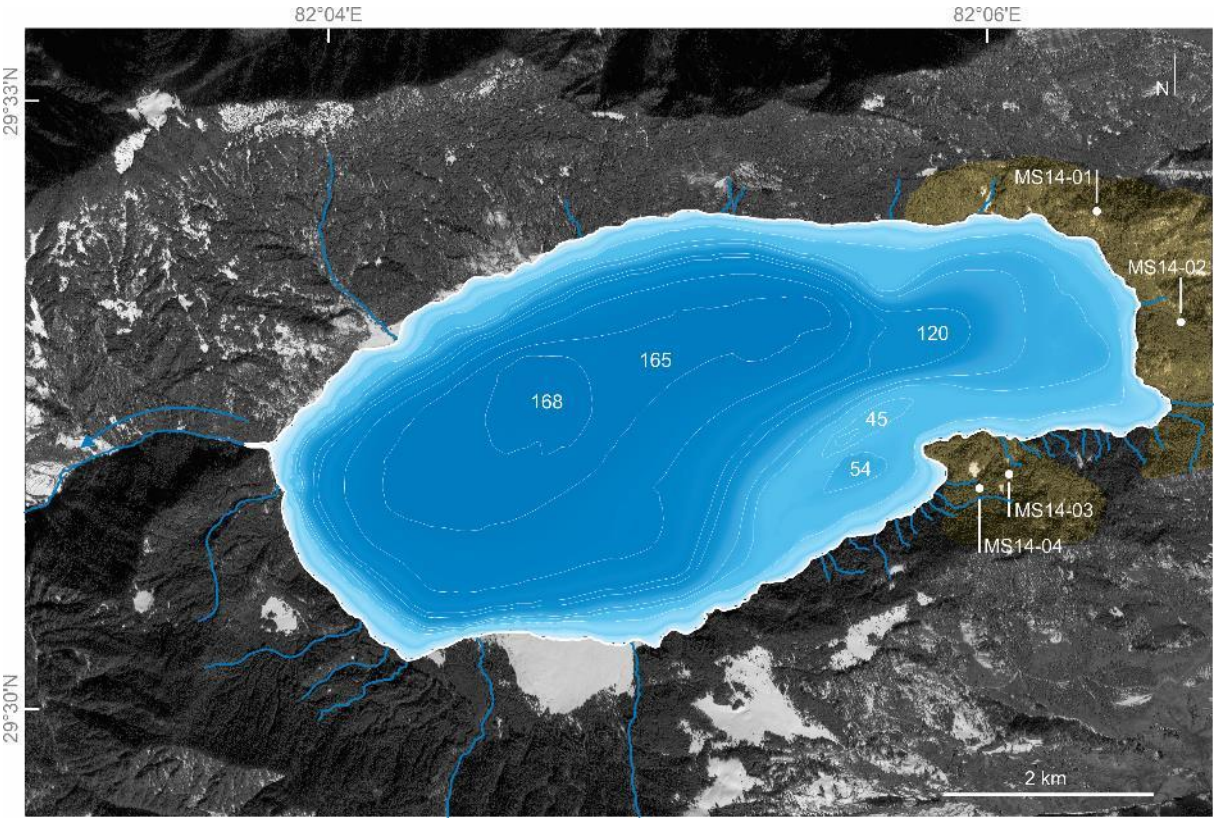

Figure 3.5. Aerial photograph and bathymetric map of Lake Rara. Yellow transparent areas represent the frontal and lateral moraines. White dots are the 10Be samples collected on quarzitic boulders from the moraine crests.

2.3.2 The Suli Gad Valley and Lake Phoksundo

The Suli Gad Valley forms a deep gorge between Dunai and Lake Phoksundo (Fig. 3.4). The valley exposes a transect through some of the main geological features of the Himalaya (Fig. 3): its southern end at Dunai is in the Lesser Himalaya (LH), and the rest of the valley is within the Tibetan Sedimentary Zone (TSZ). At Lake Phoksundo, the Tethyan Sedimentary Sequence (TSS) or TSZ is exposed, in particular the mainly Ordovician Dhaulagiri limestone (Fuchs,

1977). The Suli Gad Valley (Fig. 3.4) has been the site of detailed geological and tectonic investigations by Carosi et al. (2002, 2006), but no detailed geomorphological studies have been performed. During our trek through the valley, we identified glacial landforms and fluvial-glacial deposits. Due to the presence of numerous landslides, the water level of the rivers, the dense vegetation and the steepness of the cliffs we were not able to collect samples for dating. In the vicinity of Lake Phoksundo, numerous hummocky moraines cover the hillside of the valley. As the valley opens up, it gives way to a glacial deposit of several hundred metres high, suggesting a glacial knob. At the top of this till deposit, Lake Phoksundo lies between the limestone slopes of the TSS. Lake Phoksundo is situated in the upper course of the Suli Gad River, at the border of the lower and higher Dolpo (Fig. 3.4). It is the second-largest lake of Nepal, with very steep sides plunging to a 135-m deep flat lake bottom (Fig. 3.6), giving the lake a fjord-like appearance.

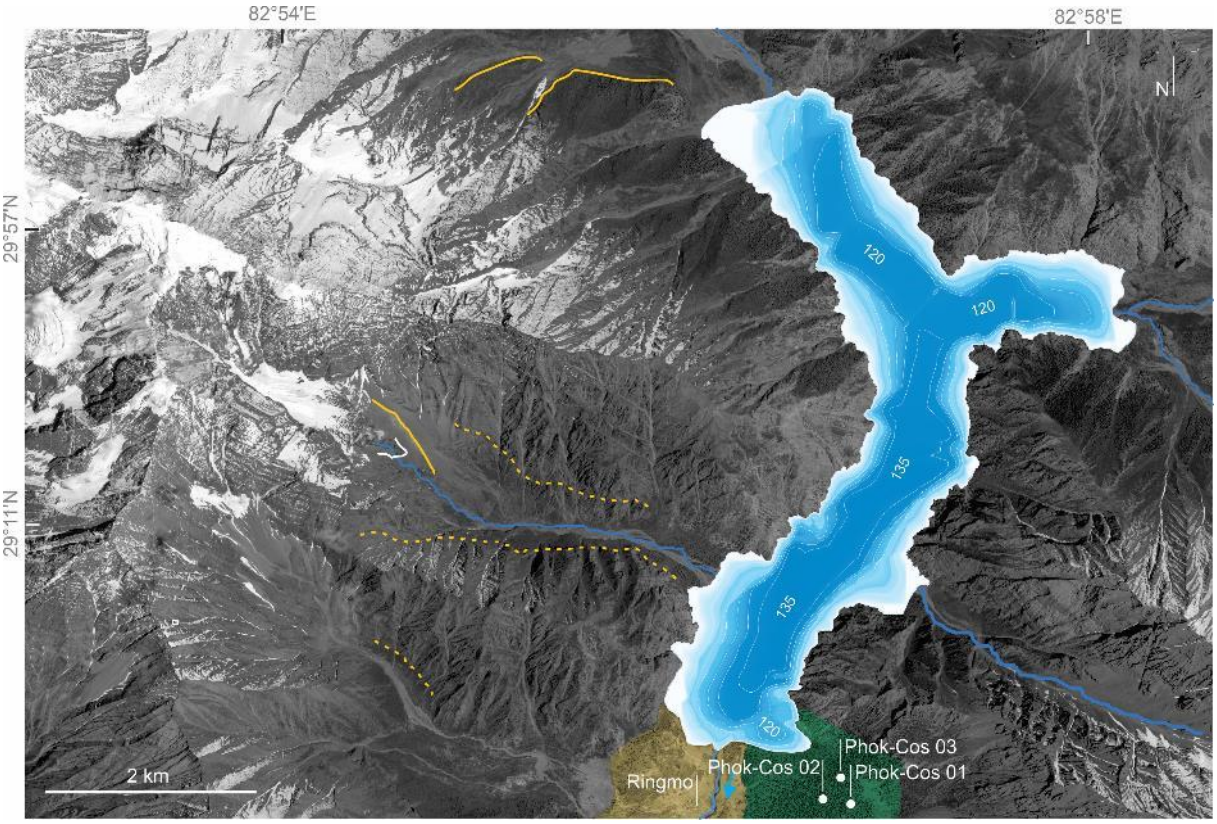

Figure 3.6. Aerial photograph and bathymetric map of Lake Phoksundo. Yellow and green transparent areas represent frontal moraines and rockslide deposits, respectively. White dots are the locations of ^{36}Cl samples collected by Fort et al. (2013) on the rockslide deposit. The white line is the 2016 front of an unnamed glacier. Thick yellow lines are inferred Little Ice Age (LIA) lateral moraines. The dashed yellow lines represent lateral and hummocky moraines that we attribute to the maximum glacial extent.

The lake has been suggested by Yagi (1977) and Weidinger and Ibetsberger (2000) to result from damming of the Suli Gad River by the collapse of a mountain wall of Dhaulagiri limestone (Fuchs, 1977), culminating at 5148 m SE of the lake (Fort et al., 2013). The collapse, which led to a 4.5-km^3 rockslide dam, was suggested to have occurred at 30 to 40 ka (Yagi, 1977), although more recent dating by Monique Fort (results published with this study) has revised this chronology (see below). The rockslide morphology presents a series of complex landforms,

including mounds and depressions of varying size. Massive interlocked blocks of several tens of meters dominate the deposit, included in fine-grained material.West of and beneath the rockslide deposit, fine sediments appearing as till/moraine material and overlain by orange conglomerates including metre-sized dolomite boulders, in contrast, suggest a glacial origin.

2.3.3 The Bheri Valley

The Bheri River is a major tributary of the Karnali River, draining the western Dhaulagiri Range in western Nepal (Fig. 3.4) from its source in the Dolpo highlands. Between the villages of Khani Gaun and Kukot, numerous fluvial-glacial deposits, lake sediments and moraines have been preserved (Fig. 4). The valley section between Khani Gaun and Kukkot presents a series of rapid and significant differences in elevation that resemble glacial knobs, rising rapidly from ~2700 to ~3300 m. However, a large number of landslides, which vary greatly in magnitude, also occur on both sides of the river. From Khani Gaun to Mukot, the Bheri River flows along the South Tibetan Detachment (STD) and within the Tethyan Sedimentary Sequence (TSS) (Fig. 3.3). In Kukkot, the valley opens up rapidly and gives way to a relatively large alluvial plain with numerous channels. On the edges of this plain, a series of small fluvial terraces are developed on top of a thick deposit of white lacustrine sediments, mainly composed of clay. The characteristic rhythmic parallel laminated sediment deposit (e.g. Ashley, 2002), which are characteristic of lake bottom deposits, are visible from afar and can be followed along the alluvial plain. The limits of the lacustrine deposits could, however, not be established due to the widespread presence of landslides.

2.4 Samples and methods

Our analysis and interpretation is based on field observation and interpretation of satellite imagery, as well as existing and new surface-exposure dating using the Terrestrial Cosmogenic Nuclides (TCN) ^{10}Be and ^{36}Cl.

2.4.1 Field observations and mapping.

Field observations were collected both in a notebook and using FieldMove software developed by Midland Valley. Photos were described, geolocated and directly plotted on a map. Geomorphological mapping was also performed using FieldMove, drawing the boundaries of each unit and describing them.

2.4.2 ^{10}Be Terrestrial Cosmogenic Nuclide (TCN) surface-exposure dating.

Four samples were collected from quarzitic boulders on the crests of the frontal and lateral moraines exposed east of Lake Rara (Fig. 3.7) for ^{10}Be TCN surface-exposure dating following the protocol outlined below. Monique Fort provided the ^{36}Cl TCN ages of the Phoksundo rockslide; a short description of the dating methods for these samples is available in Fort et al. (2013). Samples were crushed and sieved to obtain the 200–500 μm size fraction. The chemical extraction protocol is adapted from Brown et al. (1991) and Merchel and Herpers (1999) and was carried out at Ghent University, Belgium and the ISTerre cosmogenic laboratory in Grenoble, France. Quartz was isolated through repeated leaching in an H_2SiF_6-HCl (2/3-1/3) mixture. Meteoric Be was removed with three sequential baths in diluted HF (Kohl and Nishiizumi, 1992). The purified quartz samples (weighing between 14 g and 52 g) were spiked

with ~300 µl of a 1 $mg.g^{-1}$ Be carrier solution (Scharlab ICP Standard) before being totally dissolved in concentrated HF. After evaporation of HF, perchloric and nitric acids were added and evaporated to remove organic compounds and fluorides, respectively. Anion and cation exchange columns allowed the separation of Fe and Ti and the isolation of the Be fraction. Be hydroxide was extracted by alkaline precipitation (Von Blanckenburg et al., 1996). The final BeO targets were oxidized and mixed with Nb powder prior to loading them on cathodes for Accelerator Mass Spectrometer (AMS) measurements, which were carried out at ASTER, the French National AMS facility at CEREGE, Aix-en-Provence. The measured $^{10}Be/^{9}Be$ ratios were calibrated against a CEREGE in-house standard, using an assigned value of $1.191 \pm 0.01 \times 10^{-11}$ (Braucher et al., 2015) and a ^{10}Be half-life of $1.387 \pm 0.012 \times 10^{6}$ yr (Chmeleff et al., 2010; Korschinek et al., 2010). The ^{10}Be concentrations inferred from the measured $^{10}Be/^{9}Be$ ratios were corrected for the corresponding full process blank ratios (3.901×10^{-15}). AMS analytical uncertainties (reported as 1σ) include the uncertainties associated with the AMS counting statistics, the chemical blank corrections, and the ASTER AMS external error (0.5%; Arnold et al., 2010).

Figure 3.7. (a) View of Lake Rara from the north summit bordering the lake. Moraines are outlined in yellow and the ^{10}Be sample locations are indicated. The dashed arrow indicates the past outflow direction, the plain one the modern outflow. (**b**, **c**) Quartzitic boulders in Lake Rara moraine; (**b**) Example of boulder not sampled, present at the shore of the frontal moraine and (**c**) sampled boulder on the crest of the frontal moraine.

Exposure ages were computed with the online CREp calculator (Martin et al., 2017; http://crep.crpg.cnrs-nancy.fr). Production-rate scaling to the sample locations was made according to the recent, physically based, LSD model (Lifton et al., 2014), which performs

similarly to older empirical models (Borchers et al., 2016). Chosen parameters include the ERA40 atmospheric model (Uppala et al., 2005) and the Lifton-VDM2016 geomagnetic database (Lifton, 2016). Topographic shielding was estimated in the field through skyline survey using a clinometer. We retained the production rate derived by Balco et al. (2009), as no regional production rates are available for the Himalaya (Owen et al., 2010). The Balco et al. (2009) production rate has a value of 3.93 ± 0.19 at g^{-1} yr^{-1} for LSD scaling and is consistent with other recently derived Northern-Hemisphere production rates (Fenton et al., 2011; Ballantyne and Stone, 2012; Briner et al., 2012; Goehring et al., 2012; Young et al., 2013; Small and Fabel, 2015; Stroeven et al., 2015). We did not apply erosion- or snow corrections, because we have no indication for significant erosion of the sampled blocks and most sampled boulders lie in windswept locations where little snow would build up.

2.4.3 Reconstruction of the paleo-Equilibrium Line Altitude (ELA)

Using our field observations and satellite imagery, we attempted to reconstruct the paleo-Equilibrium Line Altitude (ELA) during the inferred most recent glacial extension as well as depicting roughly the maximum glacial extension of the glaciers in the vicinity of the Suli Gad and Bheri Valleys (Fig. 3.4). To do so, we used the toe-to-headwall altitude ratio (THAR; Louis, 1955) based on the assumption that the ELA lies at a fixed altitudinal ratio between the lowest and highest altitude (i.e., the headwall) of a glacier (Louis, 1955). We used the THAR value of 0.4 suggested by Owen and Benn (2005) for the reconstruction of paleo-ELAs along the Himalaya.

2.4.4 Reconstruction of the maximum glacial extent

Given the relatively good preservation of lateral moraines compared to that of frontal moraines in the study areas, we used the latter to estimate and reconstruct the maximum glacial extent. As lateral moraines are deposited below the Equilibrium Line Altitude (ELA), the maximum altitude of lateral moraine (MALM) method (Benn and Evans, 1998) assumes that the uppermost elevation of a remnant lateral moraine marks the paleo-ELA (Andrews, 1975; Dahl et al., 2003). However, our intention was not to reconstruct the paleo-ELA given the data at our disposal, but rather to estimate the maximum expansion of the glaciers from the minimum elevation of lateral moraines. In addition, we used the occurrence of cirque lakes as a marker of past glaciations. In both cases, we used both our field observations and satellite imagery.

2.5 Results and discussion

2.5.1 Lake Rara

Rock samples were taken from the frontal moraine rising about ten metres above the lake (Figs. 3.5 and 3.7). The moraine is composed of eroded boulders on which glacial erosion figures (i.e., striae) can be discerned and is covered by a pine forest. The blocks are metre-sized or larger and their lithology is quarzitic. The whole is consolidated by glacial till.

From the five dated samples, four have valid measurements, whereas one (MS14-05) showed to low and instable current during AMS measurement and is therefore not reported. The ^{10}Be exposure ages of these four boulders are listed in Table 2.1.

Sample	Lat (N°)	Lon (E°)	Altitude (m asl)	Shield, Corr.	Thickness (cm)	Local Production rate (at g^{-1} yr^{-1})	Age (ka)	1σ (ka)	1σ without production rate error
MS14-01	29.54187	82.11869	3016	0.9961	5.0	27.7	61.6	6.3	5.6
MS14-02	29.54405	82.11071	3009	0.9954	4.0	24.7	60.3	12.3	11.9
MS14-03	29.53874	82.11956	3002	0.9962	8.0	27.1	354.5	21.7	7.9
MS14-04	29.53773	82.12009	3006	0.9954	8.0	27.1	242.3	13.1	3.7

Table 2.1. Lake Rara exposure ages. The ages are from four boulders respectively from the frontal (MS14-01/02) and lateral (MS14-03/04) moraine.

Two boulders from the frontal moraine of Lake Rara (MS14-01 and 02; Fig. 2.7; Tab. 2.1) yielded consistent exposure ages of 62 ± 6 ka and 60 ± 12 ka, respectively. The other two boulders (MS14-03 and 04), collected from the lateral moraine, have significantly older ages of 355 ± 22 ka and 242 ± 13 ka, respectively. These unexpectedly old ages raise questions on issues associated with the application of surface exposure dating methods to date moraines in the Himalaya, Tibet and elsewhere, which have been discussed at length in several studies (e.g. Benn and Owen, 2002; Putkonen et al., 2008; Owen and Dortch, 2014). Such issues can be related to uncertainty introduced in the calculation of the TCN production rates, geological complexities affecting surfaces such as weathering as well as previous exposure and shielding of the surface by snow and/or sediments (Owen et al., 2010). In previous studies, Balco et al. (2008) and Owen and Dortch (2014) showed that the uncertainty related with different scaling models for low-latitude and high-altitude areas such as the Himalaya can reach 40% between scaling models over the last glacial cycle. In view of these issues, we applied the Lifton et al. (2014) time-independent production-rate model, acknowledging the uncertainty associated to our calculated ages, and use caution while assigning our numerically dated moraines to a specific climatic stage.

For such very old moraines, geological factors may complicate the dating results and overshadow the uncertainty related to the production rates (Owen et al., 2010). Commonly reducing the concentration of TCN in rock surfaces, these factors may lead to an underestimate of the true age of the landforms (Owen et al., 2010). In contrast, episodes of prior exposure of rock surfaces, which may result in an overestimation of the age of the moraine (Owen et al., 2010), are relatively rare (Putkonen and Swanson, 2003). These issues may be partially assessed by collecting multiple samples in order to obtain a statistically robust population, with some studies inferring that the oldest age in a cluster of ages on a moraine is the most appropriate measure of the age of the landform (e.g. Briner et al., 2005; Owen et al., 2010).

We will first address the question of the unusually old ages of MS14-03 and 04. Based on our limited results, the lateral moraines would be considerably older than 200 ka. The evidence of extremely old glaciations in the Himalaya is subject to intense debate (e.g. Owen and Dortch, 2014). Very old moraines can be well preserved in the semi-arid regions of Tibet and the Transhimalaya, but in most regions of the Himalaya, such old moraines are expected to be eroded. Amongst the oldest moraines are those of the Indus glacial stage (130 to 385 ka) in Ladakh (Owen et al., 2006). Other extremely old moraines have been described on the west

flank of Gurla Mandata in southernmost central Tibet (Owen et al., 2010). The large uncertainties associated with dating these old moraines and sediments preclude regional correlations (Owen and Dortch, 2014). Moreover, it is difficult to correlate convincingly the old moraines within a region (Owen and Dortch, 2014). Therefore, we hesitate to ascribe significant implications to these two very old ages.

Since samples MS14-01 and 02 were taken from stable boulders on the crest of the moraine (Fig. 7), we are fairly confident that these overlapping boulder ages reliably reflect the moraine age (Benn and Owen, 2002). The age of the moraine (~60 ka) corresponds to Marine Isotope Stage (MIS) 4. Owen and Dortch (2014) have shown significant evidence for extensive glaciation at 60–75 ka (MIS 4) for the Pamir and Tien Shan, but an absence of glacial ages at this time for the Himalaya. However, erosional processes could easily remove evidence of >30 ka glaciations in the latter region, while such evidence may be preserved more easily in the Pamir and Tien Shan due to very dry conditions (Owen and Dortch, 2014).

Another possible explanation could be the varying glacial response to climate forcing. The western Himalaya, Pamir and Tien Shan are dominated by the mid-latitude westerlies, whereas the rest of the Himalaya is monsoon-dominated. It is likely that glaciation in the Pamir, Tien Shan and western Himalaya is forced by Northern-Hemisphere climate change and is broadly synchronous with oscillations in the Northern-Hemisphere ice sheets (Owen and Dortch, 2014). In contrast, as suggested by numerous researchers, glaciers in other parts of the Himalaya respond to changes in the South Asian monsoon. In particular, a major peak in glacial ages centred around MIS 3 supports the view that glaciers advanced during a time of increased insolation, which helped drive the monsoon influence farther into the orogen, resulting in increased precipitation and cloudiness, and positive glacier mass balances (e.g., Finkel et al., 2003; Owen et al., 2003, 2005, 2006, 2009; Rupper et al., 2009).

As a preliminary conclusion, the morphology of the lake itself is linked to glacial erosion and suggests that it was covered by a cirque-glacier flowing towards the northeast. The occurrence of a cirque glacier at this elevation is consistent with ELA reconstructions from regional studies in the Annapurna massif of central Nepal (e.g. Harper and Humphrey, 2003; Pratt-Sitaula et al., 2011). It appears that Lake Rara was the site of a maximum glacial extent during MIS 4. When the present-day outflow, opposed to the moraine dam, was established remains unclear. A plausible explanation of the flow reversal could be the damming of the pre-existing outlet (3003 m of elevation) by morainic deposits and lake overflow through the low saddle in the northwest (9 m lower than the moraine crest, 3012m).

2.5.2 Suli Gad Valley and Lake Phoksundo

The glacial landforms observed in the Suli Gad Valley (Fig. 2.8), including roches moutonnées (Fig. 2.8c) and fluvial-glacial deposits (Fig. 2.8g, h, i) weathered into characteristic Hoodoos (Fig. 2.8e and f), reflect a dynamic glacial history. The age of these glacial landforms and deposits cannot be established given the absence of samples, but we assume that it coincides with the maximum extent of glaciers in the Lake Phoksundo area. Two geomorphic features suggest a significant glacial imprint on Lake Phoksundo: first, the bathymetry and elongated

nature of the lake (Fig. 2.6), consisting of a flat, deep (135 m) bottom surrounded by steep slopes, suggest it is a glacially carved trough. Second, the base of the outlet dam of the lake is composed of a compact moraine (Figs. 2.9 and 2.10). The outflow from the lake is through a large waterfall cut into the side of this moraine (Fig. 2.9a). However, a major rockslide is also present at the lake outlet (Figs. 2.9 and 2.10), the origin of which, as well as its impact on the lake, are debated. Therefore, the origin of the lake appears complex: the initial glacial lake was likely subsequently affected and enlarged by the massive rockslide. The Phoksundo rockslide is considered as one of the largest rockslides in the Himalaya (Weidinger and Ibetsberger, 2000). Its detritus is covered by loess, in which intercalations of reddish soil layers were dated by radiocarbon dating at ~30–40 ka, from which Yagi (1977) inferred that both the landslide and Lake Phoksundo dated from that time. However, based on two consistent ^{36}Cl ages of 20.9 ± 1.7 ka (Fig. 4), Fort et al. (2013) argue for a single, massive rockslide event of paraglacial origin, fitting with the most recent chronologies of the LGM (Owen, 2006).

Both Weindeinger (2011) and Fort et al. (2013) inferred that this giant rockslide dammed the valley and created the lake (Figs. 2.9 and 2.10). However, neither of these studies discussed the moraines or their chronologies. Based on the field relationships, the moraine was in place before the rockslide and the role of the rockslide was mostly to stabilize the moraine dam and expand the life span of Lake Phoksundo.

As a preliminary conclusion, the origin of Lake Phoksundo dates from (at least) the LGM. The presence of a morainic system and a rockslide deposit allowed the lake to stabilize and last over time. The origin of the giant rockslide may be due to a combination of factors including glacier retreat and significant regional seismicity.

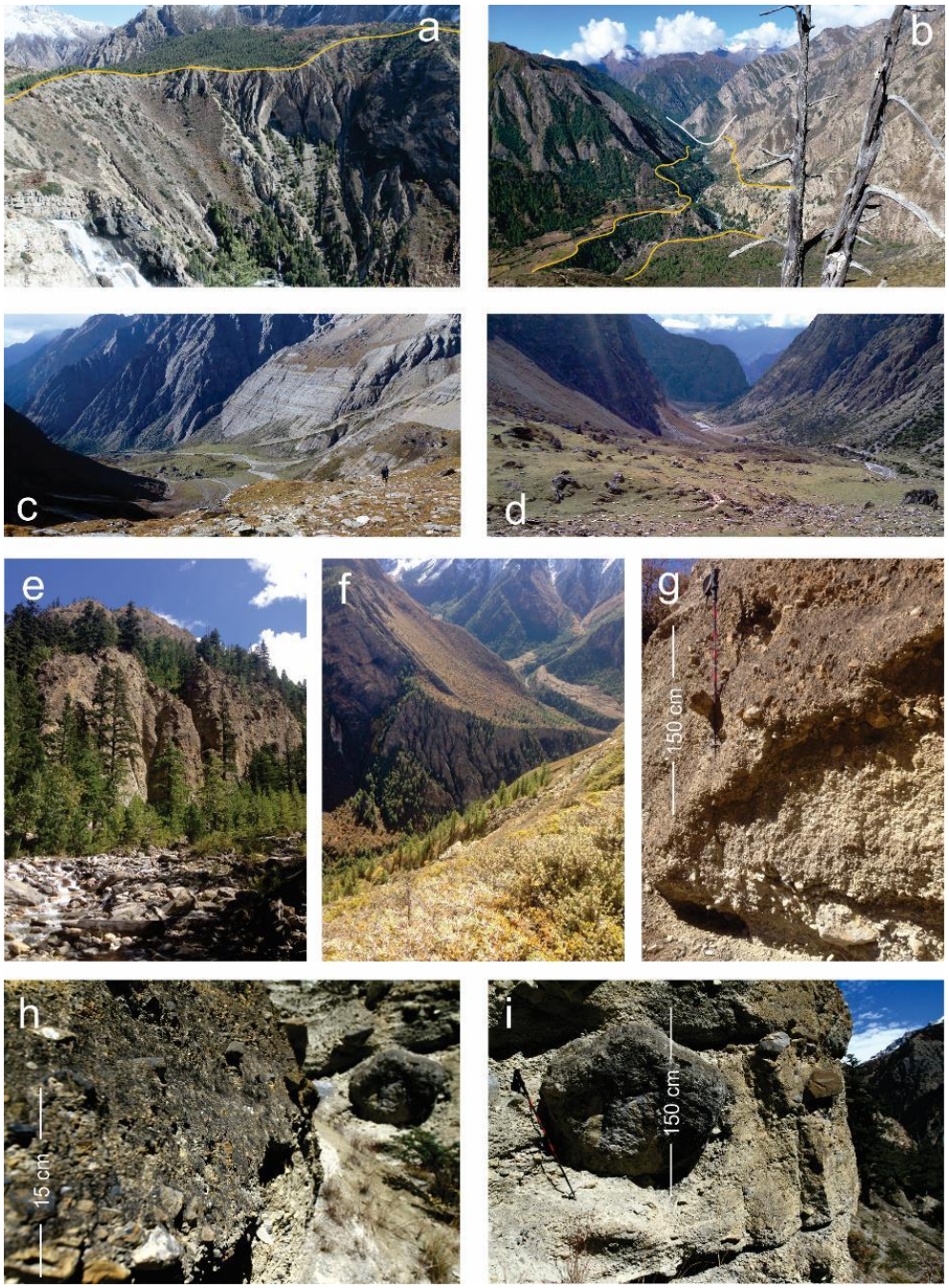

Figure 2.8. Principal glacial landforms encountered in the Suli Gad valley, an unnamed eastern tributary valley to Lake Phoksundo and beneath Lake Phoksundo. (**a**) Suli Gad waterfall and outlet of Lake Phoksundo, the background shows massive glacial deposits covered partly by the rockslide. The yellow line highlights the summit of the glacial deposits (for location see Fig. 4; locality I and Fig. 9; locality A). (**b**) View into the V-shaped Suli Gad valley (white line) and the fluvioglacial deposits (outlined in yellow; locality II in Fig. 4 and C in Fig. 9). (**c**) and (**d**) illustrate the glacially sculpted U-shaped valley indicating the former glacier extent in an eastern tributary valley to Lake Phoksundo (localities III and IV in Fig. 2.4). (**e**) Hoodoos in fluvioglacial deposit in the Suli Gad valley (locality VI in Fig. 2.4). (f) View of the glacial and fluvioglacial deposits of Lake Phoksundo (locality I in Fig. 2.4; A in Fig. 2.9). (**g**) Matrix-supported diamictons of supraglacial tills that comprise a lateral moraine associated with the former Phoksundo glacier, capped by a calcrete crust (locality V in Fig. 2.4; B in Fig. 2.9). (h) Zoom on the calcrete crust capping the lateral moraine of former Phoksundo glacier and cementing gravels (locality V in Fig. 2.4; B in Fig. 2.9). (i) Section within the lateral moraine showing an important glaciofluvial component of the lateral moraine containing metre-sized boulders (locality V in Fig. 2.4; B in Fig. 2.9).

Figure 2.9. Digital Globe imagery illustrating the association of the different glacial landforms and the rockslide around Lake Phoksundo. The white dots with shaded triangles depict the viewpoints of the photos in Figure 2.10. The Green shaded area is the Phoksundo rockslide. The yellow shaded area highlights the complex morainic landforms. We suggest the existence of a glacial knob under the Ringmo till.

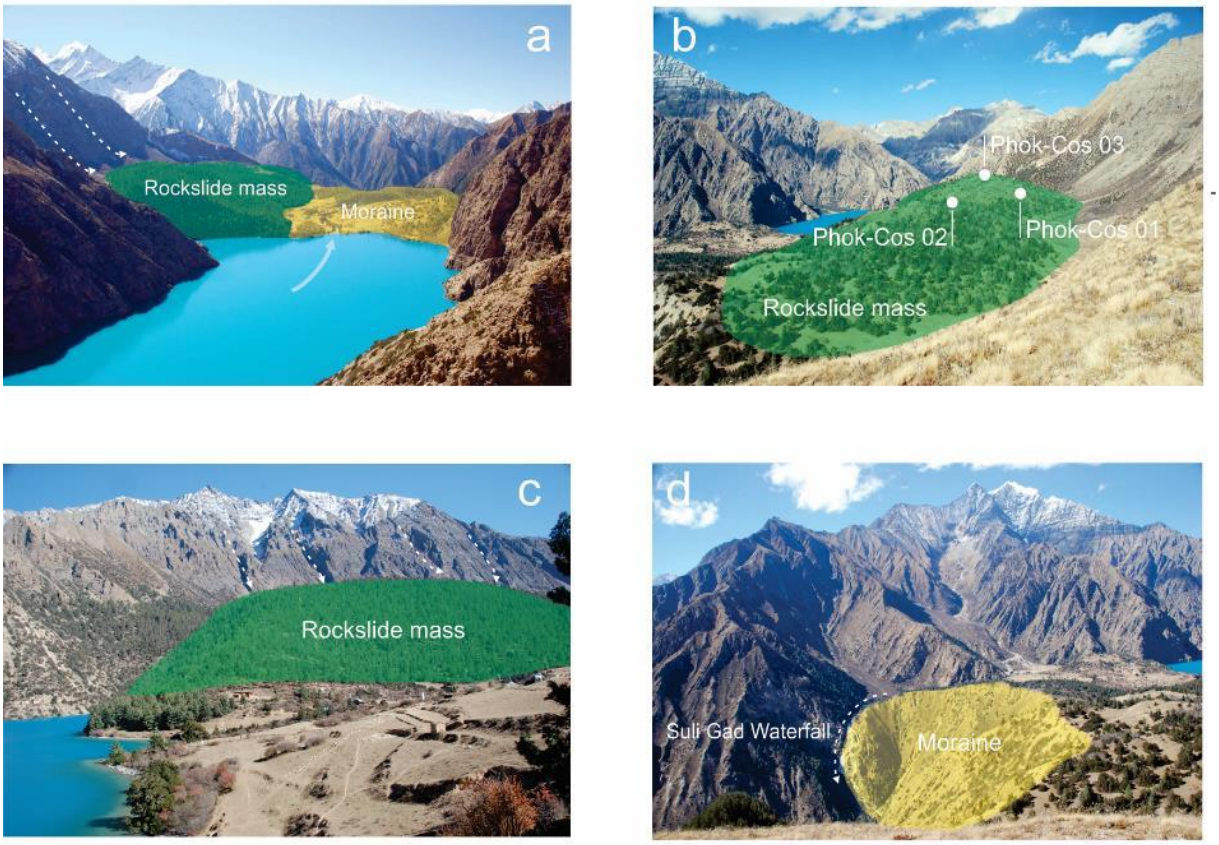

Figure 2.10. Views of Lake Phoksundo, the rockslide and the moraine. (**a**) Shows the interpreted juxtaposition of the rockslide deposits and the moraine. The arrow indicates the outflow direction. (**b**) Another perspective on the rockslide. White dots are the ^{36}Cl sampling locations from Monique Fort. (**c**) and (**d**) show the rockslide and moraine of Lake Phoksundo, respectively.

2.5.3 Bheri Valley

At Khani Gaun, the Bheri valley (Fig. 2.4b) presents finely laminated deposits composed of white sediments, with a thickness of several tens of meters and identified as rhythmic lacustrine deposits (Fig. 2.11a). Distinctive multiple graded laminae are present (Fig. 2.11b) and likely reflect temporal pulses in the inflow (e.g., winter clay layers and summer silty-fine sand deposits; Ashley, 2002). A sharply indented deposit (Fig. 2.11a) possibly indicates a catastrophic rupture of what appears to have been a pro-glacial lake. In this chapter, the term proglacial lake includes all lakes that are or have been under the influence of (i) a glacier ice margin or (ii) subaerial meltwater (for review: Ashley, 2002; Ballantyne, 2002). Pro-glacial lakes can be dammed by ice, moraine, landslide debris or bedrock (Costa and Schuster, 1988). Their evolution and persistence are strongly linked to the nature of the surrounding environment, the climate condition and the glacier dynamics (e.g. Ashley, 2002; Carrivick and Tweed, 2013).

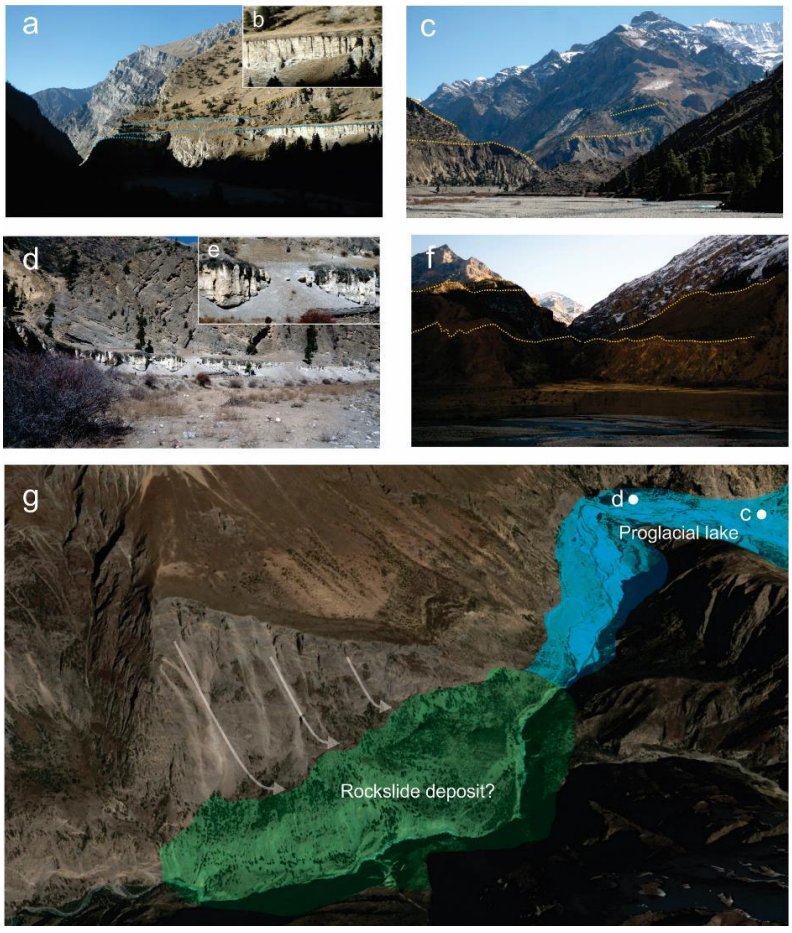

Figure 2.11. Glacial landforms in the Bheri Valley. (**a**) View of the thick rhythmic lacustrine deposits with (**b**) a zoom of the clay lamination (locality VII in Fig. 2.4). (**c**) View of the wide modern alluvial plain and the hummocky moraine landscape.

Several hoodoos are sculpted in the lacustrine sediments. The yellow dashed line represents the limits of different lateral moraines (locality IX in Fig. 2.4). (**d**) Varved lacustrine deposits overlying the alluvial plain with (**e**) a zoom of the clay lamination (localities VIII and IX in Fig. 2.4). (**f**) River terraces developed below the rhytmic lacustrine deposits; the yellow dashed lines represent the limits of different lateral moraines (locality X in Fig. 2.4). (**g**) Interpretational view with the plausible rockslide deposit that should have dammed the valley allowing the development of a proglacial lake and it's characteristic rhythmic deposit.

Close to Kukkot, a number of glacial features (Figs. 2.11 and 2.12), including fluvio-glacial deposits, lake sediments and remnants of hummocky moraines (containing eroded meter-sized boulders) on the hillside of the valley have been preserved. We suggest that they constitute lateral moraine complexes similar to those described from modern glacier settings in the Karakorum (Iturrizaga, 2003). Hence, a series of remnant moraines were encountered at an altitude of about 4000 m (Fig. 2.11), but also a series of lacustrine sediments have been recognized (Fig. 2.11). Within the wide alluvial plain, we found rhythmites deposits on top of a series of alluvial terraces, suggesting that the alluvial plain once hosted a large (possibly pro-glacial) lake. Its origin can only be suspected and linked to the withdrawal of ancient glacial tongues (Figs. 2.11g and 2.13), the rockslide or the moraines would have acted as dams at a minimum elevation of 2690 m. This would imply that glaciers in the Dolpo reached terminal elevations well below 4000 m. Furthermore, glacial landforms are widespread over a considerable horizontal range and occur between 3200 m and 5000 m elevation (Fig. 2.11), in accordance with several other Himalayan studies (e.g. Benn and Owen, 2002; Iturrizaga, 2003). However, we did not identify the damming frontal moraine; therefore, we cannot exclude other plausible hypotheses such as rockslide damming of the lake (Fig. 2.11g).

2.5.4 Reconstruction of the Holocene Equilibrium Line Altitude (ELA)

Our regional reconstruction of the Holocene-ELA was based on the toe-to-headwall altitude ratio (THAR) introduce by Louis in 1955. The satellite imagery allowed us to complement our field survey and to access to the headwall elevation. We used a value of 0.4 for the THAR calculation as suggested by Owen and Benn (2005) in the Himalayan context. By comparing the most recent glacier extension with those in eastern Nepal, it appears that the Holocene ELA for the Suli Gad glaciers was significantly lower (on average 4365 m, see Table 2.2) than the glaciers along the Dhaulagiri ranges (on average 5144 m, see Tab. 2.2). While cautious in view of the biases present in our identification of the ELAs, this difference suggests that the dynamics of these glaciers in response to changing temperature/precipitation were also different, with glaciers around the Bheri valley potentially not as sensitive to climate change as those bordering the Suli Gad valley. Previous studies have suggested that glaciers from the eastern Himalaya, which was more humid throughout the Quaternary glaciations (for review: Qiao and Yi, 2017), tend to be more sensitive to changes in temperature than glaciers in semi-arid areas like the Dolpo (Zech et al., 2013; Hu et al., 2015; Qiao and Yi, 2017). As discussed earlier, the Dhaulagiri range creates a barrier that blocks ISM precipitation, leading to a rain shadow in the Bheri Valley (Bookhagen and Burbank, 2010; Boos and Kuang, 2010; Bothe et al., 2011). The contrast in precipitation due to the rain shadow effect would have driven the Holocene ELA to a higher value on the northern and western slopes in comparison to the southern and eastern slopes (Qiao and Yi, 2017). By comparing our Holocene ELA reconstruction for the Bheri and Suli Gad valleys it appears that the average ELA value are in both cases lower than the recent

estimation made by Qiao and Yi (2017) with an average value for the LIA ELA for the central and western Himalaya reaching 5748 m. Accordingly, we agree with the observations and conclusions of Loibl et al. (2014) and Qiao and Yi (2017) that glaciers appear to advance more extensively on southern and western slopes than on the eastern and northern slopes during the Holocene. As also suggested by both these studies, this would imply that the westerlies intensified around the southern border of the Tibetan Plateau and transported more moisture/precipitation along the central and western Himalaya.

Mountain	Abbreviation	Valley	Latitude (N°)	Longitude (E°)	Toe altitude (m asl)	Headwall altitude (m asl)	LIA ELA (m asl)
Unnamed I	UI	Bheri	28.82132	83.08673	3839	5556	4526
Unnamed II	UII	Bheri	28.80823	83.80823	4657	5767	5101
Unnamed III	UIII	Bheri	28.79763	83.08424	4669	5712	5086
Unnamed IV	UIV	Bheri	28.78268	83.08157	4669	5690	5077
Unnamed V	UV	Bheri	28.75409	83.10264	4669	6279	5313
Unnamed VI	UVI	Bheri	28.74679	83.12922	4178	6361	5051
Unnamed VII	UVII	Bheri	28.73401	83.35694	4426	7514	5661
Putha Hiunchuli	PH	Bheri	28.74788	83.14599	4574	7197	5623
Churen Himal	CH	Bheri	28.74605	83.23574	3964	7330	5418
Dolpo Himal I	DI	Bheri	28.97984	83.18154	4129	6107	4920
Dolpo Himal II	DII	Bheri	28.97984	83.18154	4394	6107	5079
Dolpo Himal III	DIII	Bheri	28.97984	83.18154	4393	5597	4875
Phoksundo Himal	PH	Suli Gad	29.20744	82.90001	3646	5766	4494
Kanjeralwa I	KI	Suli Gad	29.21154	82.88964	3672	5061	4228
Kanjeralwa II	KII	Suli Gad	29.22102	82.88907	3694	5097	4255
Kanjeralwa III	KIII	Suli Gad	29.23261	82.87400	3694	5293	4334
Kanjeralwa IV	KIV	Suli Gad	29.23261	82.87400	3693	5746	4514

Table 2.2. Reconstructed ELAs of Holocene advances for glaciers in the Bheri and Suli Gad valleys based on the THAR method.

2.5.5 Reconstruction of the maximum glacial extension

Our reconstruction of maximum glacier extent during the Quaternary, based on the observation of lateral moraines, suggests minimum altitudinal values of inferred maximum glacier extension of about 2690 m for the Bheri valley and ~2730 m for the Suli Gad valley. On average, the observed remnant moraines lie just below 4000 m in the main alluvial plain of the Suli Gad and Bheri valleys. As lateral moraines are deposited below the ELAs, those values support our

conclusion on our Holocene ELA reconstruction, suggesting that the paleo-ELAs for the Suli Gad and Bheri valley must have been significantly lower than inferred from previous LIA-ELA Himalayan studies (e.g. Benn and Owen, 2002; Iturrizaga, 2003; Pratt-Sitaula et al., 2011; Qiao and Yi, 2017).

In order to test this prediction, we have attempted to delineate the maximum extent of glaciation over the Quaternary using satellite imagery, focusing in particular on proglacial and cirque lakes as markers of glaciations (Fig. 2.13). Such lakes are found at altitudes ranging from 2700 to ~4300 m in western Nepal, and appear to occur relatively frequently on the relict landscapes previously described by Harvey et al. (2015). These relict landscapes would be subject to relatively low erosion and uplift rates, potentially promoting preservation of these landforms. By mapping the occurrence of moraines as well as proglacial and cirque lakes, we have been able to approximately reconstruct the maximum impact zone of glaciations for different areas in western Nepal (i.e. Mugu District, Bheri and Suli Gad valleys). Our results suggest that this impact zone was more extended to the south than previously assumed, reaching the latitude N28°57' at the most widespread glacial Quaternary extent. In addition, glacial landforms believed to be relics of the maximum glacial extension where found at elevations of around 2700 m in the Bheri and Suli Gad valleys. Those observations would suggest that the maximal extension of glaciers was more significant than commonly accepted.

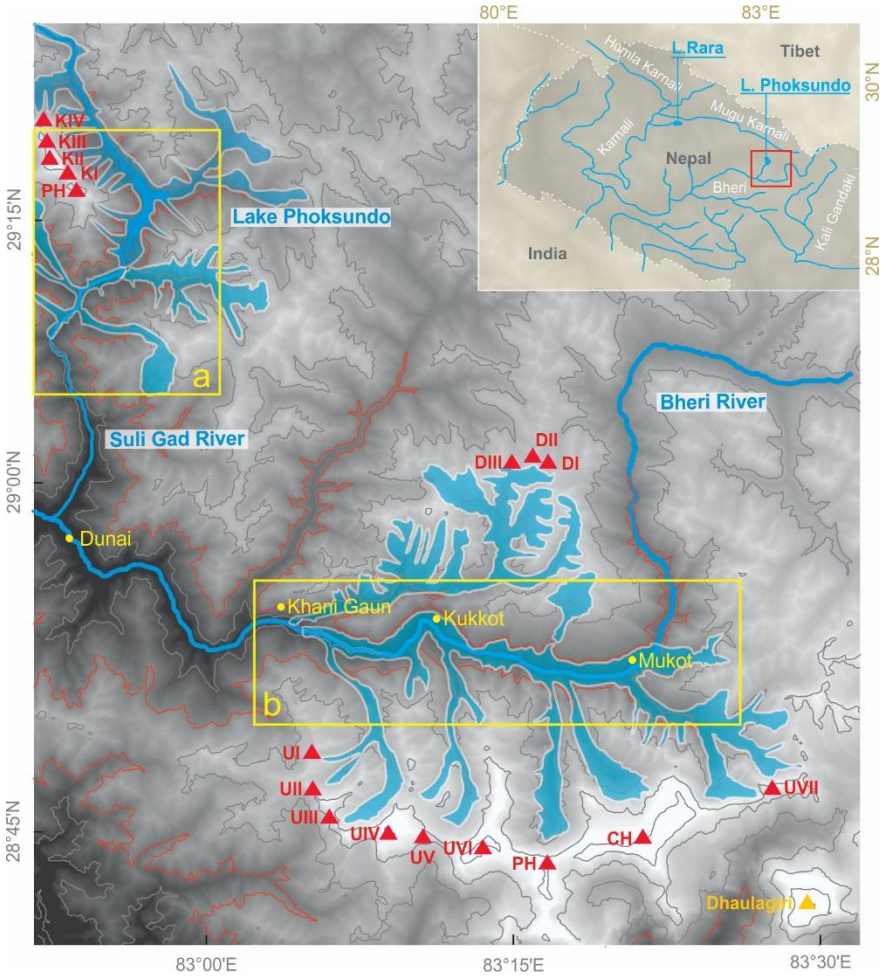

Figure 2.12. Holocene-ELA reconstruction based on satellite images and our field observations. ASTER digital terrain model of the Suli Gad valley, Lake Phoksundo and the Bheri valley. (**a**) Suli Gad valley and Lake Phoksundo. (**b**) Bheri valley. The red triangles with abbreviations and romans number illustrate the summit of the related glacier used for our Holocene ELA reconstruction. Yellow dots are the main villages of the area. White lines are 1000-m contour lines; the red contour marks 4000 m elevation. The shaded blue areas depict the reconstructed maximum glacial extension.

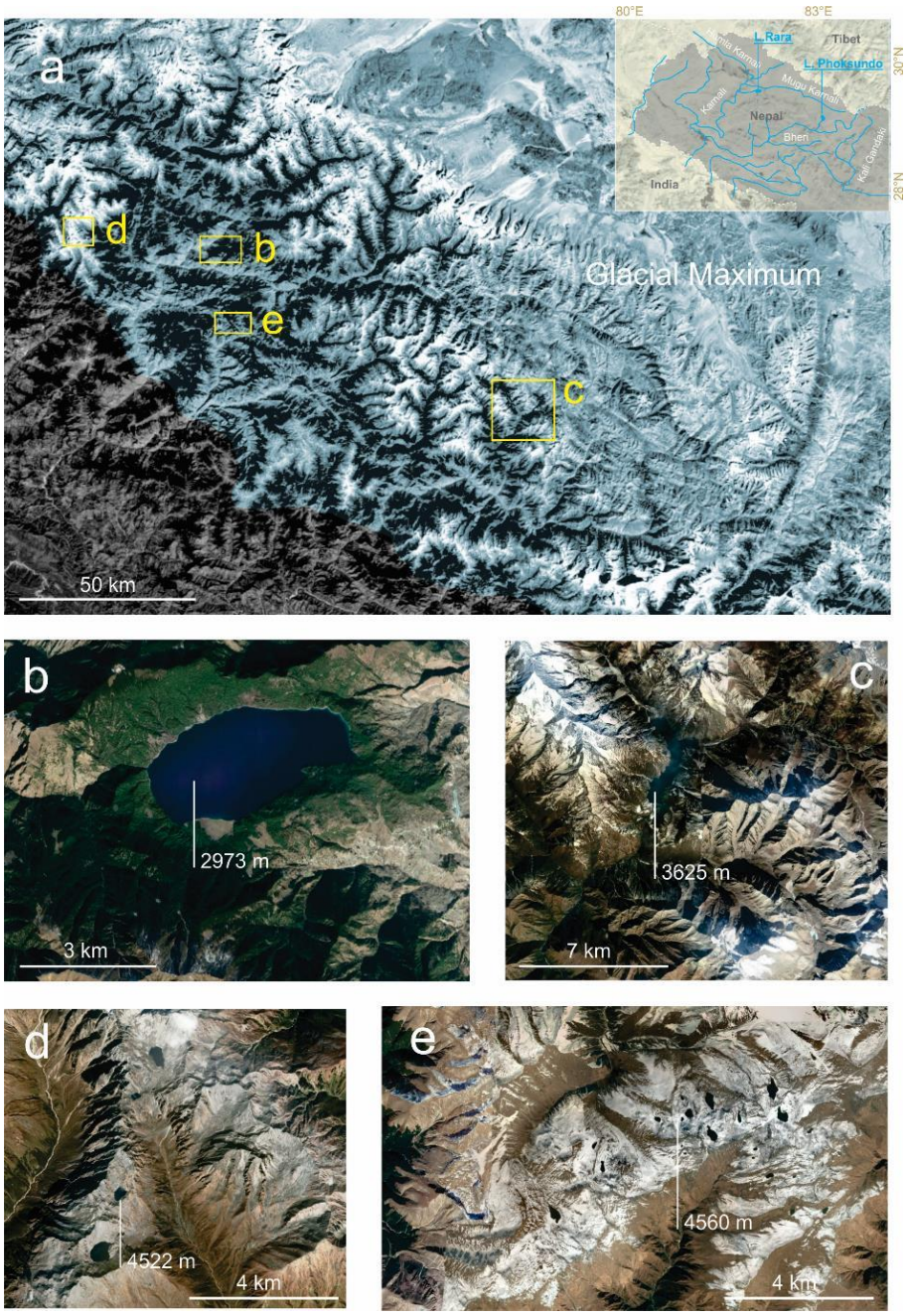

Figure 2.13. Maximum glacier extension based on occurrence of proglacial and cirque lakes. (**a**) Maximum glacially impacted area in shaded blue. NB: This representation of the area impacted by the maximum glacial extension does not mean that the area was covered by an extended ice cap. (**b**), (**c**), (**d**) and (**e**) are images of different lakes. The existence of proglacial and cirque lakes is directly related to the presence of glaciers and can thus serve as a marker of glacial extension. (**b**) and (**c**) are respectively Lakes Rara and Phoksundo.

2.6 Conclusions

The glacial dynamics of western Nepal through the Quaternary have been affected by fluctuations in the Northern Hemisphere climate system through a shift of intensity in the westerlies and the monsoon. Our new ^{10}Be dates suggest that the traces of glaciations at Lake Rara date back to at least MIS 4, while further east, in Phoksundo, the Suli Gad and Bheri valleys, the sparse chronological correlation suggests an LGM age. The extension of glaciers had a lasting effect on the landscape, both directly and possibly indirectly via the generation of rockslides, the origin of which may lie in a combination of climatic and structural factors. The development of two of Nepal's largest lakes, Lakes Rara and Phoksundo, appears to be directly controlled by glacial activity. Our estimate of the maximum glacial extent is at odds with earlier studies (e.g. Fanzel, 1960; Shi et al, 1992; Fig. 2.1) and appears to support the view of a larger extension (but not of an extended ice cap) put forward originally by Klute (1930) and Kuhle (1985; Fig. 2.1). This preliminary study opens up new avenues for on-site research and investigation to complement our observations and allow for a more robust discussion in the future.

Chapter 3

Large post-1505 AD earthquakes in western Nepal revealed by a new lake sediment record

Z. Ghazoui [1,2], S. Bertrand [2], K. Vanneste [3], Y. Yokoyama [4], J. Nomade [1], A.P. Gajurel [5], P.A. van der Beek [1]

[1] ISTerre, Institut des Sciences de la Terre, Université Grenoble Alpes, Grenoble, France.
[2] Department of Geology, Ghent University, Ghent, Belgium.
[3] Royal Observatory of Belgium, Department of Seismology and Gravimetry, Brussels, Belgium.
[4] Atmosphere and Ocean Research Institute, The University of Tokyo, Chiba, Japan.
[5] Department of Geology, Tribhuvan University, Kathmandu, Nepal.

In final revision in *Nature Communications*

According to historical archives and paleoseismological studies, the last earthquake that ruptured the Main Frontal Thrust in western Nepal occurred in 1505 AD. No evidence of large earthquakes has been documented since, giving rise to the concept of a seismic gap in western Nepal and adjacent areas in northern India. Here, we report on a new record of earthquake-triggered turbidites from Lake Rara, western Nepal. Our lake-sediment record contains eight earthquake-triggered turbidites during the last 800 years, and it registered all three previously reported $M_w \geq 7$ events in western Nepal (1165-1400 AD, 1505 AD and 1916 AD). Modelling of shaking intensity, together with the instrumental record, shows that even near-field earthquakes should have a magnitude $M_w > \sim 6.5$ to trigger turbidites in the lake. The five previously undocumented post-1505 AD earthquakes imply that western Nepal is as seismically active as central Nepal and call for a revaluation of the risk of a major earthquake affecting western Nepal and northern India.

3.1 Introduction

The Himalayan collision, in which India underthrusts below Tibet and the Himalaya along a major crustal detachment known as the Main Himalayan Thrust (MHT), regularly produces major destructive earthquakes, as elastic deformation accumulated during underthrusting of the Indian Plate is released periodically by slip along the MHT fault plane (Bilham et al., 2001; Avouac, 2003; Feldl and Bilham, 2006; Mugnier et al., 2013). The destructive 2015 M_w 7.8 Gorkha earthquake (Avouac et al., 2015; Hayes et al., 2015) represented an intermediate-size event in this process as it ruptured only the lower, northern part of the MHT without breaking through to the surface (Mugnier et al., 2013; Avouac et al., 2015). Evaluation of seismic hazard in the Himalaya has been based on the comparison of geodetic strain rates with the amount of seismic moment release, measured by instrumental seismicity and inferred from paleoseismology (Bilham et al., 2001; Stevens and Avouac, 2016). Whereas historical seismicity and trenching studies record at least four, and possibly up to eight, major earthquakes over the last 800 years in central and eastern Nepal (Bollinger et al., 2016), the last known major event to have affected western Nepal and northern India, rupturing a long portion of the Main Frontal Thrust (MFT), was the M_S ~8.2 earthquake of 1505 AD (Fig. 3.1; Kumar et al., 2006; Yule et al., 2006). The intervening 500 years have resulted in the accumulation of a >10 m slip deficit along this segment of the MHT, leading to the concept of a seismic gap in western Nepal and adjacent areas in northern India, which could potentially trigger a great earthquake in the near future (Bilham et al., 2001; Rajendran and Rajendran, 2015; Stevens and Avouac, 2016).

However, both historical and paleoseismic records of earthquakes are inherently incomplete (Ambraseys and Jackson, 2003; Bilham, 2004; Bollinger et al., 2016) and the age, extent, and correlation of surface ruptures inferred from paleoseismic trenching studies in the central Himalaya are the subject of significant controversy (Hayes et al., 2015; Bollinger et al., 2016; Lavé et al., 2005; Sapkota et al., 2012; Pierce and Wesnousky, 2016; Wesnousky et al., 2018).

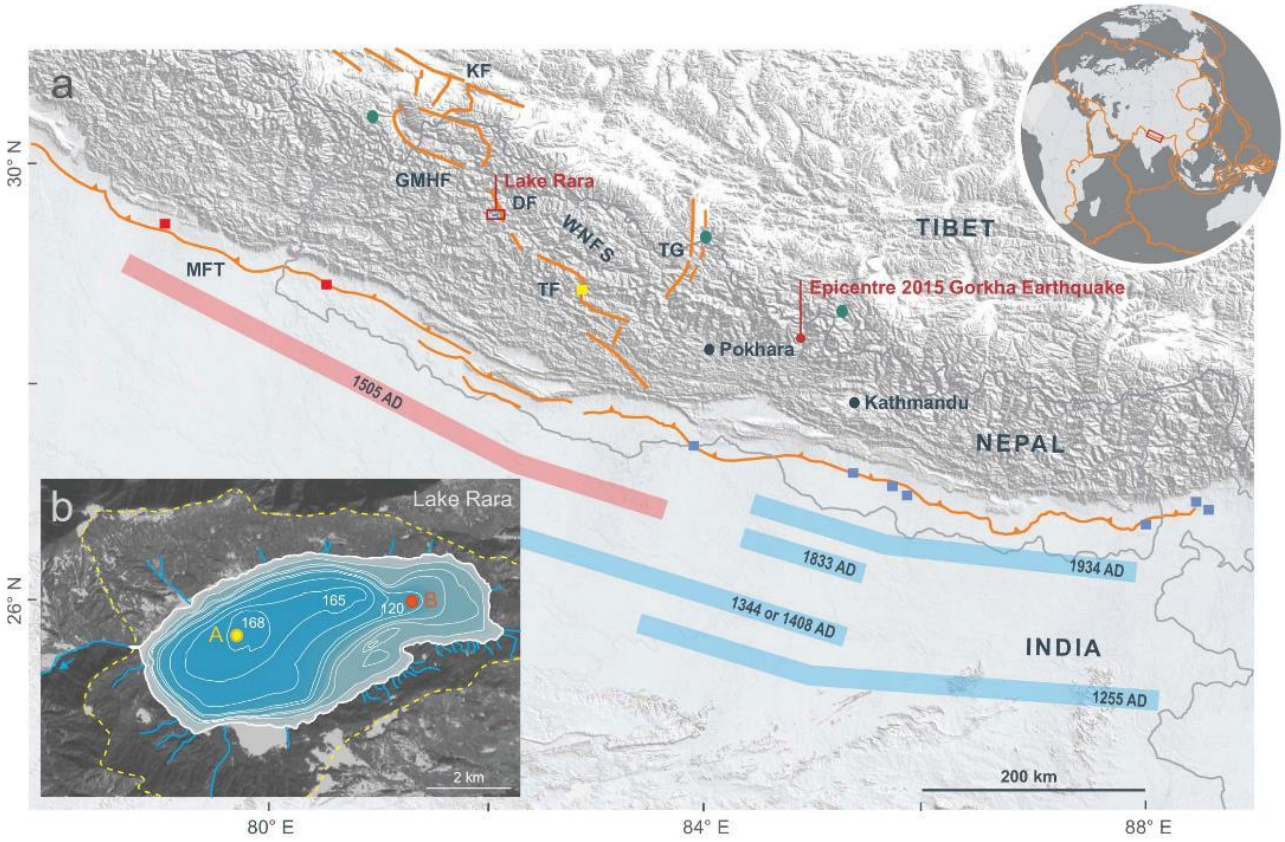

Figure 3.1. Geomorphic and seismotectonic setting of Lake Rara. (**a**) Digital terrain model of the central Himalaya, showing active faults (Murphy et al., 2014; Taylor et al.,2009) and inferred rupture lengths of historical earthquakes (dates as indicated). Squares indicate paleoseismological trenching sites, in red for the great 1505 AD earthquake, in yellow for the Tibrikot earthquake and in blue for central Nepal earthquakes (see main text for references). Green dots are locations for which historical chronicles record destruction during the 1505 AD earthquake (Jackson, 2002). Active faults are: KF - Karakoram Fault; MFT - Main Frontal Thrust; TG - Thakkola Graben; WNFS - Western Nepal Fault System (composed in part by: DF - Dharma Fault; GMHF - Gurla Mandhata-Humla Fault system; TF - Tibrikot Fault). The red rectangle shows the location of Lake Rara (inset **b**). (**b**) Bathymetric map of Lake Rara (from Okino and Satoh, 1986 and our own measurements) showing the sampling sites A and B, overlain on a satellite image of the lake catchment (outlined by yellow dashed line, the full catchment is shown in Supplementary Fig. 1).

Historical written archives in western Nepal are limited due to several factors. For the period prior to the 20th century, references to earthquakes in western Nepal and the northern Himalaya are scattered throughout Tibetan literature and, until the mid-20th century, access to Tibet and Tibetan documents was extremely restricted to foreign researchers (Ambraseys and Jackson, 2003). Moreover, translation and interpretation of traditional references to earthquakes is complicated by the religious undertone in the Tibetan hagiographic literature (Ambraseys and Jackson, 2003). In addition, western Nepal has always been much less densely populated than central Nepal, lacking major urban centres (such as Kathmandu, Pokhara or Gorkha) and it was virtually inaccessible to foreign researchers during the Nepal civil war of 1996-2006. Furthermore, seismic activity based on written archives is exclusively evaluated in terms of macroseismic effects and is subject to misinterpretations (Ambraseys and Jackson, 2003) as the vulnerability of buildings exposed to earthquakes varies greatly in the Himalayan region depending on the type of architecture. In particular, traditional timber-laced buildings common

to the western Himalaya (including western but not central Nepal; Rai and Murty, 2006; Langenbach, 2016) have proven their ability to resist earthquake loading much better than modern structures, but their exceptional resistance is not taken into account in any of the intensity scales (Ambraseys and Jackson, 2003; Rai and Murty, 2006; Langenbach, 2016).

Trench-based paleoseismic records are rendered equivocal by the strong vegetation cover and erosional activity of the Himalayan front, leading to poor access and preservation potential of fault scarps. Furthermore, the unknown and variable age inheritance in the charcoals used for radiocarbon dating of observed surface ruptures, i.e. the time lapse between charcoal formation and its incorporation in the sediments from which it is sampled (Frueh and Lancaster, 2014), may lead to significant overestimation of the ages of seismic events (Bollinger et al., 2016).

Finally, trenches on the Himalayan front only record surface-breaking earthquakes. However, not all earthquakes produce slip that reaches the surface (e.g., the 2015 M_w 7.8 Gorkha earthquake; Avouac et al., 2015; Hayes et al., 2015) and, therefore, would be detected from trenches. Moreover, while some ruptures reach the surface at the MFT, producing fault escarpments or fault-related folds, others (e.g., the 2005 M_w 7.6 Kashmir earthquake; Mugnier et al., 2013) reach the surface through out-of-sequence thrusting.

Compared to the historical and terrestrial archives discussed above, lake sediments may provide a complementary and more continuous paleoseismic record, as earthquake-triggered slope failures and surficial sediment remobilization form turbidite deposits (Strasser et al., 2006; Howarth et al., 2014; Moernaut et al., 2014; Wilhelm et al., 2016; Kremer et al., 2017; Monecke et al., 2004; Moernaut et al., 2017). In spite of their potential to complement the paleoseismic inventory, lake records have hitherto not been investigated in the Himalaya.

In order to reconstruct past earthquake activity in the inferred seismic gap, we collected three short sediment cores from Lake Rara in western Nepal (29°32'N, 82°05'E; Fig.3.1; Supplementary Fig. 3.1). We cored two sites within the lake, in the deepest basin at water depths of 168 m (site A) and in the shallower northeastern arm of the main basin at 120 m depth (site B), using a gravity corer operated from an inflatable dingy (Fig. 3.1). The cores were analysed using X-ray Computerized Tomography (CT), X-ray Fluorescence (XRF) core scanning, logging of physical properties, bulk organic geochemistry, and high-resolution grain-size measurements (Fig. 2; Supplementary Figs. 3.2, 3.3; see Methods). Chronology was established on cores RA14-SC05 and RA14-SC06 by combining radionuclide (^{210}Pb and ^{137}Cs) and radiocarbon (^{14}C) dating (Supplementary Fig. 3.4, Supplementary Tables 3.1–3.3). Radiocarbon dating was performed on terrestrial leaf material and thus does not suffer from age inheritance.

3.2 Results.

The cored sediments are mainly composed of mud, interrupted by 10–25 mm thick, dense, magnetic and Ti-rich micaceous sandy silt layers (Fig. 3.2), which are characterized and differentiated on the basis of variations in mean grain size, magnetic susceptibility, Ti concentration, C/N ratios and radio-density (see Methods). As their distinctive signatures on

the magnetic susceptibility and XRF profiles clearly contrast with the homogeneous muddy background, these fining-upward deposits were readily identified as turbidites (see Supplementary text). Up to eight of these deposits were identified in the cores; they are most clearly represented in core RA14-SC05 (Fig. 3.2; Supplementary Fig. 3.2). Age-depth models (Supplementary Fig. 3.4; Methods) show that sedimentation rates are ~0.4 mm/yr at site A, located in the deepest part of the lake (168 m), and approximately half that at site B. Both the lake physiography and the sedimentation rates at site A favour the ability of this site to record a complete event history (Moernaut et al., 2014; Wilhelm et al., 2016); we therefore focus here on the interpretation of core RA14-SC05.

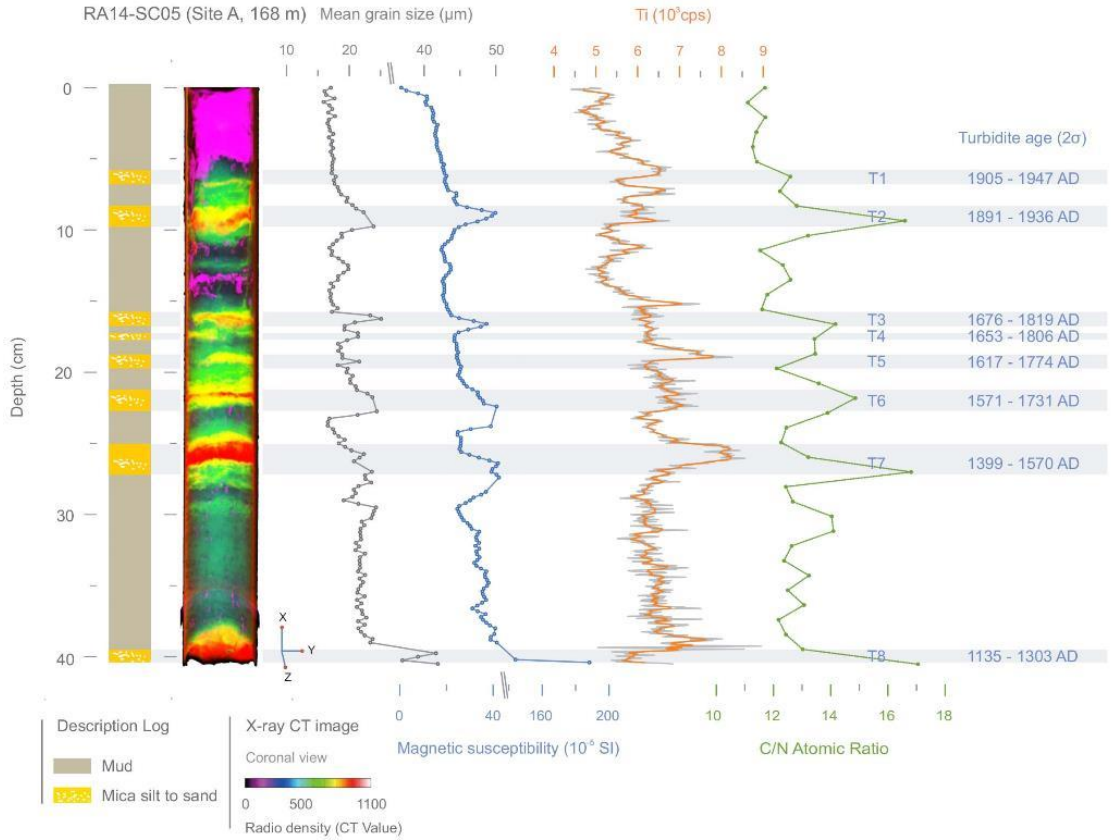

Figure 3.2. Sediment core RA14-SC05. From left to right are shown: a synthetic log, 3D coronal view of computed X-ray tomography images in pseudo-colour, mean grain size, magnetic susceptibility, Itrax XRF Ti profile (grey curve: raw data; orange curve: 5 pt-weighted average) and carbon to nitrogen (C/N) atomic ratio. These five parameters were used to identify turbidites T1 to T8. Their ages were extracted from the age-depth model (see Methods).

3.3 Discussion.

Origin of turbidites. Turbidites within lake sediments can be triggered by various processes such as floods, landslides, spontaneous slope failures, or earthquakes (see Supplementary text). The small size, limited hydrographic system (streams entering the lake are typically less than 30 cm wide and 15 cm deep), and relatively low relief of the Lake Rara catchment (Fig. 3.1, Supplementary Fig. 3.1) render floods and landslides unlikely triggering mechanisms. This inference is consistent with the very low sedimentation rates measured at the shallowest site RA14-SC06 (~0.2 mm/yr), which reflects the low hydrodynamic activity in the catchment of

Lake Rara, and render spontaneous slope failures also unlikely. Hence, the turbidites identified in the sediments of Lake Rara most likely represent either earthquake-triggered slope failures or earthquake-triggered remobilization of surficial lake sediments. This interpretation is supported by their C/N ratios, which range between 13 and 17 (Fig. 3.2), reflecting a mixture of organic matter of aquatic (C/N <8) and terrestrial (C/N >20) origin (Howarth et al., 2014). Although the absolute values depend on grain size (Supplementary Fig. 3.3), these results suggest that the turbidites originated from the reworking of sediment previously deposited on shallower parts of the slopes within the lake, where C/N values are slightly higher than in the centre of the lake due to continuous input of terrestrial organic matter from the catchment. Flood or landslide-triggered turbidites, in contrast, would have a purely terrestrial C/N signature.

The strongest argument for attributing an earthquake origin to lake turbidites is a temporal correlation with known historical events (Howarth et al., 2014; Moernaut et al., 2014; Monecke et al., 2004). A good starting point for this correlation is the great 1505 AD earthquake. Historical records describe widespread devastation in western Nepal, northern India and southern Tibet (Fig. 1), from which a magnitude M_s=8.2 has been estimated (Ambraseys and Jackson, 2003). Surface ruptures on the MFT immediately south and southwest of Lake Rara have been attributed to the 1505 event (Kumar et al., 2006; Yule et al., 2006). This earthquake therefore seems an obvious candidate to have triggered slope failures within Lake Rara. We interpret turbidite T7 in core RA14-SC05 (1399–1570 AD) as representing the 1505 AD earthquake. This is the most prominent event deposit; it can be correlated to turbidite TA in core RA14-SC06 from site B based on the independent age models (Supplementary Figs. 3.4, 3.5), and it is present in all three cores (Supplementary Fig. 3.2). Another known earthquake that affected the region of Lake Rara is the 1916 Dharchula earthquake (Szeliga et al., 2010). The ages of the two topmost turbidites in our record (T1 and T2; Fig. 2; Supplementary Fig. 3.4) both overlap with this earthquake, with the weighted-mean age of T2 (1917) being very close to it. Therefore, it appears likely that the 1916 earthquake triggered T1 or T2, but the age overlap between these does not allow us to pick one or the other (Supplementary Fig. 3.4). The association of these two turbidites with known earthquakes confirms the seismic nature of the lake turbidites recorded in Lake Rara. The others (Fig. 3.2) most likely represent previously undocumented earthquakes.

Earthquake turbidite-triggering threshold. Observations in lakes worldwide suggest that earthquake-triggered turbidites can originate either from subaqueous slope failures or from surficial sediment remobilisation, when local shaking exceeds Modified Mercalli Intensities (MMI) 6–7 and 6, respectively (Strasser et al., 2006; Howarth et al., 2014; Moernaut et al., 2014; Wilhelm et al., 2016; Monecke et al., 2004; Moernaut et al., 2017). In order to predict shaking intensity and constrain the local earthquake turbidite-triggering threshold (E_QTT; Wilhelm et al., 2016) for Lake Rara, we produced MMI shaking maps for several historical and instrumental events (Fig. 3.3) based on a set of Intensity-Prediction Equations (IPEs: Allen et al., 2012; Ambraseys and Douglas, 2004; Szeliga et al., 2010; Bakun and Wentworth, 1997; Atkinson and Wald, 2007; Ghosh and Mahajan, 2013; see Methods).

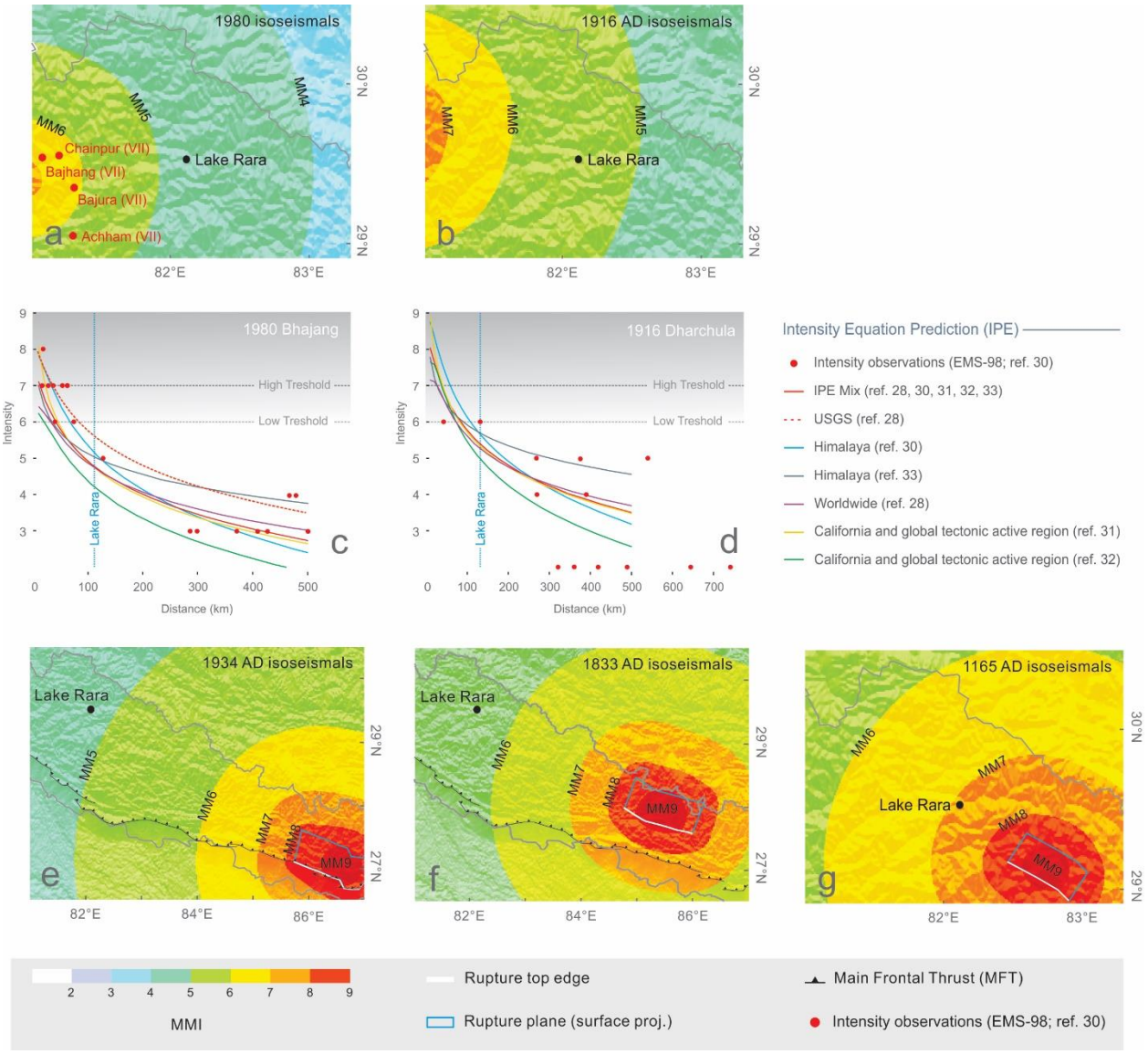

Figure 3.3. Modified Mercalli Intensity (MMI) isoseismals modelled for historical and instrumental earthquakes in central/western Nepal, and plots of observed and predicted intensity versus distance. (**a**, **b**) Modelled isoseismals and observed intensities for earthquakes in western Nepal; (**a**) instrumental 1980 (MHT?) Bhajang earthquake (M_w 6.5; intensity observations from Szeliga et al, 2010 (ref. 30) in map region are indicated), (**b**) instrumental 1916 (MHT?) Dharchula earthquake (M_w ~7.2; no intensity observations in map region). (**c**, **d**) Plots of observed and predicted intensity versus distance for the 1980 Bhajang (**c**) and 1916 Dharchula (**d**) earthquakes, respectively. The vertical blue line corresponds to the epicentral distance of Lake Rara; the dashed grey lines indicate the lower and upper bounds of a generally accepted earthquake turbidite-triggering threshold. Red dots are observed intensities (Szeliga et al, 2010; ref. 30), coloured lines show predicted intensity versus distance according to the different IPEs (ref. 28, Allen et al., 2012; ref. 30, Szeliga et al., 2010; ref. 31, Bakun and Wentworth, 1997; ref. 32, Atkinson and Wald, 2007; ref. 33, Ghosh and Mahajan, 2013) and our average. Also shown is USGS Shakemap fit for the 1980 Bhajang earthquake (see Methods for discussion). (**e**, **f** and **g**) Modelled isoseismals for historical earthquakes in central/western Nepal; (e) 1934 AD MHT earthquake (M_w 8.4), (**f**) 1833 AD MHT earthquake (M_w 7.8) and (**e**) 1165-1400 AD Tibrikot Fault (part of the WNFS) earthquake (M_w ~7.9) The surface projection of the rupture plane is represented by the grey rectangle; the top edge of the rupture is shown by a solid white line. Rupture scenarios for (**e**) and (**f**) are from Hubbard et al., 2016; for (**g**) from Murphy et al., 2014. The location of Lake Rara is indicated by a black dot.

The E_QTT for Lake Rara was estimated using two instrumental earthquakes; the 1980 Bajhang and 1916 Dharchula earthquakes. The most recent update of the ISC-GEM catalogue (Storchak et al., 2013) reassessed the location and magnitude of the M_w≈7.0–7.2 1916 Dharchula earthquake (Szeliga et al., 2010; Storchak et al., 2013) at an epicentral distance of ~130 km from Lake Rara (29.730°N 80.745°E; Supplementary Fig. 3.8). As discussed above, this earthquake can be correlated to T1 or T2 in the sediments of Lake Rara. At some 30 km east of Dharchula, the 1980 Bajhang earthquake (Storchak et al., 2013) constitutes the largest instrumental earthquake (M_w 6.5; Supplementary Fig. 3.8) recorded in western Nepal over the last half-century, but its age is much younger than the most recent turbidite T1 in Lake Rara (Fig. 3.2) and we infer that this earthquake did not trigger slope failure or surficial sediment remobilization in the lake. The E_QTT for Lake Rara should therefore lie between the shaking intensities felt at the lake for these two earthquakes. Mean shaking intensities obtained with our IPE selection suggest that the E_QTT is situated between MMI ~4.5 and MMI ~5.5 (Figs. 3.3a and b. However, comparison with observed intensities for the 1980 Bajhang earthquake (Szeliga et al., 2010) implies that our modelled near-field intensities may underestimate actual intensities by a half to one unit (see Methods; Figs. 3.3c and d). Hence, with the available data and the associated uncertainties, we cannot tightly constrain the E_QTT for Lake Rara, although a value close to the lower bound of the range reported in literature is likely. In the following, we will therefore use the conservative E_QTT estimate of MMI ≥6.

Possible correlation with other historical earthquakes. Attributing T1 or T2 to the M_w≈7.0–7.2 1916 Dharchula earthquake and turbidite T7 to the 1505 event implies that five other post-1505 AD events are recorded in Lake Rara sediments (Fig. 3.2), some of which may correspond to known events that occurred in Nepal or northern India during the last two centuries. In particular, the 1833/08/26 and 1934/01/15 earthquakes affecting central and eastern Nepal are well documented and surface ruptures on the MFT were attributed to the latter event(Bollinger et al., 2016; Bilham et al., 2004; Sapkota et al., 2012; Ambraseys and Douglas, 2004), although this interpretation has recently been questioned (Wesnousky et al., 2018). Both earthquakes ruptured the MHT east of Kathmandu and have been attributed moment magnitudes M_w≈7.3–7.7 and 8.1–8.4, respectively (Bollinger et al., 2016; Ambraseys and Douglas, 2004; Szeliga et al., 2010). Published isoseismals for these earthquakes vary significantly but in most of these, Lake Rara lies outside the MMI=6 isoseismal (Sapkota et al., 2012; Ambraseys and Douglas, 2004; Szeliga et al., 2010). We have modelled the isoseimals for both earthquakes using the rupture planes and magnitudes inferred by Hubbard et al. (2016), to confirm that Lake Rara lies outside the MMI=6 isoseismals (Fig. 3.3, Supplementary Fig. 3.6). For the 1934 earthquake, modelled intensities at the lake are MMI<5, whereas they are 5<MMI<6 for the 1833 earthquake. For this far-field earthquake, our predicted intensities correspond much better to the observed intensities than for the near-field earthquakes discussed above. We thus conclude that these modelled intensities are reasonable and that neither of these events is likely to have generated a turbidite in the lake. Likewise, the 1803/09/01 Kumaon earthquake has been attributed a magnitude M_w≈7.3–7.5 (Ambraseys and Douglas, 2004; Szeliga et al., 2010). Published isoseismals (Supplementary Fig. 3.7) suggest an intensity of IV (MSK) for Lake Rara (Ambraseys and Douglas, 2004), which is clearly insufficient to trigger a turbidite.

The Lake Rara sediment record also includes at least one medieval earthquake (T8 in core RA14-SC05; Fig. 3.2, Supplementary Fig. 3.4). Although two or three great medieval earthquakes were inferred from paleoseismic trenches in Nepal, of which the historic 1255 earthquake has attracted most attention, their exact magnitude and extent of slip remain controversial (Bollinger et al., 2016; Lavé et al., 2005; Sapkota et al., 2012; Pierce and Wesnousky, 2018). Surface ruptures attributed to the 1255 earthquake have recently been documented from locations to the south and southwest of Kathmandu (Wesnousky et al., 2017). However, given the apparent similarity of the 1255 and 1934 events (Bollinger et al., 2016; Hubbard et al., 2016), we consider it unlikely that T8 was triggered by the 1255 AD earthquake.

The Western Nepal Fault System (WNFS) has been recognised as an active trans-tensional fault system that accommodates oblique convergence in the western central Himalaya and connects to the Karakorum Fault (Fig. 3.1; Murphy et al., 2014; Silver et al., 2015). Although the activity of this system cannot be resolved from geodetic data (Jouanne et al., 2017), it presents features that are diagnostic of active faulting. In particular, a surface-rupturing event has been documented on the Tibrikot Fault (Fig. 3.1), tentatively dated between 1165–1400 AD and attributed to an $M_w \approx 7.9$ earthquake (Murphy et al., 2014). Our modelling shows that Lake Rara is within the MMI=7 isoseismal for this rupture scenario (Fig. 3.3e). We therefore suggest that turbidite T8 (1135–1303 AD) records seismic shaking associated with the Tibrikot earthquake (Murphy et al., 2014).

Significance of previously unknown events. Overall, five turbidites post-dating the great 1505 earthquake cannot be attributed to any previously described earthquake (Fig. 3.4). To evaluate whether or not background seismicity ($M_w < 5.6$) could have triggered these turbidites, we consider all earthquakes reported by the USGS within a radius of 20 km of Lake Rara between 1974-2018, the period during which the USGS catalogue is considered complete. Our search yielded 11 earthquakes with M_w ranging from 4 to 5.6, none of which is recorded as a turbidite in Lake Rara. These results suggest that background seismicity, i.e. events $M_w < \sim 6$, do not significantly remobilize surficial sediments to generate turbidites in Lake Rara. In addition, we tested the sensitivity of the lake site to near-field moderate to large earthquakes. In this test (see Methods), we used the aforementioned IPEs to infer the magnitude required to reach the threshold intensity of MMI≥6 at Lake Rara for hypothetical mid- to upper-crustal moderate-magnitude events on the closest known faults (Supplementary Fig. 3.8): one on the MHT directly below the lake (at a depth of 26 km; Jouanne et al., 2017), and two others on the Dharma (DF) and Hula (HF) Fault segments of the WNFS, at epicentral distances <15 and 80 km, respectively. The results (Supplementary Fig. 3.8) indicate that, in order to be recorded in Lake Rara sediments, nearby earthquakes should have a minimum magnitude $M_W \geq 5.8$ for the Rara-MHT and DF scenarios, with the required magnitude increasing rapidly with epicentral distance, and $M_W \geq 7.1$ for the HF scenario. This range of magnitudes is above the regional background seismicity during the past decades. The rapid increase in required magnitude with epicentral distance is indicated by the fact that the 1980 M_w 6.5 earthquake at an epicentral distance of ~100 km, and other instrumental $M_w > 6$ earthquakes in western Nepal and northern India, failed to trigger turbidites in the lake. Hence, it is likely that the turbidites present in our cores have been triggered by large ($M_W \geq \sim 6.5$) earthquakes.

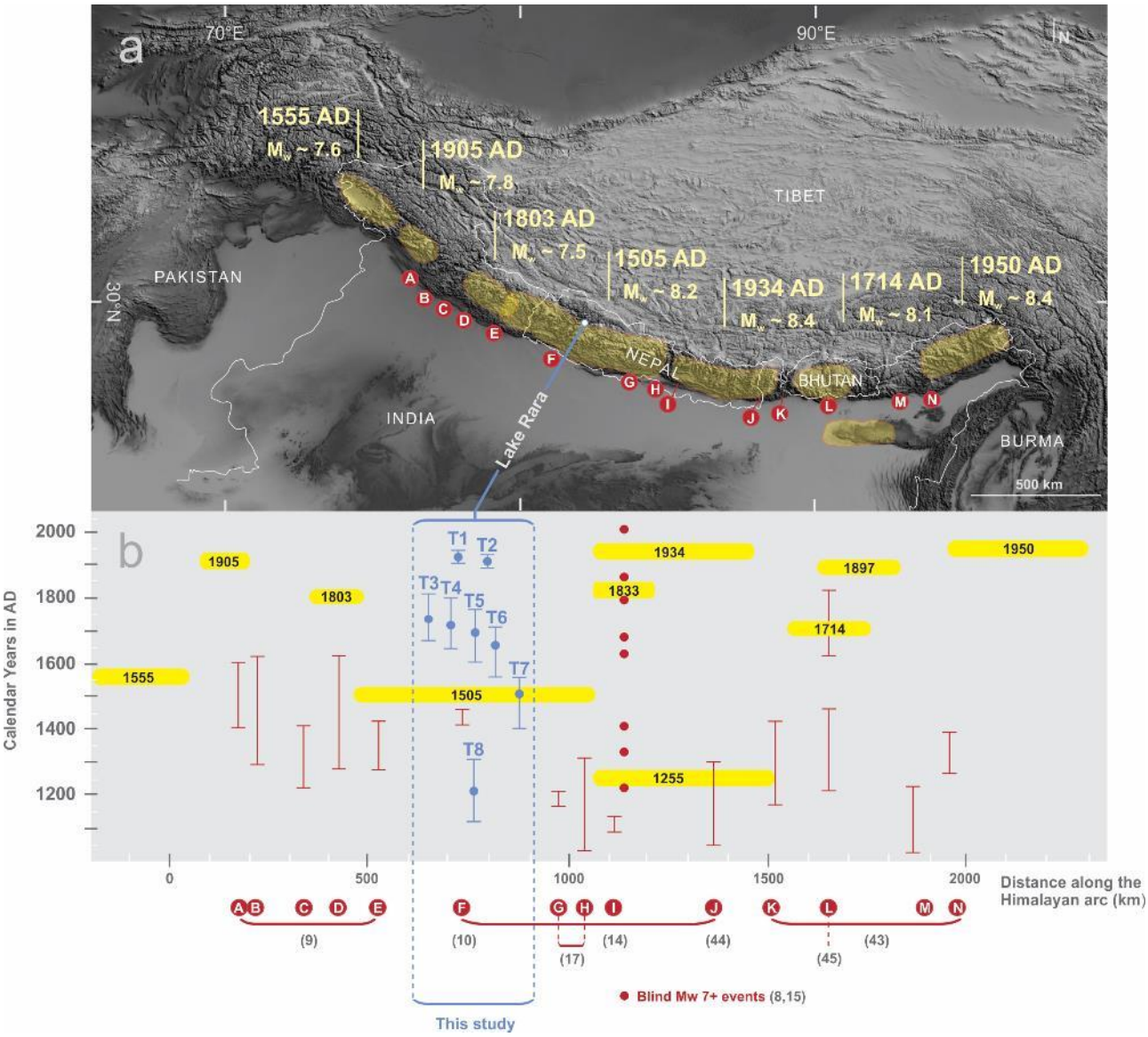

Figure 3.4. Overview of historical and paleoseismic data along the Himalayan front. The map is modified and updated after Kumar et al., 2010. (**a**) Digital terrain model of the Himalayan region. Yellow areas correspond to inferred ruptures of historical earthquakes (the surface ruptures of the 1255 AD and 1833 AD earthquakes overlap that of the 1934 earthquake, and are not represented); their timing and magnitude are indicated. Red dots labelled A to N represent paleoseismic trenches along the MFT; references are given in parentheses below plot (**b**). (**b**) Ages and extents of historical Himalayan M_w > ~7.5 earthquakes (horizontal yellow bars). Red vertical bars reflect ^{14}C ages that bracket the age of surface ruptures in calendar years AD, with 2σ uncertainties. Blue vertical bars represent the turbidite ages extracted from the age-depth model (2σ; this study); blue dots indicate the weighted mean age (ref. 9, Kumar et al., 2006; ref. 10, Yule et al., 2006; ref. 14, Lavé et al., 2005; ref. 17, Wesnousky et al., 2018; ref. 43, Kumar et al., 2010; ref. 44, Nakata and Rockwell, 1998; ref. 45, Le Roux-Mallouf et al., 2016).

3.4 Implications for the notion of a seismic gap in western Nepal

The above findings strongly suggest that, on average every 50–100 years since 1505, earthquakes of significant magnitude (M_w≥~6.5) produced turbidites in Lake Rara, potentially

significantly reducing the missing slip reported for the western Nepal seismic gap. Such earthquakes could occur on either the MHT or the WNFS. However, since the latter accommodates oblique convergence in the western-central Himalaya through slip partitioning (Murphy et al., 2014; Silver et al., 2015), slip on that system also contributes to reducing the stored seismic moment in western Nepal. Our data indicate that western Nepal may be as seismically active as central Nepal (Fig. 3.4), and that the notion of a seismic gap in western Nepal and northern India should be reconsidered. Future studies involving other lakes should allow correlating these events over a broader region. We also note the critical need for IPE calibration in this region. By using lake-sediment records as a paleo-seismometer for the first time in the Himalaya, this study complements the record obtained from paleoseismological and historical archives, demonstrating the importance of a holistic and diversified approach in paleoseismology to improve seismic hazard assessment.

3.5 Methods

Sediment core collection and analysis. In order to reconstruct the past earthquake activity of the Lake Rara area, we collected three short sediment cores with an average length of 40 cm. The coring sites were selected after a preliminary bathymetric survey that complemented existing depth information (Okino and Satoh, 1986). The coring sites are located in two different areas at water depths of 168 m and 120 m, respectively (Supplementary Figs. 3.1, 3.2). The cores were obtained in October 2014 with an Uwitec gravity corer operated from an inflatable dingy.

Cores were split lengthwise using a Geotek core splitter and described macroscopically. Their physical properties, including γ-ray attenuation density and magnetic susceptibility, were obtained using a Geotek multi-sensor core logger at 2-mm resolution. High-resolution grain-size analysis was performed on core RA14-SC05 with a step of 2.5 mm using a Malvern Mastersizer 3000 after removing organic matter, calcium carbonate and biogenic silica (McGregor et al., 2009). Grain-size distribution parameters were obtained using Gradistat V8 (Blott and Pye, 2001) and were calculated according to Folk and Ward, 1957. The relative concentration of major elements was obtained by X-ray fluorescence spectrometry (Itrax XRF core scanner) at 500-µm resolution at the Stockholm University Slamlab (Sweden). Bulk organic geochemistry (TOC, TN) was measured with an elemental analyser (PDZ Europa ANCA-GSL) at the UC Davis Stable Isotope Facility. Before analysis, samples were placed in silver capsules and decarbonated using 1N sulphurous acid (Verardo et al., 1990). The amount of sediment was optimized based on preliminary LOI_{550} measurements.

To reconstruct the 3D structure of the split cores we made use of a Siemens Somatom Definition Medical X-ray Computerized Tomography (CT) scanner (Kak and Slaney, 1988), which produces CT-slice images composed of voxels (volume elements) with a resolution of 0.15 × 0.15 × 0.60 mm. The 3D reconstruction was obtained by processing the contiguous set of CT slices with VGStudio v2.1. Radio-density values were extracted from the grey levels of the CT-slice images and represented using a colour chart to highlight variations in density within the cores. The CT grey levels correspond to X-ray attenuation, reflecting the proportion of X-rays absorbed or scattered as they pass through each voxel, which is primarily a function of X-ray

energy and the density and composition of the material being analysed.

Age models. A chronology for the Lake Rara sediment record was established on cores RA14-SC05 (site A) and RA14-SC06 (site B) by combining radiocarbon (Supplementary Table 3.1) and radionuclide (^{210}Pb and ^{137}Cs; Supplementary Tables 3.2, 3.3) dating. Samples for radiocarbon dating were picked outside of the turbidites, as these are considered to be instantaneous deposits. Radionuclides ^{210}Pb and ^{137}Cs were measured respectively on 11 and 9 bulk-sediment samples from core RA14-SC05 (Supplementary Fig. 3.4) by Flett Research Ltd. (Winnipeg, Canada) following the methods of Eakins and Morrison (1978) and Mathieu et al. (1988). Radiocarbon ages for cores RA14-SC05 and RA14-SC06 were obtained by dating four and five leaf samples, respectively. After acid-alkali-acid pre-treatment, the samples were converted to graphite following the procedure of Yokoyama et al. (2007). Isotopic analysis of the graphite targets was performed using Accelerator Mass Spectrometry (AMS) at the University of Tokyo, Japan (Yokoyama et al., 2010). All ages were calibrated using the calibration curve for Northern Hemisphere terrestrial ^{14}C dates IntCal13 (Reimer et al., 2013). Age-depth models of cores RA14-SC05 and RA14-SC06 (Supplementary Fig. 3.2) were produced using Bacon 2.2 software (Blaauw and Christen, 2011) after removal of the turbidites. The ages indicated in Fig. 2 and Supplementary Fig. 3.4 correspond to the base of each turbidite

Modelling shaking intensity. In order to evaluate the potential impact of historical earthquakes on the Lake Rara sediment record, we used custom software built on top of the core Python library of the open-source seismic hazard engine OpenQuake (Pagani et al., 2014) to compute shaking intensities based on the rupture parameters inferred for these earthquakes and on a set of Intensity-Prediction Equations (IPEs). We evaluated five events: a surface-rupturing earthquake (M_W=7.9) on the Tibrikot fault (Western Nepal Fault System; WNFS) between AD 1165 and 1400 (Murphy et al., 2014), the ruptures inferred in Hubbard et al. (2016) for the 1833 (M_w=7.8) and the 1934 (M_W=8.4) earthquakes on the Main Himalayan Thrust (MHT) and the instrumental 1916 (M_w≈7.2; Szeliga et al., 2010; Storchak et al., 2013) and 1980 (M_w=6.5; Stochark et al., 2013) earthquakes inferred to involve the MHT. The rupture parameters are summarized in Supplementary Table 3.5. A large number of IPEs is available in the literature, predicting shaking intensity as a function of source and path parameters (mainly magnitude and distance). They differ in the intensity scale (MMI, EMS-98, MSK), magnitude scale (M_W, M_S) and distance metric (epicentral, hypocentral or rupture distance) that is considered, in the geographic area or tectonic region for which they are representative, and in the number and quality of input macroseismic data points. As it is currently not possible to identify a single IPE that is best suited to model shaking intensities for fault ruptures in western Nepal, we applied a mix of five different IPEs: we selected three IPEs (Allen et al., 2012; Bakun and Wenworth, 1997, Atkinson and Wald, 2007) that were developed for California and other tectonically active regions globally, and performed best in an evaluation for application in the Global Shakemap (Cua et al., 2010), supplemented with two IPEs developed specifically for the Himalaya (Szeliga et al., 2010; Ghosh and Mahajan, 2013). The main parameters of these IPEs are summarized in Supplementary Table 4. Unfortunately, the Himalayan IPEs use a different intensity scale (EMS-98 and MSK, respectively, versus MMI), but the difference with MMI is probably less than the variability among different IPEs, and one of these studies (Szeliga et al.,

2010) made a direct comparison with the two Californian IPEs (Allen et al., 2012; Bakun and Wentworth, 1997), concluding that there is good agreement in intensity attenuation between the two regions. Using the selected IPEs, we computed maps of mean shaking intensity (Fig. 3a, b, e, f and g) as the arithmetic average of the mean intensity predicted by the different IPEs. We note that, whereas the predicted and observed intensities for the 1934 and 1833 central Nepal earthquakes (Figs. 3.3e and f) appear to overlap reasonably well (Supplementary Fig. 3.6), significant discrepancies appear between predicted and observed intensities for the west Nepal 1980 earthquake (Fig. 3.3a). These discrepancies result both from poorly constrained locations (hypocentre, epicentre, depth) and magnitudes of the modelled events[34], as well as from the use of IPEs (Allen et al., 2012; Szeliga et al., 2010; Bakun and Wentworth, 1997; Atkinson and Wald, 2007; Ghosh and Mahajan, 2013) that are not well-calibrated for the region and possibly underestimate intensities (Figs. 3.3c and d). In particular for the 1916 Dharchula earthquake, the closest recording station used for constraining the source parameters was in Calcutta, at a distance of ~10° (>1000 km; Storchak et al., 2013). Our intensity map for the 1980 Bajhang earthquake, based on the IPE mix (Allen et al., 2012; Szeliga et al., 2010; Bakun and Wentworth, 1997; Atkinson and Wald, 2007; Ghosh and Mahajan, 2013) appears to underestimate the observed near-field intensities (Figs. 3.3c and f; Szeliga et al., 2010). In the USGS Shakemap solution, based on one of the IPEs in our mix (Allen et al., 2012), it appears that a value of 0.76 has been added to the event magnitude to obtain predicted intensities matching with the observations (Szeliga et al., 2010), explaining why the published Shakemap (https://earthquake.usgs.gov/earthquakes/eventpage/usp0001959#shakemap) shows higher intensities at the site of Lake Rara than our solution. From the IPEs in our selection, it appears that the Himalayan IPE (Szeliga et al., 2010) shows the best match with the observed intensities (Szeliga et al., 2010) in the distance range of interest to this study (up to about 150 km) although this is not surprising as ref. 30 fitted their IPE to the same observations, which are in EMS-98.

Modelling sensitivity to near-field background seismicity. To assess the sensitivity of Lake Rara to smaller-magnitude near-field earthquakes, we estimated the magnitude necessary to cause shaking of intensity MMI ≥ 6 at the lake for different scenarios using the same IPE mix as above. We computed intensities (mean ± 1 standard deviation) for a range of possible magnitudes, and interpolated the magnitude corresponding to MMI = 6 from the obtained magnitude-intensity curves (Supplementary Fig. 3.8). We considered three different rupture scenarios on the faults that are closest to Lake Rara: one on the MHT directly below Lake Rara ("Rara-MHT"), and two others on the Dharma (DF) and Humla (HF) Faults, which are both part of the Western Nepal Fault System (WNFS; Fig. 3.1, Supplementary Fig. 3.8). These scenarios are modelled by selecting a fixed hypocentral location, which is the midpoint of ruptures that increase in size with the considered magnitude. In the Rara-MHT scenario, the hypocentre is directly below Lake Rara at a depth of 26 km (Jouanne et al., 2017). The DF and HF scenarios were modelled at locations corresponding to recent earthquakes, which occurred respectively 2008/12/08 (M_W=5.3), and 1980/06/22 (M_W=5.1). Their source parameters were taken from the Global Centroid Moment Tensor database (Dziewonski et al., 1981; Ekström et al., 2012), and we selected the nodal plane that agrees best with the corresponding faults and style of faulting (Silver et al., 2015; Taylor et al., 2009). The rupture parameters are summarized in Supplementary Table 3.6. Because epicentral distance is zero in the Rara-MHT scenario, we

decided to leave out IPEs that use epicentral distance, as this may lead to unrealistically high or undefined intensities for this case. In the other scenarios, the distance between the lake and the rupture decreases with increasing magnitude. The magnitude versus intensity plots obtained for the three scenarios are shown in Supplementary Fig. 3.8.

3.6 Supplementary Information

Supplementary Text

Identification of turbidite layers. The turbidites were identified using a series of sedimentological and geochemical criteria that included grain size, magnetic susceptibility, Ti concentrations, bulk organic geochemistry and radio-density. From the mean grain-size profiles, the turbidites are identified by their coarse base and a fining-upward sequence of fine sand to very fine silt, in sharp contact with the underlying background mud. The magnetic susceptibility, the Ti XRF profiles and the C/N ratio exhibit similar patterns as their behaviour is directly related to grain size (Fig. 3.2; Supplementary Fig. 3.3). The spikes in magnetic susceptibility are interpreted as recording an input of para- to ferro-magnetic minerals, which are concentrated in the coarse and dense fraction of the sediment. Likewise, it has been shown that Ti concentrations reflect silt content in sediments (Cuven et al., 2010; Bertrand et al., 2012). The turbidites are most visible on the 3D CT images of the cores, which highlight their dense bases due to their high contents of fine sand to silt, contrasting with the lower radio-densities of the muddy background.

Turbidite triggering mechanism. Turbidites within lake sediments can be triggered by various factors such as floods, spontaneous slope failures, or earthquakes. In the main text, we argue why we think that we can exclude floods or slope failures as triggering mechanisms for the Lake Rara turbidites.

In the case of Lake Rara the "synchronicity criterion" (Moernaut et al., 2014; Schnellmann et al., 2002) cannot be directly applied as the lake is composed of a single basin, which means that the two coring sites are not entirely independent. Our best argument for attributing an earthquake origin to Lake Rara turbidites is a temporal correlation with known historical events (Howarth et al., 2014; Moernaut et al., 2014; Bertrand et al., 2012; Meyers and Terranes, 2001). We have been able to relate turbidite T7 (1399–1570 AD; Fig. 3.2; Supplementary Fig. 3.4) to the great 1505 AD earthquake that ruptured the MFT, but also T8 (1135–1303 AD) to the rupture of Tibrikot fault segment of the WNFS in 1165–1400 AD (Murphy et al., 2014). In addition, our T2 turbidite (1891–1936 AD; Fig. 2; Supplementary Fig. 3.4) can be correlated to the 1916/08/28 earthquake (M_w 7, 29.730°N 80.745°E), which was added to the ISC-GEM catalogue (Storchak et al., 2013) in 2017. By doing so, we have demonstrated that the occurrence of turbidites in Lake Rara is not due to random slope-failure processes but related to seismic activity implying ruptures on both the MFT/MHT and the WNFS.

As stated in the main text, the geomorphologic and hydrographic context rules out the potential of flood-triggered turbidites. The hydrographic system of Lake Rara contains 37 small streams flowing along gentle (<30°) and densely forested slopes (Supplementary Fig. 3.1). These

streams have an average width of 30 cm and a depth of about 15 to 30 cm. The purely sub-aquatic origin of the turbidites is additionally supported by the C/N signature of the turbidites, which ranges between 13–17, representing a mixture of aquatic (C/N <8) and terrestrial (C/N >20) sources (Meyers and Teranes, 2001). In contrast, turbidites resulting from a hydrometeorological event would have a terrestrial C/N ratio >20 (Meyers and Teranes, 2001). The C/N values measured in Lake Rara turbidites are similar to (in fact somewhat more aquatic than) the values measured by Howarth et al. (2014) in subaqueous mass-wasting deposits in New-Zealand lakes. Although the absolute values depend on grain size (Supplementary Fig. 3.3), these results suggest that the turbidites originate from the reworking of sediment previously deposited at shallower locations within the lake.

The low hydrodynamic activity in the catchment of Lake Rara is also suggested by the very low inferred sedimentation rates (0.3–0.5 mm/yr at site RA14-SC05 and 0.2–0.3 mm/yr at site RA14-SC06). These are less than half of the accumulation rates generally observed in lakes used in paleoseismic research (~1 mm/yr or higher; Howarth et al., 2014; Moernaut et al., 2017), resulting in higher slope stability and therefore rendering spontaneous slope failures unlikely. Finally, it is worth noting that sediment accumulation rates in Lake Rara have not significantly changed during the last millennium (Supplementary Fig. 3.4a). This observation implies that land-use activities have had little effect on soil erosion and therefore did not affect the rate of sediment remobilisation and the earthquake recording sensitivity of the lake.

Of the eight turbidites recorded in core RA14-SC05 (site A; Fig. 1; Supplementary Figs. 1 and 2), only turbidite T7 (1399–1570 AD), which is attributed to the great 1505 AD earthquake, is also expressed in the sediments of the shallower site 2 (core RA14-SC06; Supplementary Fig. 2). The age of turbidite TA (1285–1606 AD) is statistically indistinguishable from that of turbidite T7 (1399–1570 AD), as demonstrated by the similarity of the Probability Density Functions (PDF) of both turbidites, which both peak around 1500 AD (Supplementary Fig. 3.5). This synchronicity strongly suggests that turbidites T7 and TA represent the same event, and were likely generated by the same slope failure, which triggered a turbidity current affecting the entire basin of Lake Rara. The reason why the 1505 AD event is the only one recorded at both locations likely reflects the particularly large magnitude of this event, combined with the lower recording sensitivity at site B.

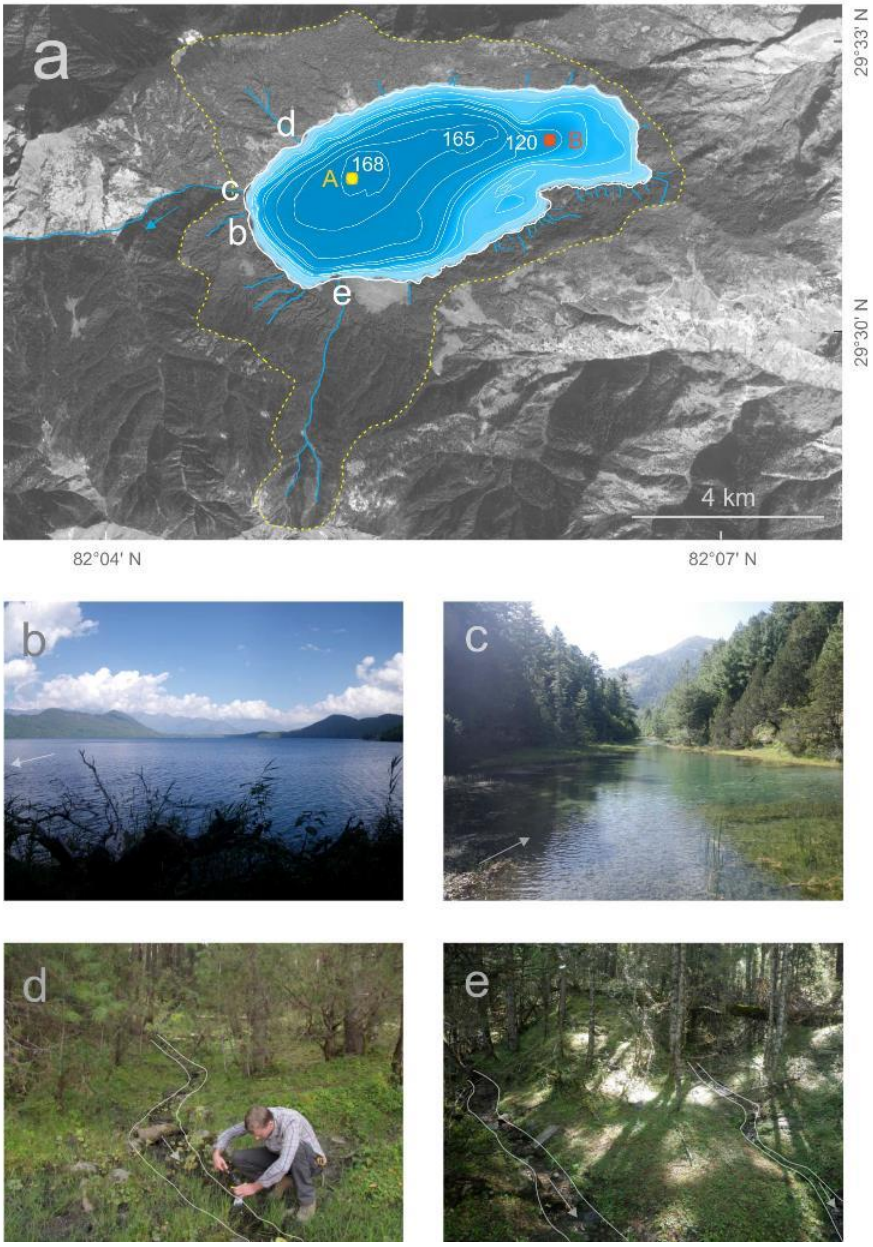

Supplementary Figure 3.1. Field photos highlighting hydrographic features of the Lake Rara watershed. The photos were taken in October 2014, i.e., immediately after the monsoon season (June to early September in 2014), when the rivers are at their highest level. (**a**) DigitalGlobe image of Lake Rara. The wastershed is illustrated by the yellow dashed curve. The letters b, c, d, e indicates the locations of the corresponding field photos. (**b**) Southern bank of the lake with view on the dense forest and gentle slopes around the lake. The arrow indicates the outflow. (**c**) Lake outflow. The arrow indicates flow direction. (**d**) One of the 37 streams flowing into the lake. The arrow indicates the flow direction. The cobbles and boulders in the streambed and along the banks of the river originate from moraine deposits intersected by the river intersects; they were probably not transported. (**e**) Two streams on the eastern bank of the lake, which are representative by their size and depth of the 37 streams that we have observed along the banks of Lake Rara.

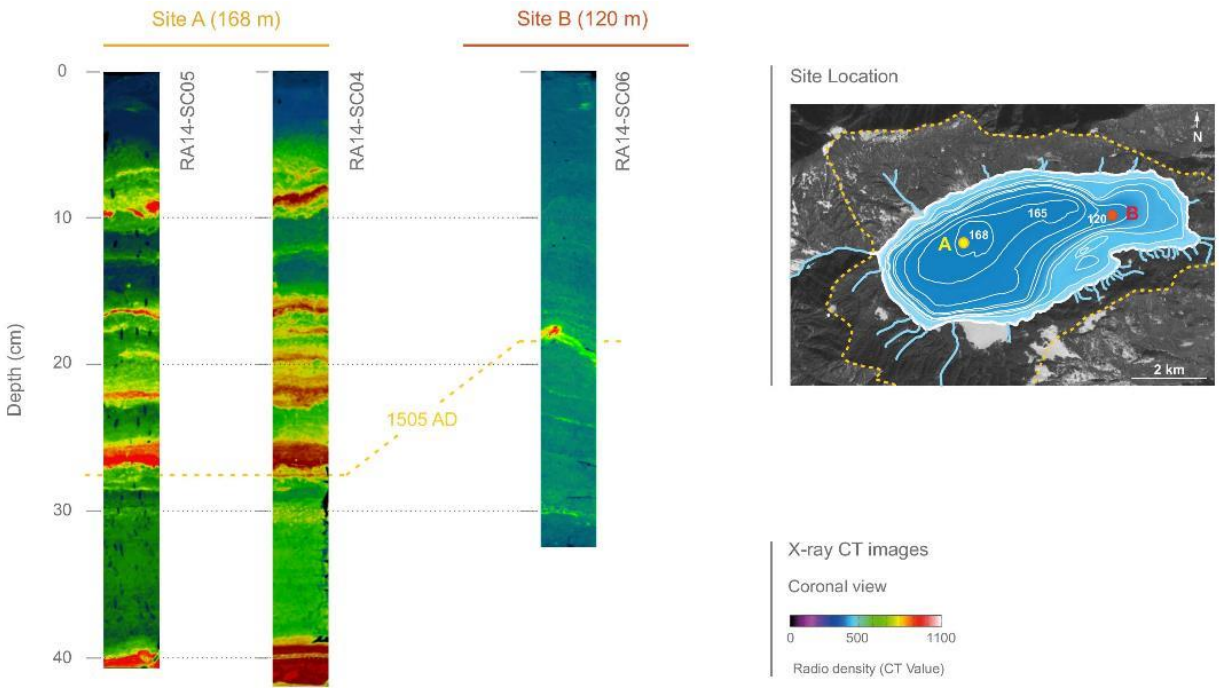

Supplementary Figure 3.2. Pseudo-colour x-ray computed tomography images of the three sediment cores. The images are coronal views of the two cores from site A (168 m water depth) and the core from site B (120 m water depth).

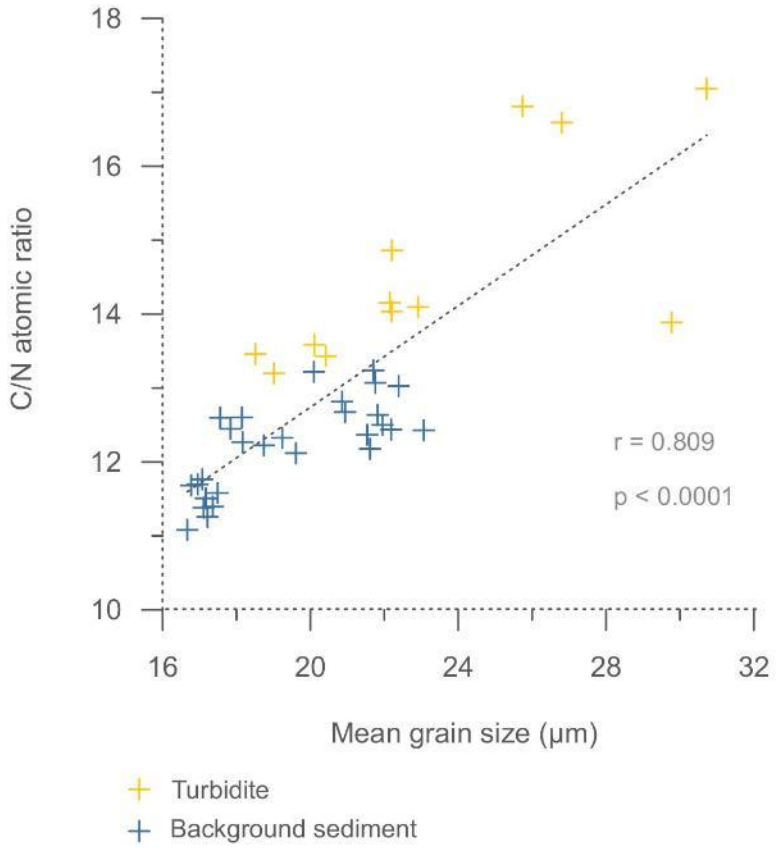

Supplementary Figure 3.3. C/N atomic ratio versus mean grain size for samples from sediment core RA14-SC05 (site A). The C/N ratios are significantly positively correlated to grain size ($r = 0.809$, $p < 0.0001$). Note that the C/N values obtained on the turbidites are aligned with the C/N values obtained on the background sediments, which means that the only reason the turbidites display higher C/N values is their coarse grain size.

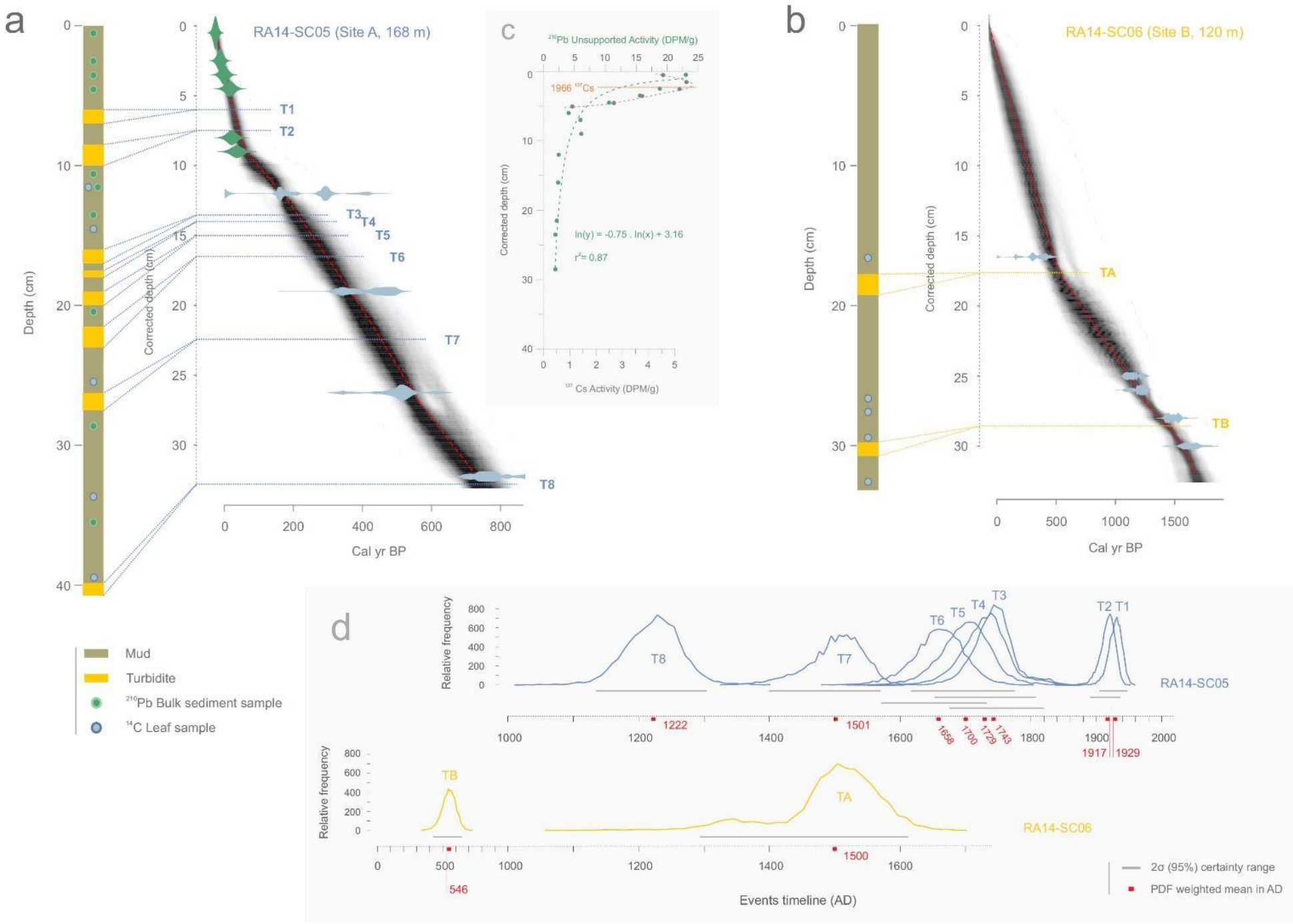
a
RA14-SC05 (Site A, 168 m)
Depth (cm)
Corrected depth (cm)
Cal yr BP
T1
T2
T3
T4
T5
T6
T7
T8
c
^{210}Pb Unsupported Activity (DPM/g)
1966 ^{137}Cs
ln(y) = -0.75 . ln(x) + 3.16
r^2= 0.87
Corrected depth (cm)
^{137} Cs Activity (DPM/g)
b
RA14-SC06 (Site B, 120 m)
Depth (cm)
Corrected depth (cm)
Cal yr BP
TA
TB
Mud
Turbidite
^{210}Pb Bulk sediment sample
^{14}C Leaf sample
d
Relative frequency
T8
T7
T6
T5
T4
T3
T2 T1
RA14-SC05
1222
1501
1658
1700
1729
1743
1917
1929
TB
TA
RA14-SC06
546
1500
2σ (95%) certainty range
PDF weighted mean in AD
Events timeline (AD)

Supplementary Figure 3.4. Age models. Bacon age-depth models (Blaauw and Christen, 2011) for (a) core RA14-SC05 (site A) and (b) core RA14-SC06 (site B). The corrected depths were calculated by removing instantaneous event deposits (turbidites) from the total depths in order to apply a continuous model in Bacon. The samples analysed for radiocarbon and radionuclides are located on the log. Grey levels on the age-depth curves represent confidence levels. The red dashed lines represent the overall best fit. Blue dashed lines in (**a**) and yellow dashed lines in (**b**) represent the projection of the turbidites on the age-depth models of core RA14-SC05 and core RA14-SC06, respectively. (**c**) Radionuclide (^{210}Pb and ^{137}Cs) activities as a function of corrected depth for core RA14-SC05. Corrected depth was calculated by removing instantaneous event deposits. ^{210}Pb ages were calculated from the unsupported ^{210}Pb activity using a Constant Rate of Supply (CRS) model. Unsupported ^{210}Pb concentrations were calculated as total − supported (deduced from ^{226}Ra concentrations) ^{210}Pb. The model assumes constant input of ^{210}Pb and a core that is long enough to include all of the measurable atmospheric source ^{210}Pb, i.e. it contains a complete ^{210}Pb inventory. The extrapolated ages were implemented in the Bacon age-depth model. ^{137}Cs concentrations were used as control points for recent deposits since their peak is expected to represent 1963-1966 AD (Arnaud et al., 2002). (**d**) Timeline of the earthquake-triggered turbidites identified in cores RA14-SC05 and RA14-SC06 (in years AD). The Probability Density Function (PDF) of the age of each turbidite is represented in blue for RA14-SC05 and in yellow for RA14-SC06. The grey lines at the bottom of the PDF represent the 2σ (95%) age range for each turbidite. The red squares highlight the weighted mean ages of the events (in years AD).

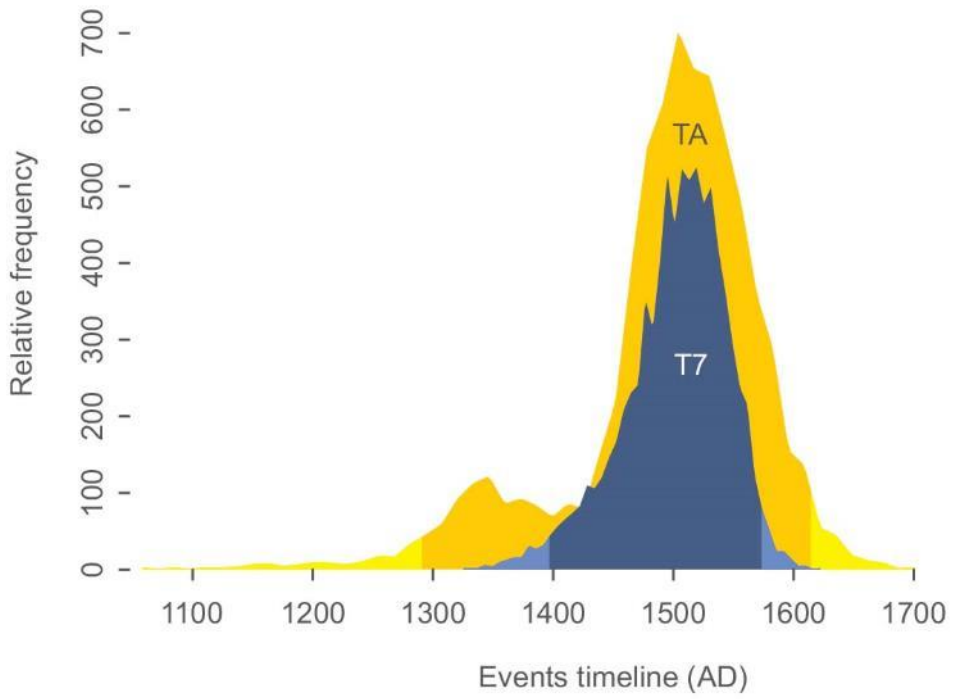

Supplementary Figure 3.5. Probability Density Functions (PDF) for ages of turbidites T7 (RA14-SC05, site A) and TA (RA14-SC06, site B). Dark blue/yellow represent the 2σ (95%) uncertainty range. Both PDFs peak around 1500 AD, suggesting that the entire body of Lake Rara was affected by a synchronous event. We relate this event to the 1505 AD earthquake.

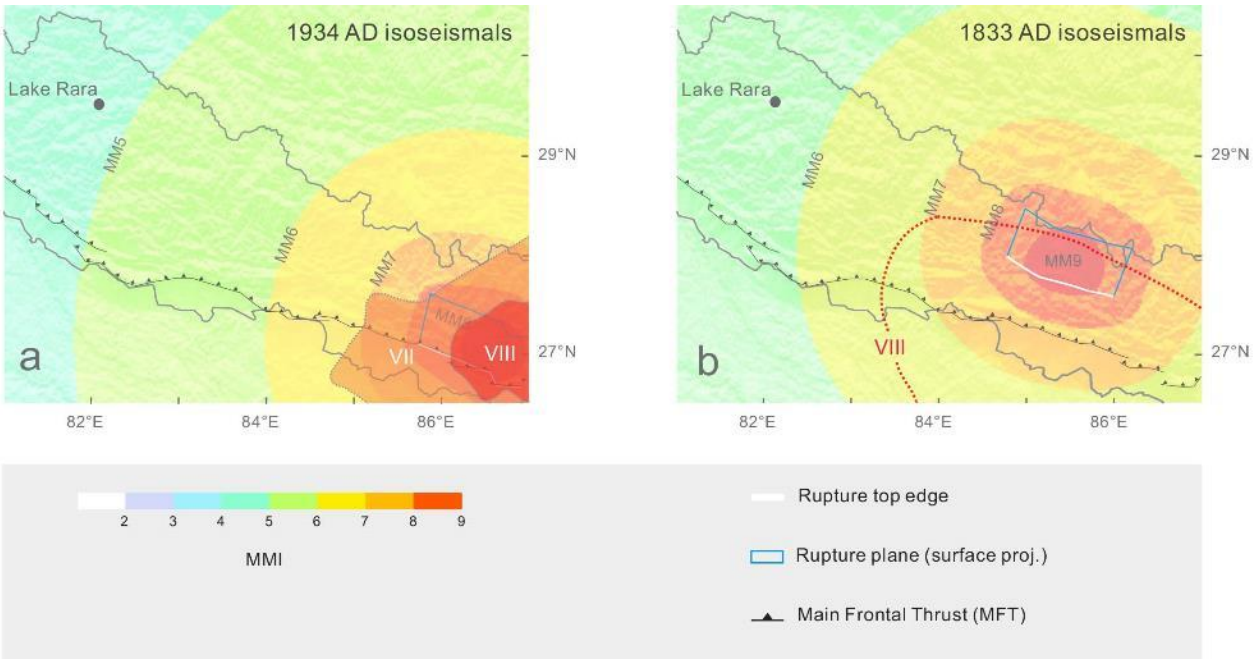

Supplementary Figure 3.6. Comparison of published and modelled isoseismals for the 1934 AD (Mw 8.4) and 1833 AD (Mw 7.8) earthquakes. (**a**) 1934 AD macroseismic isoseimals (MSK) from Pandey and Molnar (1988; shaded patches with roman numbers) compared to our modelled MMI isoseismals. (**b**) 1833 AD MMI=8 isoseismal from Bilham (1995; dotted contour with roman number) compared to our modelled MMI isoseismals.

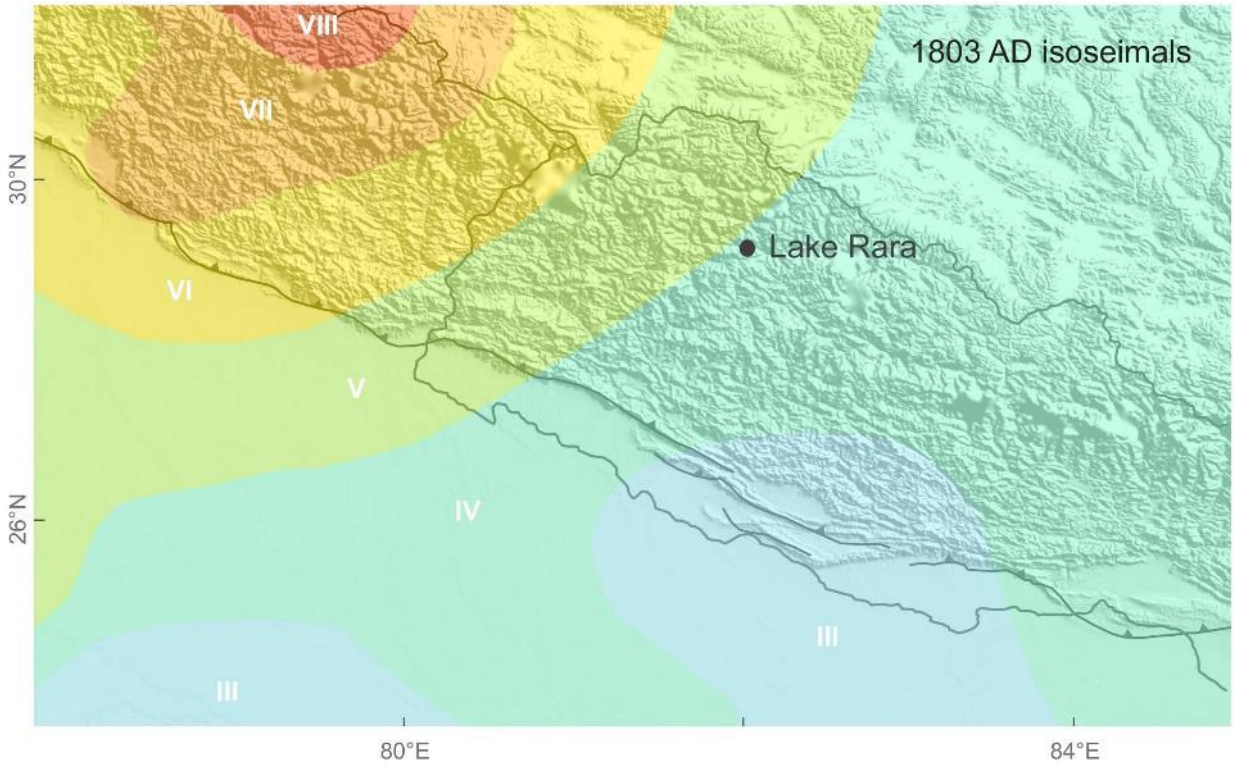

Supplementary Figure 3.7. Isoseismal maps (MSK) of the 1803/09/01 Kumaon earthquake (M_w≈7.3-7.7). The map is redrawn from Ambraseys and Douglas (2004) and based on 33 intensity observations.

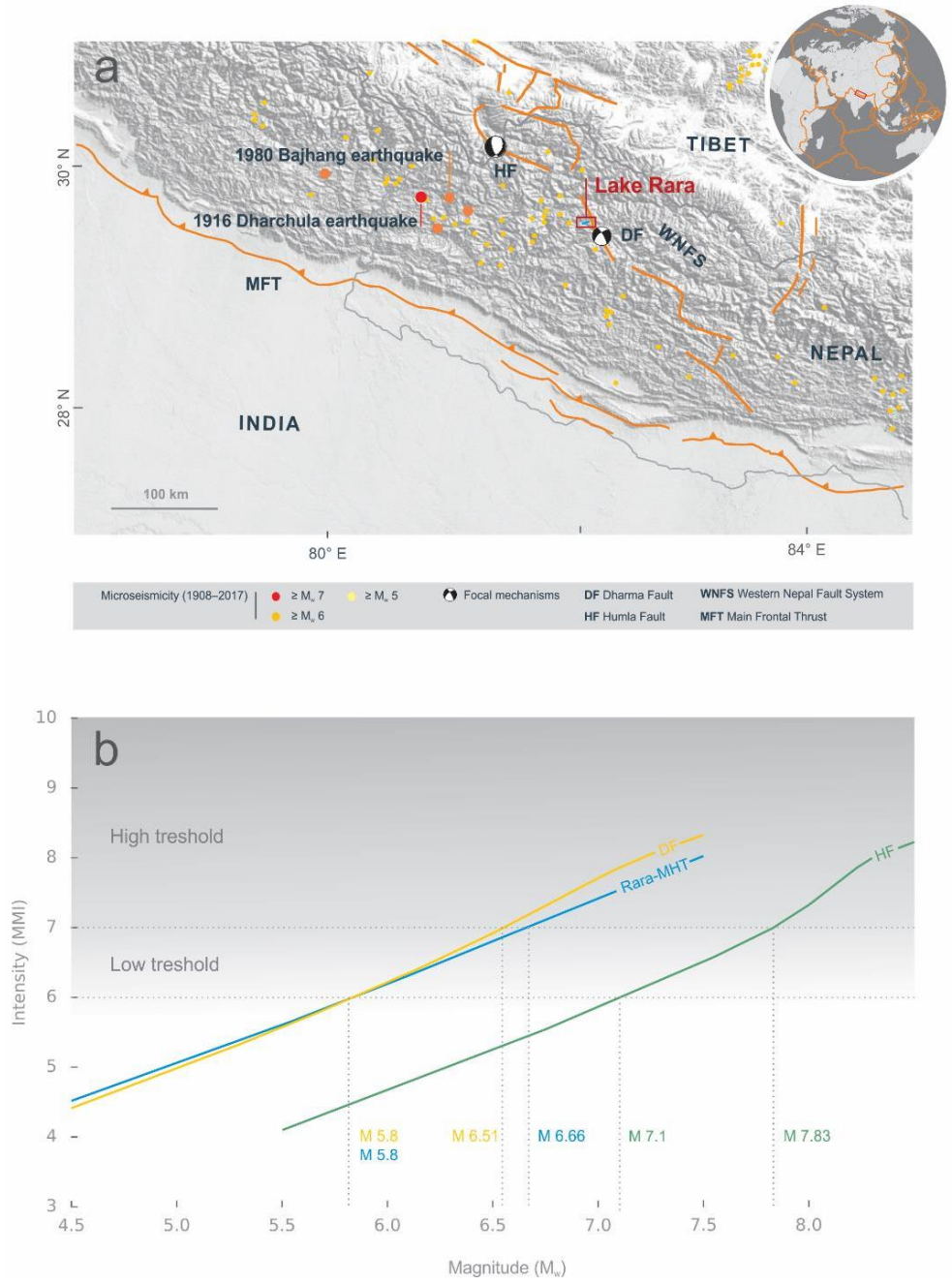

Supplementary Figure 3.8. **Proximal rupture scenarios and earthquake sensitivity assessment.** The first rupture scenario involves a hypothetical earthquake at 26 km (Hubbard et al., 2016) below Lake Rara on the MHT, while the other two involve rupture on the Dharma (DF) and Humla (HF) Faults, respectively. (**a**) Map of Western Nepal illustrating the background seismicity ($M_w \geq 5$) from 1908–2017 (2017 update of ISC-GEM; Storchak et al., 2013). Representative focal mechanisms from the Global Centroid Catalogue database (Dziewonski et al., 1981; Ekström et al., 2012) for the Dharma (DF) and Humla (HF) Faults are represented. (**b**) Magnitude versus intensity plot for each rupture scenario, computed using the same IPEs as in Fig. 3 and the source parameters in Supplementary Table 3.6 (see Methods). The solid curves are the mean magnitude-intensity curves (average of different IPEs) for each scenario. The blue curves correspond to the scenario of rupture on the MHT directly below the lake at a depth of 26 km (Hubbard et al., 2016). The DF and HF scenarios are represented in yellow and green, respectively.

Supplementary Table 3.1. AMS ^{14}C ages obtained on sediment cores RA14-SC05 and RA14-SC06.

ID	Lab Code	Sample depth (cm)	Material	$\delta^{13}C$ (‰)	^{14}C age (yr. ±1σ)
SC05	YAUT-022721	14-15	Leaf	-17.81	234 ± 35
SC05	YAUT-022723	25-26	Leaf	-25.95	379 ± 47
SC05	YAUT-023023	33-34	Leaf	-18.69	469 ± 51
SC05	YAUT-022724	39-40	Leaf	-27.31	858 ± 44
SC06	YAUT-022725	16-17	Leaf	-22.65	267 ± 48
SC06	YAUT-022726	26-27	Leaf	-19.81	1221 ± 35
SC06	YAUT-022727	27-28	Leaf	-27.45	1258 ± 35
SC06	YAUT-022730	30-31	Leaf	-20.41	1605 ± 36
SC06	YAUT-023013	32-33	Leaf	-31.04	1717 ± 56

Supplementary Table 3.2. ^{210}Pb data and corresponding CRS ages of samples from sediment core RA14-SC05. The CRS model assumes constant input of ^{210}Pb and a core that is long enough to include all of the measurable atmospheric source ^{210}Pb, i.e., it contains a complete ^{210}Pb inventory. The model assumes that the ^{210}Pb activity of 2.38 DPM/g in the 20-21 cm section (corrected depth 16 cm) corresponds to the background level. The results are plotted in Supplementary Figure 3.4.

Depth (cm)	Corrected depth (cm)	^{210}Pb Total Activity (DPM/g)	^{210}Pb Unsupported Activity (DPM/g)	CRS age (yr. ± 15%)
0–1	0.5	23.04	19.70	25.8 ± 3.8
2–3	2.5	18.81	15.48	36.8 ± 5.5
3–4	3.5	15.61	12.28	51.0 ± 7.6
4–5	4.5	10.62	7.29	62.0 ± 9.3
10–11	6	4.08	1.02	79.5 ± 11.9
11–12	7	5.99	2.93	84.0 ± 12.6
13–14	9	6.11	3.05	98.8 ± 14.8
16–17	12	2.48	0.00	
20–21	16	2.38		
28–29	21.5	2.15		
35–36	28.5	1.92		

Supplementary Table 3.3. ^{137}Cs activities measured on samples from sediment core RA14-SC05. The results are plotted in Supplementary Figure 3.4.

Sample ID	Sample depth (cm)	^{137}Cs Activity (DPM/g dry wt.)	1σ Counting error (DPM/g dry wt.)
RA14-SC05 (0-1 cm)	0-1	3.70	0.32
RA14-SC05 (1-2 cm)	1-2	4.59	0.62
RA14-SC05 (2-3 cm)	2-3	4.33	0.46
RA14-SC05 (3-4 cm)	3-4	2.91	0.38
RA14-SC05 (4-5 cm)	4-5	1.83	0.37
RA14-SC05 (5-6 cm)	5-6	1.31	0.49
RA14-SC05 (7-8 cm)	7-8	0.44	0.26
RA14-SC05 (9-10 cm)	9-10	0.25	0.20
RA14-SC05 (35-36 cm)	35-36		

Supplementary Table 3.4. Main parameters of Intensity Prediction Equations used to model macroseismic intensities of different rupture scenarios.

Intensit Prediction Equations	Intensity measure	Magnitude scale	Distance metric	Standard deviation	Region
Bakun and Wentworth, 1997	MMI	M_w	Epicentral	Not specified	California
Atkinson and Wald, 2007	MMI	M_w	Rupture	Fixed (0.4)	California
Allen et al., 2012	MMI	M_w	Rupture	Distance-dependent (0.94 at 10 km, 0.76 at 100 km)	Global active crust
Szeliga et al., 2010	EMS-98	M_w	Hypocentral	Not specified	Himalaya
Ghosh and Mahajan, 2013	MSK	M_s	Epicentral	Fixed (~0.246)	NW Himalaya

Supplementary Table 3.5. Rupture parameters used to compute the intensity maps in Fig. 3.3.

Events	M_W	Length (km)	Mean strike (°)	Dip (°)	Top depth (km)	Bottom depth (km)
Tibrikot Fault	7.9	50	302	40	0	20
MHT 1833	7.8	130	290	10	10	20
MHT 1934	8.4	170	283	10	0	10
Instrumental earthquake	M_W	Latitude (°)	Longitude (°)	Depth (km)	Strike (°)	Dip (°)
1916 Dharchula	7.2	29.73	80.75	20	290	21
1980 Bajhang	6.5	29.42	80.95	22.3	290	21

Supplementary Table 3.6. Source parameters used for near-field rupture scenarios in Supplementary Fig. 3.8.

Fault	Latitude (°)	Longitude (°)	Depth (km)	Strike (°)	Dip (°)	Rake (°)
Rara-MHF	29.52925	82.0925	25	304	26.5	90
DF	29.65	82.01	19.5	328	75	-151
HF	30.10	81.59	15	162	63	-115

Chapter 4

Seismic hazard minimized by the cycle concept

Zakaria Ghazoui [1, 2], Jean-Robert Grasso [1], Arnaud Watlet [3], Corentin Caudron [2], Abror Karimov [1], Sebastien Bertrand [2], Yusuke Yokoyama [4] and Peter van der Beek [1]

[1] Université Grenoble Alpes, CNRS, ISTerre (Institut des Sciences de la Terre), Grenoble, France.
[2] Department of Geology, Ghent University, Ghent, Belgium.
[3] Royal Observatory of Belgium, Department of Seismology and Gravimetry, Brussels, Belgium.
[4] Atmosphere and Ocean Research Institute, The University of Tokyo, Chiba, Japan.

Will be submitted to *Science* before the PhD defense

Seismic hazard estimates are based on the distribution of time intervals between earthquakes with a reference magnitude and are significantly influenced by the model of temporal distribution (i.e., periodical to random). In the Himalaya, given the present knowledge of past earthquakes, recurrence times are generally described by a cyclic model, leading to substantial variations in hazard assessment within Himalayan countries. We propose a paradigm shift supported by statistical analyses on a 6000-year seismic record derived from a lake-sediment core in western Nepal. Our results imply that intervals between large (M≥7) earthquakes are robustly described by a Poisson distribution. Second-order event clustering further evidences correlated events. These patterns are calibrated against data from the instrumental catalogue for the entire Himalaya and are inconsistent with a periodic or quasi-periodic time distribution for long-term seismicity in the Himalaya. This shift in paradigm shows that the occurrence of major to moderate events is as uncertain as smaller events on any time scale, increasing drastically the seismic hazard in the Himalaya. From a global perspective, applying instrumental statistical seismology methods to paleo-seismology data validates the necessary complexity in any conceptual seismic cycle dogma.

4.1 Introduction

With a total length of about 2400 km, the Main Himalayan Thrust (MHT) and its surface-breaking frontal ramp, the Main Frontal Thrust (MFT), is considered to be the largest and most rapidly slipping continental megathrust worldwide (e.g. Cattin and Avouac, 2000). Convergence across the Himalayan belt occurs at a rate increasing from ~14 to ~21 mm/yr from west to east (e.g. Stevens and Avouac, 2015). The strain accumulated during convergence is released by major earthquakes, the magnitude, time and location of which remain unpredictable (e.g. Cattin and Avouac, 2000; Bilham et al., 2001). The possible occurrence of major earthquakes poses a significant threat to the densely populated Himalayan region and its foreland; therefore, characterizing the return time of large earthquakes remains both a socio-economic necessity and a scientific challenge. Most studies have focused on paleo-seismological techniques to assess characteristic return times (see Bollinger et al., 2014 for a review). However, along most segments of the MFT, paleo-seismic trenches have generally revealed only a single event over the past 1000 years per site (e.g. Bollinger et al., 2014). In the absence of significant paleoseismological time series, the mean return times of large earthquakes cannot be robustly ascertained (e.g. Bollinger et al., 2014). The absence of reliably constrained recurrence times leaves open the possibility that much larger earthquakes (up to $M_w > 9$) than those recorded until now could occur on a multi-millennial time scale (e.g., Lavé et al., 2005; Feldl and Bilham, 2006; Gupta and Gahalaut, 2015; Stevens and Avouac, 2015; 2017). In this context and mainly due to lack of evidence or speculative interpretation of insufficient data, the return period of major Himalayan earthquakes remains subject to significant debate (e.g., Ader et al., 2012; Kumahara and Jayangondaperumal, 2013; Mugnier et al., 2013; Srivastava et al., 2013; Schiffman et al., 2013; Bollinger et al., 2014; Wesnousky et al., 2017).

On a global scale, the analysis of temporal and spatial distributions of paleo-earthquakes has led to diverging conclusions (e.g. Wu et al., 1995; Sykes and Menke, 2006; Satake and Atwater, 2007). These distributions are suggested to span a wide range of patterns including (i) quasi-

periodic recurrence (e.g. Sykes and Menke, 2006; Scharer et al., 2010; Berryman et al., 2012; Corbi et al., 2013), (ii) recurrence times varying according to the "supercycles" concept (e.g. Goldfinger et al., 2013; Herrendörfer et al., 2015), (iii) time-independent (Poissonian) distributions (e.g. Wu et al., 1995; Gomez et al., 2015), and (iv) clustered patterns (e.g. Kenner and Simons, 2005).

In order to analyse the timing of past earthquakes and their distribution, we focus here on an alternative archive; lacustrine sediment cores (e.g., Monecke et al., 2004; Howarth et al., 2014; Moernaut et al., 2014; Gomez et al., 2015, Ghazoui et al., 2018). We report on a long sediment core from Lake Rara (western Nepal; Nakamura et al., 2012; Fig. 1 and S1) that allows us to analyse the longest paleo-seismologic catalogue for Nepal based on dated turbidite occurrences. The calibration of turbidite triggering against seismic shaking in terms of magnitude range and time patterns was performed for a shorter core from the same lake (Ghazoui et al., 2018). To characterize the 50-event series that occurred in a 6000 years window, we apply statistical seismology techniques that are commonly used on regular instrumental seismic catalogues (e.g. de Arcangelis et al. 2016).

Classically, two classes of earthquakes are defined. Events may be independent (uncorrelated) in the time domain or they may be correlated, i.e. clusters of events triggered by other earthquakes (e.g. aftershocks of previous shocks). These latter events are not related to any external drivers within the lithospere. These two classes of events are observed in worldwide seismic catalogues. The corresponding inter-event time (*dt*) distributions fit a power-law for short inter-event times (i.e. correlated events) and an exponential law for the largest values of inter-event times, i.e. Poissonian non-correlated events (for a review, see De Arcangelis et al., 2016). These patterns correspond to a gamma distribution for *dt* values (e.g. Saichev and Sornette, 2007; de Arcangelis et al., 2016). A Poissonian inter-event time distribution formally corresponds to earthquakes that are purely driven by plate tectonics, without interaction with other events (e.g. Gardner and Knopoff, 1974; Helmstetter and Sornette, 2002; De Arcangelis et al., 2016). In the present study, we calibrate the 50-event sediment core catalogue against a 50-event instrumental seismic catalogue for the Himalaya, in order to statistically estimate the magnitude range and time patterns of the recorded historical events.

4.2 Data

Our study is based on a 4-m long sediment core retrieved from Lake Rara in western Nepal (Fig. 1 and S1). The recent study of Ghazoui et al. (2018) presents three 40-cm length sediment cores from the same lake in which up to eight earthquake-triggered turbidites (ETT) covering the last millennium are recorded. Radiocarbon dating shows that the long sediment core covers 6000 years of sedimentary history (Nakamura et al., 2012, 2016) and is punctuated by a series of 50 turbidites (Fig. S4.2; see supplementary data). Turbidites were identified on the basis of geochemical profiles obtained by XRF, visual description and enhanced photos (Fig. S4.2; see supplementary data and Ghazoui et al., 2018). We consider that all the major turbidites have been identified while it is likely that some turbidites of smaller sizes or too close one to another remain undeciferable. The 2σ (95% confidence level) uncertainty related to age depth model is presented in the Supplementary Information (Fig. S4.3). We also present the minimum and

maximum ages for each of the 50 turbidites (Tab. S4.1). The 50 turbidites within the sediment core are inferred to have been triggered by regional earthquakes (e.g. Ghazoui et al., 2018). Ghazoui et al. (2018) constrained the local shaking-intensity threshold to trigger a turbidite within Lake Rara slope as MMI>6, based on observed and modelled intensity maps. Such a threshold corresponds to earthquakes with a magnitude Mw ≥ ~6.5 within a 150- to 200-km distance range (Ghazoui et al., 2018; Fig. 4.1).

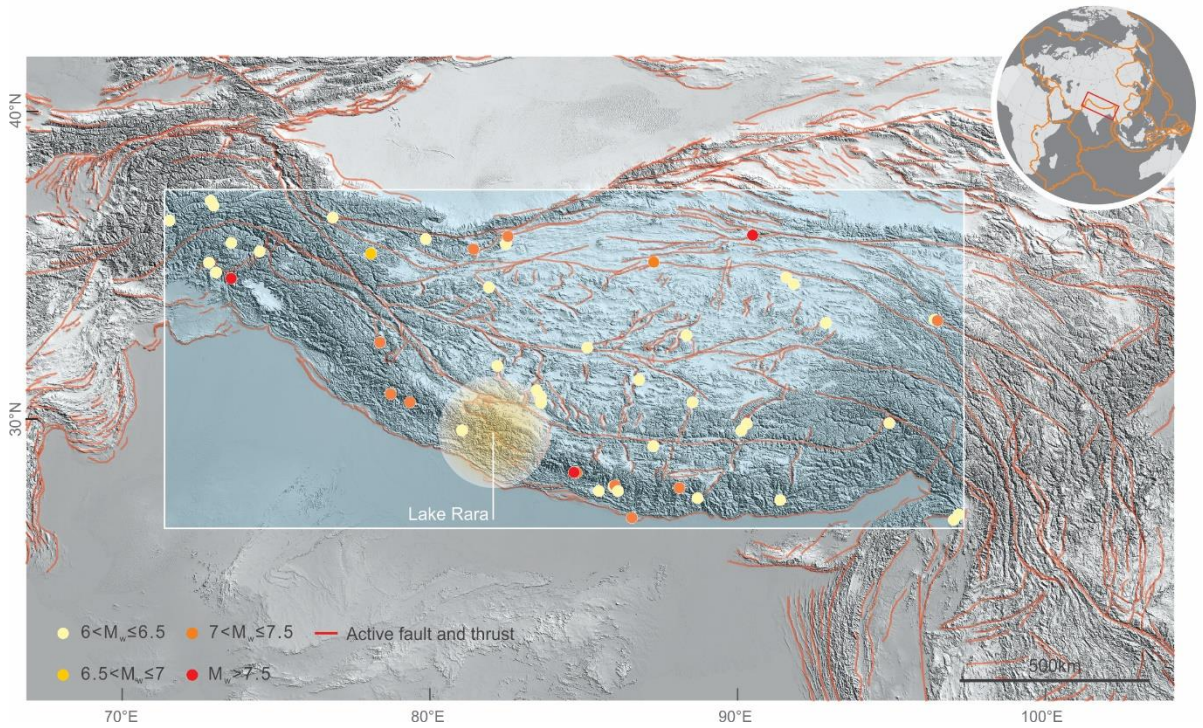

Figure 4.1. Map of the India-Asia collision zone with the 50 largest instrumental earthquakes recorded during the period 1974-2018 (from the USGS instrumental earthquake catalogue; colored according to magnitude). The yellow circle is the area seismically resolved by Lake Rara turbidites (see Ghazoui et al., 2018 for details). The blue box represents the selection area for the USGS instrumental earthquake catalogue. Orange lines are active faults.

To calibrate the ETT time series (Fig. 4.2a) against the patterns of instrumental seismic catalogues, we use the USGS regional seismicity catalogue (Fig. 4.1 and 4.2b); as extracted from a 26.68°N-37.03°N, 72.87°E-97.23°E box that covers the Himalayan range and most of Tibet (http://neic.usgs.gov/neis/epic/epic.html). In order to ensure magnitude completeness of the catalogue (e.g. Kagan and Jackson, 2010; Tahir and Grasso, 2014) and allow a quantitative comparison with the ETT catalogue, we selected the 50 largest events (7.9 ≥ Mw ≥ 6.1) occurring between 1974 and 2018 from this instrumental catalogue. We used the instrumental catalogue for combined statistical analyses and comparisons between time-series patterns of instrumental earthquakes and of ETT. Such a comparison between a regional (2300 × 1300 km^2) seismicity catalogue (Fig. 4.1) for a relatively short (44 years) duration and a local (~200 km radius) catalogue on a 6000 year time window is supported by (i) the classical ergodicity assumption for seismicity (e.g. Main, 1996; Anderson and Brune, 1999) and (ii) the scaling properties of earthquake dynamics (c.f., De Arcangelis et al., 2016). To compare quantitatively the two types of distribution we rescale the inter-event times by the mean inter-event time of each distribution (e.g. Sanchez and Shcherbakov, 2012; de Arcangelis et al; 2016; Fig. 4.2c).

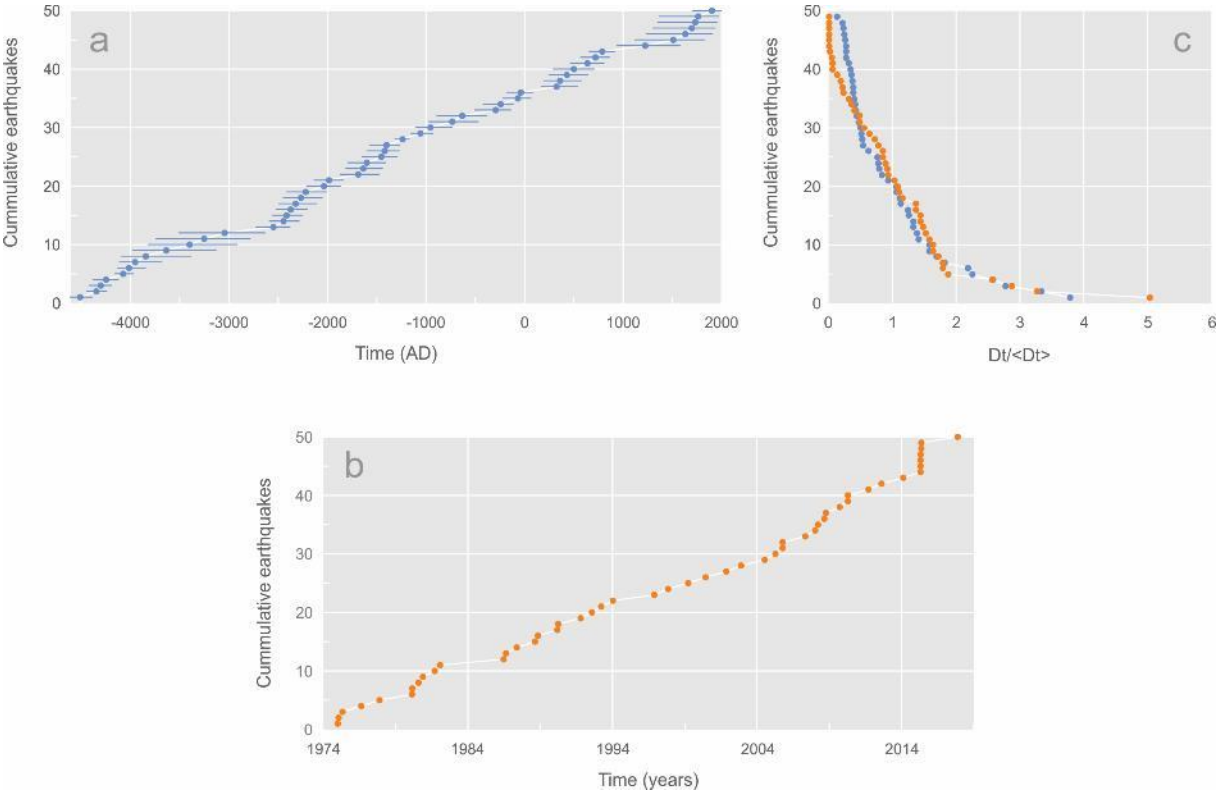

Figure 4.2. Cumulative number of earthquakes versus time. (**a**) The 50 events of the earthquaketriggered turbidite (ETT) catalogue. (**b**) The 50 largest events (M_w, 6.1-7.8) from the USGS instrumental earthquake catalogue. (**c**) Collapsed inter-event time distributions from both catalogues obtained by rescaling the inter-event times by the mean inter-event time of each distribution (orange dots: USGS instrumental earthquake catalogue; blue dots: ETT catalogue). Events are from the area defined in Figure 1.

4.3 Methods

Time distribution analysis. We aim to extract, from the turbidite time series, patterns that characterize the past 6000 years of seismicity around lake Rara, western Nepal. We analyse the inter-event time distribution to quantify the level of event interactions, i.e. whether the inter-event time distribution shows a clustered, periodic or Poissonian pattern (Fig. 4.3). Because of the relatively small number of available events (and because of the key importance of the interpretation of the time-series pattern) we use outputs from different techniques to constrain the type of inter-event time distribution we deal with and to increase the signal-to-noise ratio of the catalogue. For this purpose, we stack the time series (Fig. S4.4) in a superposed epoch analysis (e.g., Linde and Sacks, 1998; Lemarchand and Grasso, 2007: De Arcangelis et al., 2016) to resolve any possible clustering in turbidite series (Figs. 4.4 and S4.4).

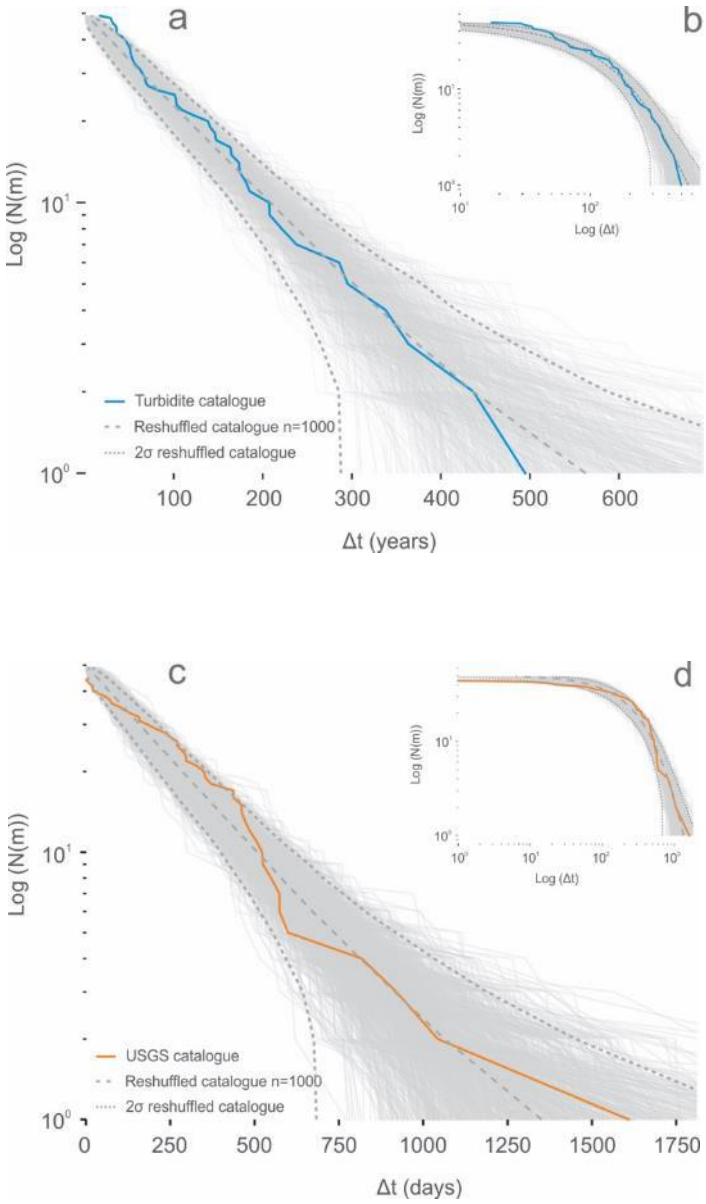

Figure 4.3. Plots of the cumulative distributions of earthquakes as a function of inter-event time. (**a**) Log-linear and (**b**) Log-Log plot for the ETT catalogue. (**c**) Log-linear and (**d**) Log-Log plot for the instrumental catalogue. Exponential distributions reproduce the data for both the ETT catalogue (**a, b**; blue curve) and the instrumental catalogue (**c, d**; orange curve). Grey bold lines are distributions from reshuffled data (n=1000). The dark grey dashed curves represent the 2σ (95%) confidence level of the exponential fit. The central dashed grey curve represents the absolute reference to the Poisson model. Note the presence of expected border effects exhibiting the resolution limit for very short time intervals for both the instrumental and ETT catalogues (Kagan, 2013).

Calibration. Using the USGS instrumental database and the statistical laws that drive earthquake interactions (i.e., Gutenberg-Richter, Omori's and Bath's laws) we aim to bound the ΔM value, i.e. the difference between the maximum recorded magnitude M_{max} and the threshold magnitude for recording M_c ($\Delta M = M_{max} - M_c$), that emerges from the turbidite time series. To increase the robustness of the analysis, we test the results against reshuffled catalogues (e.g. Kelly and Sear, 1984; Lemarchand and Grasso, 2007; Tahir et al., 2012). The

reshuffled catalogues are constructed by sampling at random with replacement (bootstrap procedure) 1000 sets of 50 event dates from both the instrumental and the ETT time series ("synthetic event catalogue"). The 1000 sets of synthetic catalogues (each with a 50-event size) are then analysed in the same manner as the real catalogues to assess the confidence levels for the real distribution.

Finally, we compare the inter-event time patterns resolved using our ETT catalogue to the distribution reported from other analyses of worldwide paleo-seismicity time series using the coefficient of variability (standard deviation/mean)

4.4 Results

The primary way to characterise the Δt distribution is based on the η ratio or coefficient of variability ($\eta = \sigma/\mu$; with σ, the standard deviation and μ the mean value; e.g., Cox and Lewis, 1976; Marzocchi and Zaccareli, 2006). Kagan and Jackson (2010) define a Poissonian (uncorrelated event) distribution as having a η=1, whereas distributions with η<1 are quasi-periodic to periodic and those with η>1 are defined as clustered. For the 50 ETT events, this ratio is smaller than unity (σ=123.84, μ=146.03, η=0.84), corresponding to an overall uniform distribution of event times. To first order, the η = 0.84 value rejects the possibility of event clustering (e.g., Cox and Lewis, 1976; Marzocchi and Zaccareli 2006). When interpreted in term of earthquake time series, this implies that the magnitude range of recorded earthquakes is too narrow to be able to record triggered seismic cascades (e.g. Hemlstetter, 2003; Traversa and Grasso, 2008; Tahir et al., 2012). We recover the same pattern from the 50 largest events of the instrumental catalogue (η=0.98).

These patterns are confirmed by testing the inter-event time distribution against reshuffled distributions (Fig. 4.3a). The observed series, for both the instrumental and the ETT catalogues, are consistent with a Poisson distribution at 2σ (95%) confidence level, as represented by the theoretical curve of the Poisson model (Fig. 4.3a and c). The Poisson distribution of the corresponding earthquake times supports these events to be primarily driven by the tectonic plate deformations, with a weak contribution of triggering by other earthquakes (e.g., Helmstetter et al., 2003; De Arcangelis et al., 2016). The fluctuation around the Poisson distribution (Figs. 4.3a and c), suggests there are correlated events in the series that may be driven by earthquake interactions (i.e. aftershocks). These patterns are identified both in the ETT and the instrumental catalogues.

In order to further constrain the clustered distribution for the smallest (correlated) inter-event times, we used superposed epoch analysis after each master event time (for a review, see De Arcangelis et al., 2016; Fig. S4.4). To avoid multiple interactions during cascading seismic cascades, we isolate master events that are followed by at least an event within a 150-year window for the ETT catalogue (e.g. Tahir et al., 2012). For these events, we resolved an increase in post-event rate, above the value of the reshuffled series (95 % confidence level), up to 300 years after the trigger events (Figs. 4.4a and S4.4a).
The analysis of inter-event time patterns in the ETT time series, using either the coefficient of variability (η) or inter-event time distributions, suggests that the turbidite time series is close to

a Poissonian series (Fig. 4.3a) to first order. It corresponds to an event catalogue where interactions are minor. Accordingly, this catalogue is equivalent to a seismic catalogue with dampened or filtered aftershocks. For validation, when using the same technique on the 50 largest events from the USGS instrumental catalogue, we recover similar patterns to those of the ETT catalogue. This finding provides further support to the inference that the turbidite catalogue records local slope response to the largest regional earthquakes (Ghazoui et al., 2018). Although these general analyses support independent event patterns, some second-order, non-poissonian patterns emerge. First, there is a change in average event rate over time (Fig. 4.4). These changes are not robust at the 2σ (95%) confidence level, as tested against reshuffled time series (Figs. 4.3a and c), but none of the 1000 random simulations reproduces the three changes of rate we observed over time. Second, superposed epoch analyses validate event clustering as resolved in the 50-300 years window. The same patterns are resolved on the USGS catalogue in the 100-400 days window. These patterns are robust at the 2σ (95%) confidence level against reshuffled series (Figs. 4.3a and c).

4.5 Discussion

The analyses of the inter-event times of the earthquake-turbidite catalogues support a global Poisson distribution of recurrence times (Fig. 4.3 and S4.4). This pattern rejects any periodic or quasi-periodic pattern for earthquake occurrence in this central Himalaya area for the past 6000 years. Within the global Poisson distribution we resolve fluctuations that we interpret to be driven by earthquake interaction, i.e. clustered earthquakes. These properties are recovered when using data from an instrumental catalogue (USGS, 1974-2018) that extends throughout the Himalayan arc and with the same number of largest events (Fig. 4.2c─4.4 and S4.4).
All the analyses of time patterns support the ETT catalogue, and its related Poisson inter-event time distribution, to be a proxy for a regional earthquake catalogue in which only the largest events are recorded. It corresponds to a catalogue with a small number of aftershocks, i.e., with a small magnitude range ($\Delta M \leq 2$) between the maximum magnitude of the catalogue (M_{max}) and the threshold magnitude value for completeness (M_c; e.g., Helmstetter and Sornette, 2003; De Arcangelis et al. 2016). While it is not possible to relate each of the turbidite event to a given magnitude, we tentatively quantify the magnitude range value, $\Delta M = M_{max}\text{-}M_c$, for the ETT catalogue.

As a first-order value, a ΔM calibration emerges from the overlap between the observed time patterns in the M_w 6.1-7.8 USGS catalogue and the ETT time series (figure 4.2c). Because the aftershock (triggered earthquake) number and inter-event time patterns both scale with the magnitude range ΔM of a given catalogue (for a review, see De Arcangelis et al., 2016), our results support the turbidite dataset to mimic an earthquake time series with a rough estimate of $\Delta M \approx 2$. With the estimate for M_{max} in the range 8.2-8.4 (1505 western Nepal earthquake; e.g., Ambraseys and Jackson, 2003; Bilham and Ambraseys, 2005; Kumar, 2010; Stevens and Avouac, 2016), the recording limit of the ETT catalogue would thus be in the range M_c=6.2-6.4; consistent with our earlier estimates (Ghazoui et al., 2018) based on modelling shaking intensities of know earthquakes at the lake.
Complementary to this global interpretation, the use of superposed epoch analyses allows us to extract correlated events for small inter-event times, i.e. within 150 years from the trigger events

recorded in the 6000 years long turbidite series (Fig. 4.4). Correlated events are similarly resolved, on the 44 years long USGS instrumental catalogue, within 420 days from the trigger events (Fig. 4.3, 4.4 and S4.4).

Similarly to the USGS instrumental catalogue, we characterize the ETT catalogue as a succession of 12 seismic cascades (event interaction). Prior to these seismic cascades, quiescence periods exist in the 100-700 yr range (Tab. S4.2─4.3 and Fig. 4.4a). The inter-event times between the 12 seismic cascade onsets (i.e. the recurrence rate of the largest trigger events) are in the 200-1200 yr range. The largest (1200 yrs) inter-event time highlight how the wide range of possible *dt* values may bias recurrence interval estimates when the number of data is small.

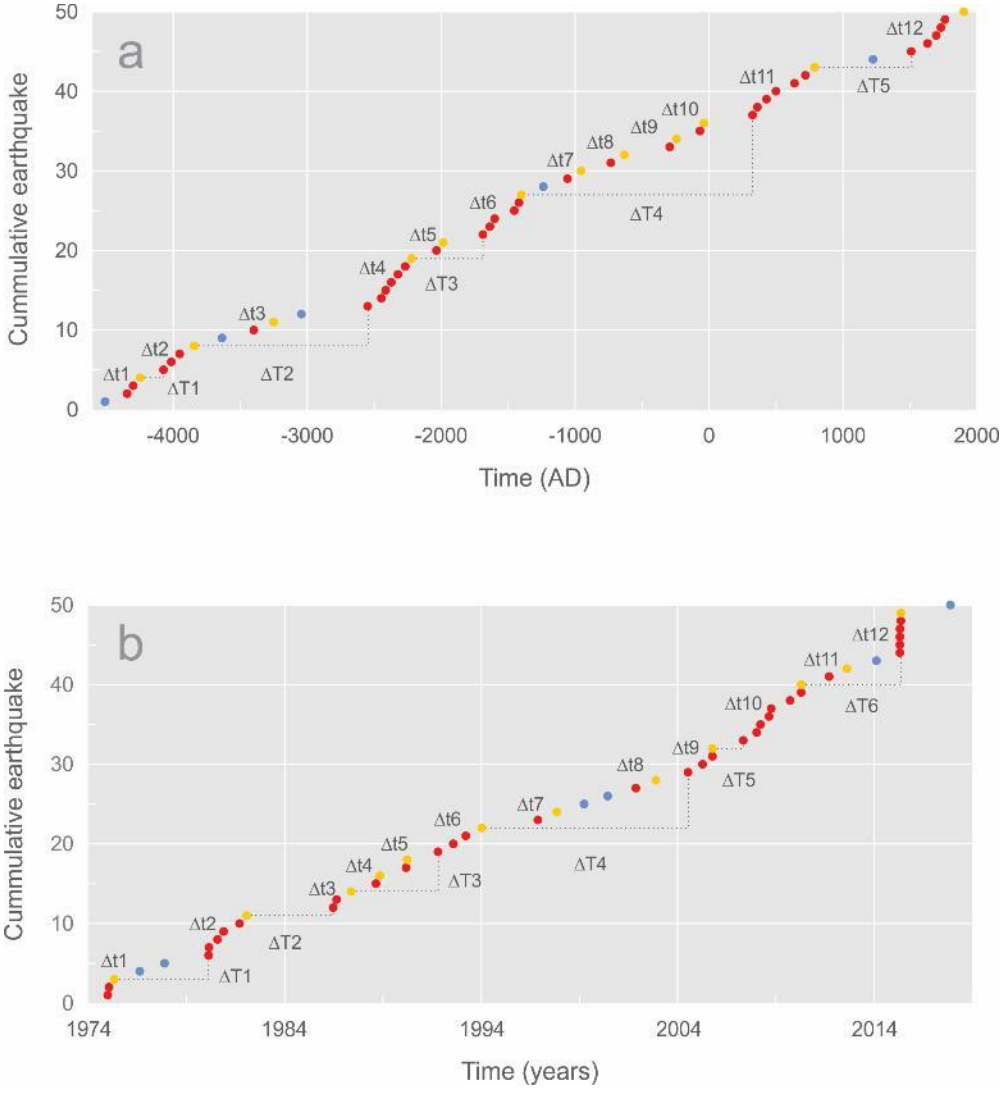

Figure 4.4. Cumulative number of earthquake as a function of time for (a) the earthquake turbidite catalogue and (b) the USGS instrumental earthquake catalogue. Red dots are events that are part of a seismic sequence. Yellow dots define the end of the sequence. The sequences are defined by subsequent events with inter-event times (dt) < 148 y (**a**) or (dt) < 422 days (**b**). The Δt_x and ΔT_x values correspond respectively to the duration of a sequence and the inter-sequence time, and are summarized in Tables S1 and S2.

When we compare our overall Poissonian distribution with existing worldwide paleo-seismic time series for earthquake seismic cascades (Fig. 4.5), there is a strong correlation between the number of recorded events and η. These observations emphasize that the larger the number of recorded event in a series, the more uniform the observed time distribution (i.e. no periodicity). When the number of events in a dataset increases (Fig. 4.5), the observed time pattern moves from a periodic or quasi-periodic organization (η<1) to Poisson-like and clustered patterns, as η=1 to η>1 respectively. These results question (i) the robustness of analyses based on small datasets (as tested against the sample size) and,(ii) the link between local, single-fault slip patterns that appear with possible periodic patterns, and the earthquake slip patterns driven by fault interactions that emerge with a uniform inter-event time distribution at a regional scale.

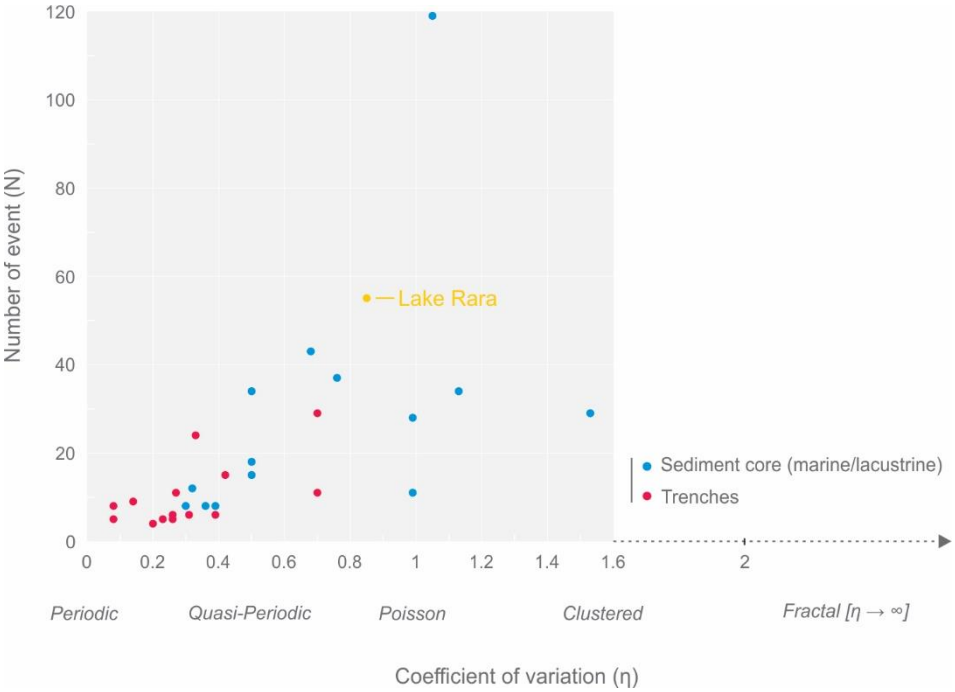

Figure 4.5. Comparison of the number of events (N) versus the coefficient of variation (η) from worldwide paleoseismic records. We compile data from a previous study (Sykes and Menke, 2006) and implemented data from lacustrine to coastal sites. The different types of seismic behavior defined by the coefficient of variation (η) are indicated below the x-axis.

4.6 Conclusion

Our turbidite catalogue demonstrates that 12 major events, which correspond to those identified as the triggers of aftershocks sequence occurred in western Nepal over the last 6000 yrs. Their associated magnitudes must be in the upper bound of the ΔM estimated for the turbidite catalogue (Fig. 4.1), i.e. around Mw=8. The reported evidence for correlated events (i.e. triggered successive events of comparable sizes) argue that clustered events as seismic seismic cascades or event pairs, (e.g. the 1833-1934 Nepal sequence) are not rare occurrences in the Himalaya.

In the Himalyan context we cannot reject that the temporal Poissonian distribution of earthquakes on a 6000 yrs duration does fit the observed patterns from instrumental catalogue of 44 yrs duration. The two-time distributions are driven by Poissonian processes on the first

order and on the second order by clusters of correlated events, thereby rejecting the model of cycles and quasi-periodicity that is advanced by numerous paleo-seismology studies. This suggests a paradigm shift that is of the utmost importance for Himalayan countries in view of the socio-economic challenges posed by the impact of the next major earthquake. In terms of seismic hazard, our results attest that the occurrence of major earthquakes is as uncertain as for moderate to small earthquakes, whatever the time scales, leaving Himalayan countries on a permanent threat.

On the global scale, this study bridges the gap between analyses based on instrumental seismic catalogues (large numbers of recent earthquakes) and catalogues based on paleo-seismology data (small number of historical earthquakes on large time scales). It points to possible biaises that may emerge from small data sets as used in paleoseismological studies. Applying instrumental statistical seismology methods to paleo-seismology data validates the necessary complexity in any conceptual seismic cycle dogma, with significant consequences for seismic risk and hazard assessment.

4.7 Supplementary Information

Supplementary Text

Identification of turbidite layers. Some turbidites were already identified by Nakamura et al. (2016). For this study, their record was revisited based on the multiproxy results of Ghazoui et al. (2018), who made use of a series of sedimentological and geochemical criteria to identify turbidites in short cores from the same lake. In Ghazoui et al. (2018), turbidite identification was based on grain size, magnetic susceptibility, Ti concentrations, bulk organic geochemistry and radio-density. In the present study, the turbidites ewere identified by their coarse base and a fining-upward sequence of fine sand to very fine silt, in sharp contact with the underlying background mud. As it has been shown that Ti concentrations reflect silt content in sediments (Cuven et al., 2010; Bertrand et al., 2012) and in the continuity of our previous study on Lake Rara (Ghazoui et al., 2018) we used the Ti/Ca ratio as a turbidite proxy. We calibrated our observations with the descriptive log of Nakamura et al. (2016) and an enhanced core photo (Fig. S1). This enhancement consists of calibrating the white value of the rightest mica layers, to facilitate the identification of the turbidite layers.

Age model. A chronology for the Lake Rara long sediment record was established on core RA09-04 by radiocarbon dating (see Nakamura et al., 2016 for the complete procedure). Samples for radiocarbon dating were picked outside of the turbidites, as these are considered to be instantaneous deposits (Nakamura et al., 2016). All ages were recalibrated using the calibration curve for Northern Hemisphere terrestrial ^{14}C dates IntCal13 (Reimer et al., 2013), and a new age-depth model (Fig. S4.2) was produced using Bacon 2.2 (Blaauw and Christen, 2011) after removal of the turbidites.

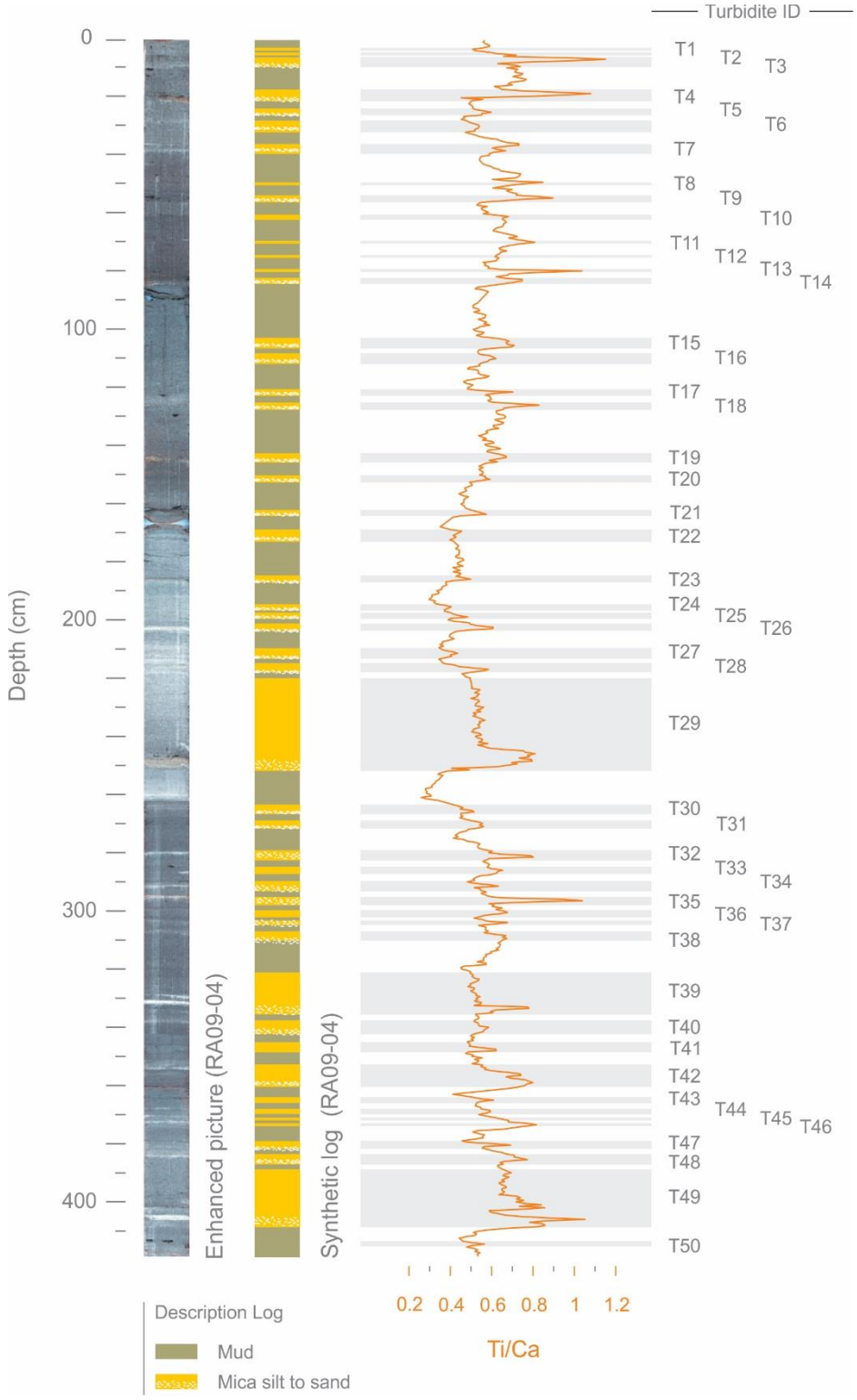

Supplementary Figure 4.1. Sediment core RA09-04. From left to right are shown: an enhanced core photo, a synthetic log, XRF Ti/Ca ratio profile and the turbidite identification.

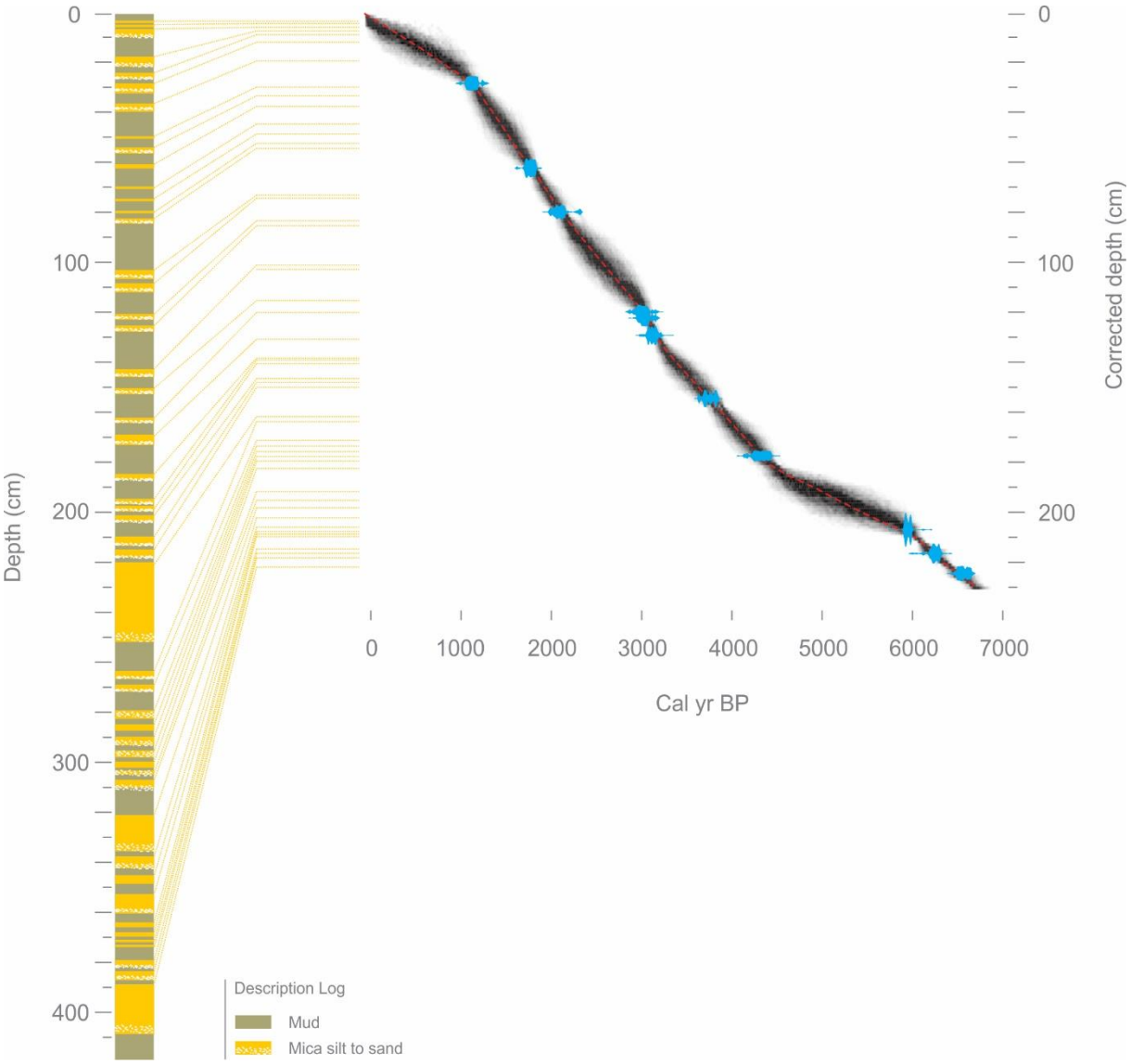

Supplementary Figure 4.2. Bacon age-depth model for core RA09-04. The corrected depths were calculated by removing instantaneous event deposits (turbidites) from the total depths in order to apply a continuous model in Bacon. Grey levels on the age-depth curves represent confidence levels. The red dashed line represents the overall best fit. Yellow dashed lines represent the projection of the turbidites on the age-depth models.

ID	n_events	Start of sequence (yr. AD)	End of sequence (yr. AD)	Δt_X (Duration; yr.)	ΔT_X (Gap; yr.)	ΔT_X * (yr.)
1	3	-4344	-4246	98	173	173
2	4	-4073	-3843	229	444	1294
3	2	-3398	-3251	147	702	531
4	7	-2548	-2220	328	185	1725
5	2	-2034	-1983	51	295	722
6	6	-1688	-1401	287	344	
7	2	-1056	-954	102	221	
8	2	-733	-632	101	338	
9	2	-293	-241	52	173	
10	2	-68	-38	29	363	
11	7	324	787	462	722	
12	6	1509	1902	392		

Supplementary Table 4.1. Synthetic table of the selected events defining a sequence for the earthquake turbidite catalogue based on a Dtmax <148 years. Δt_x is the duration of a sequence. ΔT_x is the intersequence time. ΔTx^* is the intersequence time not taking in to account the pairs of events during the stationary activity or quiescence.

ID	n_events	Start of sequence (days)	End of sequence (days)	Δt_X (Duration; days)	ΔT_X (Gap; days)	ΔT_X * (days)
1	3	0	120.9	120.9	4.801	4.801
2	6	1873.4	2583.2	709.8	4.407	4.408
3	3	4192.2	4523.5	331.3	1.262	4.426
4	2	4984.4	5060.5	76.1	1.330	10.506
5	2	5546.3	5566.1	19.7	1.570	1.572
6	4	6139.3	6953.5	814.1	2.856	5.033
7	2	7996.9	8350.9	353.9	4.018	
8	2	9817.8	10189.3	371.5	1.641	
9	4	10788.4	11241.9	453.4	1.572	
10	8	11815.8	12890.5	1074.6	1.431	
11	2	13413	13741.9	328.9	2.700	
12	6	14727.7	14744.8	17.1		

Supplementary Table 4.2. Synthetic table of the selected events defining a sequence for the instrumental USGS catalogue based on a Dtmax <422 days. Δt_x is the duration of a sequence. ΔT_x is the intersequence time. ΔTx^* is the inter-sequence time value by not taking in to account the pairs of events during the stationary activity or quiescence.

Chapter 5

Correlation between Holocene climate changes and global seismicity

Zakaria Ghazoui [1, 2], Jean-Robert Grasso [1], Corentin Caudron [2], Flor Vermassen [3], Sebastien Bertrand [2] and Peter van der Beek [1]

[1] Université Grenoble Alpes, CNRS, Institut des Sciences de la Terre (ISTerre), Grenoble, France.
[2] Department of Geology, Ghent University, Ghent, Belgium.
[3] Natural History Museum of Denmark, University of Copenhagen, Copenhagen, Denmark.

In preparation for *Geophysical Research Letters*

Until now, physical explanations of presumed seismic periodicity can only be speculated and the proposed mechanisms are the source of heated debate and controversy. They include the mutual triggering of earthquakes through different mechanisms of stress transfer, the existence of tectonic pulses, as well as the control of seismicity by processes that are external to the geosphere. Studies on climate-earthquake relationships have so far been conducted at the decadal to multidecadal, rather than centennial to millennial, timescales. Here, we compiled previously-published paleoseismic records covering the Mid and Late Holocene and we compared our global catalog with paleoclimate reconstructions. Results show that records from paleoseismic trenches show the same clustering as sediment-based records, without any significant differences between the Northern and Southern Hemispheres. Our results suggest that interhemispheric seismic clustering is driven by non-random processes at 99% confidence. Comparison between paleoseismological data and paleoclimatological records highlights a relationship between neoglacial periods and peaks in world seismic rates. This observation is in line with numerous existing studies on loading and unloading of the Earth's crust by climatic forcing, but this relation is shown here for the first time on a global scale. If confirmed, it will have important implications for seismic hazard assessment in our current rapidly changing climate.

5.1 Introduction

The response of faults to climate-driven changes in ice and water volumes on the Earth's surface poses a challenging and unique question. The lithosphere is far from an isolated entity and interacts with other components of the Earth system, such as the hydrosphere and the atmosphere in complex and often unexpected ways. Over the last 20 years, considerable efforts have been made to decipher the potential interplay between climate change and deformation of the earth's crust (e.g. Gao et al., 2000; Heki, 2003; Liu et al., 2009; Hampel et al., 2010; Godard and Burbank, 2011; Ader and Avouac, 2013; Bollinger et al., 2014; Scafetta et al., 2015; Craig et al., 2017). Recent breakthroughs, both in paleoseismology with the discovery of high-resolution sedimentary records spanning more than 6000 years of seismic history (Goldfinger et al., 2013; Gomez et al., 2015; Moernaut et al., 2017; Rubin et al., 2017; Ghazoui et al., 2018) and in paleoclimatology, have paved the way for studies aimed at improving our understanding of the dynamics of, and potential coupling between, earthquakes and climate. However, the study of the interaction between climate and the occurrence of earthquakes on timescales that extend beyond instrumental measurements is very delicate. Both dating biases and insufficient geographical coverage may lead to spurious interpretations.

Here, we compiled previously-published paleoseismic records covering the Mid and Late Holocene and we compared our stacked catalogue with paleoclimate reconstructions In doing so, we attempt to assess whether there is a relation between seismic activity and climate variability on multi-millennial timescales, and we discuss the possible forcing mechanisms.

5.2 Data and analysis

In an effort to establish whether an earthquake-climate global link exists at centennial to millennial timescales, we merged results from diverse paleo-seismological studies, taking into account only those catalogues that have a complete coverage and excluding instrumental

earthquakes to avoid over-representativeness. We decided not to take into account the existing NOAA Significant Earthquake database and the Centennial Earthquake catalogue as they go back only to 2150 BP. The paleo-earthquake catalogues were derived from paleo-seismic studies constraining rupture timing either directly (i.e. trenches) or via proxy records (i.e. tsunami deposits and lacustrine/marine turbidites). In order to increase the generality of our study, we compiled catalogues with a variety of fault types, including normal, strike-slip and reverse faults, as well as subduction interfaces. For each of the 45 available catalogues, we applied a series of selection criteria. These include: (1) each of the selected events and catalogues are independent of each other; (2) : each catalogue covers at least the last 7000 years (i.e., starts at or before 5000 yr BP); (3) a precise description of the sites is present including a paleo-seismic log, (4) a robust dating method and/or age model was used (minimum 10 radiocarbon data points for the last 5000 years). In all cases, we used the age-depth models published in the original articles. As a result, 31 catalogues (Table 1), comprising a total of 500 earthquakes, met our selection criteria. All catalogues were cut off at 5000 yr BP due to the very limited amount of data available before that period. Our combined catalogue therefore covers 5000 years of seismic history (from 5000 cal. yr. BP to 1992 AD) from 40°S to 61°N latitude (Fig. 5.1).

The vast majority of these archives are located near the convergent plate boundaries around the Pacific, with additional catalogues for the India/Asia and Mediterranean convergent plate boundaries (Fig. 5.1). Very few catalogues represent the polar regions (i.e., 90°S–60°S and N) and most of the catalogues are located between latitudes 30°S and 50°N. The western USA has the highest concentration of paleo-seismic trenches (Fig. 5.1). This seismic catalogue distribution is skewed toward the Northern Hemisphere, because of the number studies undertaken as well as the Southern Hemisphere is Ocean dominated. However, seismic catalogues derived from marine and lake-sediment cores partially compensate the geographical bias (Fig. 5.1).

Figure 5.1. Global distribution of the selected paleo-seismic sites. Blue crosses are the locations of marine/lacustrine records. Yellow crosses are the locations of paleo-seismic trenches.

Fault type	Record type	Country	Fault zone	Segment	Site	Reference
Strike-Slip	Trench	USA	San Andreas	Mendocino	Petrolia	Merrits, 1996
Strike-Slip	Trench	Japan	Tanna		Myoga	Okada and Ikeda, 1991
Strike-Slip	Trench	Japan	Okaya			Okada and Ikeda, 1991
Normal	Trench	USA	Wasatch	Brigham City	Brigham	McCalpin and Nishenko, 1996
Normal	Trench	USA	Wasatch	Weber	Various	McCalpin and Nishenko, 1996
Normal	Trench	USA	Wasatch	Salt Lake City	Various	McCalpin and Nishenko, 1996
Normal	Trench	USA	Wasatch	Provo	Various	McCalpin and Nishenko, 1996
Normal	Trench	China	Helen Mtns			Qidong and Yuhua, 1996
Normal	Trench	Italy	Ovindolli-Peza			Pantosti et al., 1996
Normal	Trench	Italy	Irpinia		Piano di Peccore	Pantosti et al, 1996
Normal	Trench	USA	S. Crater Flat		Yucca Mountain	Pezzopane et al., 1996
Normal	Trench	USA	Paintbrush Canyon		Midway Valley	Pezzopane et al., 1996
Normal	Trench	USA	Stagecoach Road		Yucca Mountain	Pezzopane et al., 1996
Normal	Trench	USA	Windy Wash		Yucca Mountain	Pezzopane et al., 1996
Normal	Trench	USA	Star Valley		Afton	McCalpin, 1993
Normal	Trench	Russia	Tunka		Arshan	McCalpin and Khromovskikh, 1995
Reverse	Trench	USA	Reelfoot			Kelson et al., 1996
Reverse	Trench	China	Dushanzi			Qidong et al., 1996
Reverse	Trench	China	Manas			Qidong et al., 1996
Reverse	Trench	Japan	Atotsugawa		Miyagawa	Okada et al., 1989
Subduction	Trench	USA	Alaska	Prince William Sound	Copper River Delta	Plafker and Rubin, 1994
Subduction	Trench	USA	Alaska	Prince William Sound	Middleton Island	Plafker and Rubin, 1978
Subduction	Trench	USA	Cascadia. S		Humboldt Bay	Carver et al., 1994
Subduction	Trench	USA	Cascadia. S		Petrolia terraces	Merrits, 1996
Subduction	Trench	USA	Cascadia. N		Sea Channels	Adams and Weichert, 1994
Subduction	Trench	New Guinea			Huon Peninsula	Ota and Chappell, 1996
Subduction	Turbidite	USA	Cascadia		Various	Goldfinger et al., 2012
Subduction	Tsunamite	Indonesia	Sumatra-Andaman		Various	Patton et al., 2015
Subduction	Turbidite	New Zealand	Hikurangi. N		Various	Pouderoux et al., 2014
Various	Turbidite	Chile	Various		Lake Rinihue	Moernaut et al., 2018
Various	Turbidite	Nepal	Various		Lake Rara	Ghazoui et al., 2018

Table 1. Selected paleo-seismic records included in our global catalogue.

In order to characterize our combined catalogues, we have distinguished the earthquakes identified from trenches from those identified based on tsunami deposits and marine/lacustrine sediment cores (Fig. 5.2). For this purpose, we used the median radiocarbon age of each event and counted the number of events using within a time window varying between 100 and 400 years (Fig. 5.2). When interpreting the results, one has to keep in mind the uncertainties inherent to radiocarbon dating and age-depth modeling. Although we set a minimum number of radiocarbon ages as a selection criteria, some records are much better dated than others.

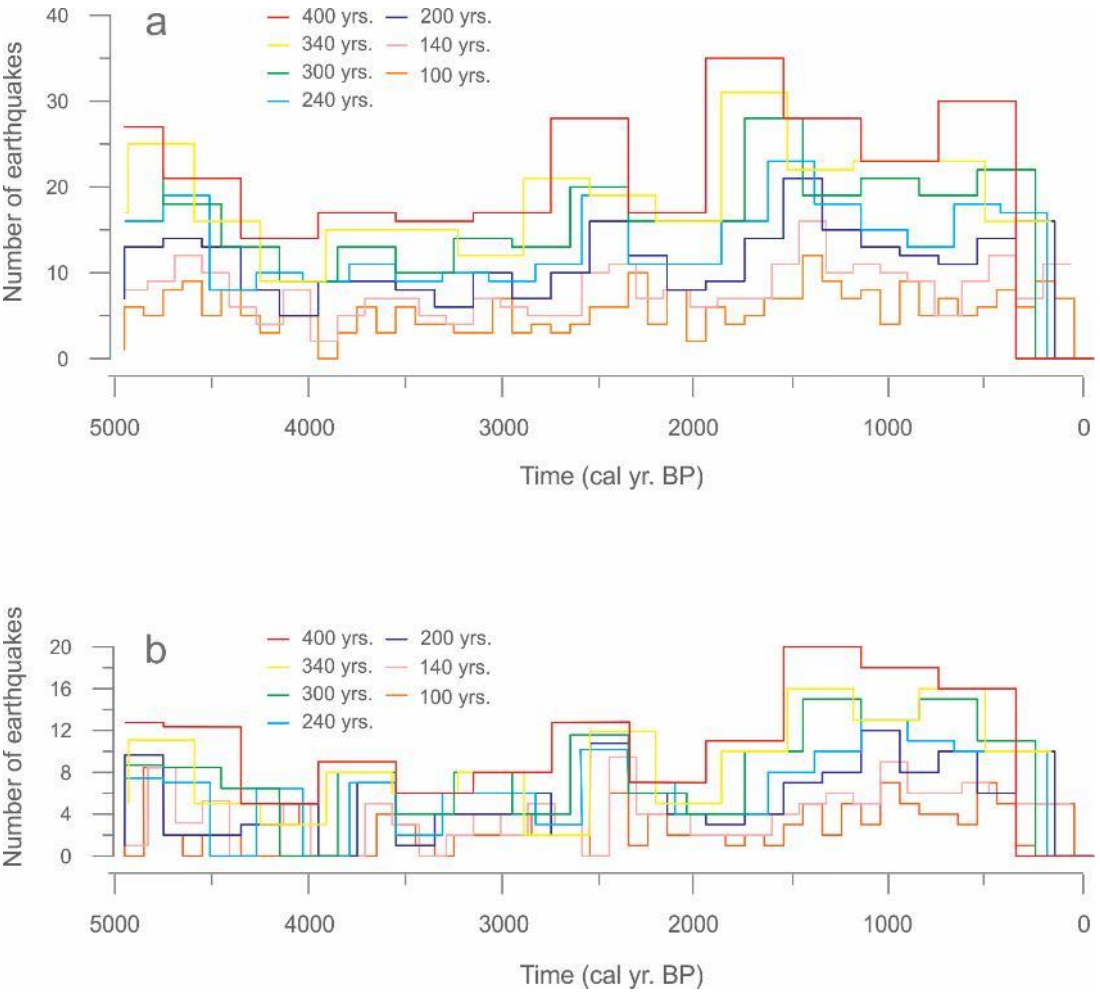

Figure 5.2. Distribution of earthquakes during the last 5000 years for different time bins between 100 and 400 years. (**a**) Events inferred from tsunami deposits and marine/lacustrine sediment cores. (**b**) Events inferred from paleo-seimic trenches

5.3 Potential regional variations in temporal distributions

A first significant observation is the similar temporal clustering of the trench-based and sediment-based catalogues (Fig. 5.2). Four clusters are identified: 5000 to ~4200 cal yr BP, ~3900 to ~3500 cal yr BP, ~2700 to ~2300 cal yr BP and ~1800 to ~400 cal yr BP (Fig. 5.2). The sub-catalogue including only events inferred from tsunami deposits and sediment cores (Fig. 5.2a) shows a higher number of recorded earthquakes than the trenches (Fig. 5.2b). One reason might be the higher recording sensitivity of sediment cores (e.g., Gomez et al., 2015), allowing them to capture earthquakes of lower magnitude than trenches. Another major difference is that trenches only record the seismicity of a particular fault segment, whereas the sediment record includes more distant earthquakes from a potentially larger number of faults.

A noteworthy observation is the apparent synchronicity of event clustering in the catalogues from both the Southern and Northern hemispheres as well as for trenches and marine/lacustrine records (Fig. 5.3).

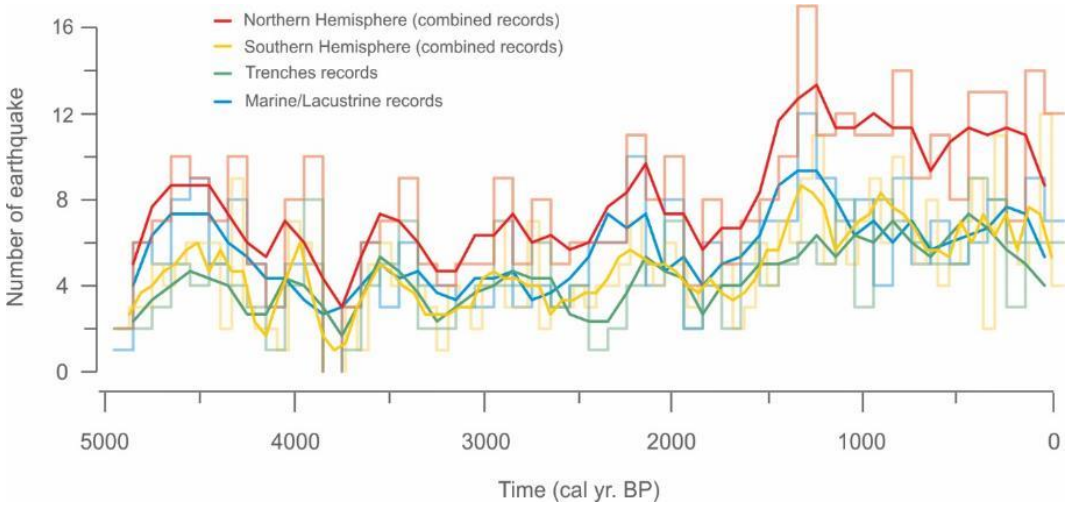

Figure 5.3. Distribution of earthquakes during the last 5000 years with a time bin of 100 years. The thick colored lines are the 5pt-moving average of the histograms.

Nevertheless, this apparent clustering could be insignificant due to under-sampling or may be dominated by a higher proportion of events present in a particular catalogue, altering the general trend. Therefore, we have divided our data regionally into two catalogues, one combining all the records from marine and lacustrine environments from the Pacific, the other combining the rest of the geological archives around the world (Fig. 5.4). We use 400-year time bins to count the occurrence of events to reduce the uncertainty associated with dating methods. The earthquake clustering during the Holocene remains and is significant at the 1σ confidence level for both catalogues (Fig. 5.4). As these different subdivisions of our catalogues show synchronized variations in earthquake probability and highlight the same patterns, we feel confident to merge them into a single global catalogue.

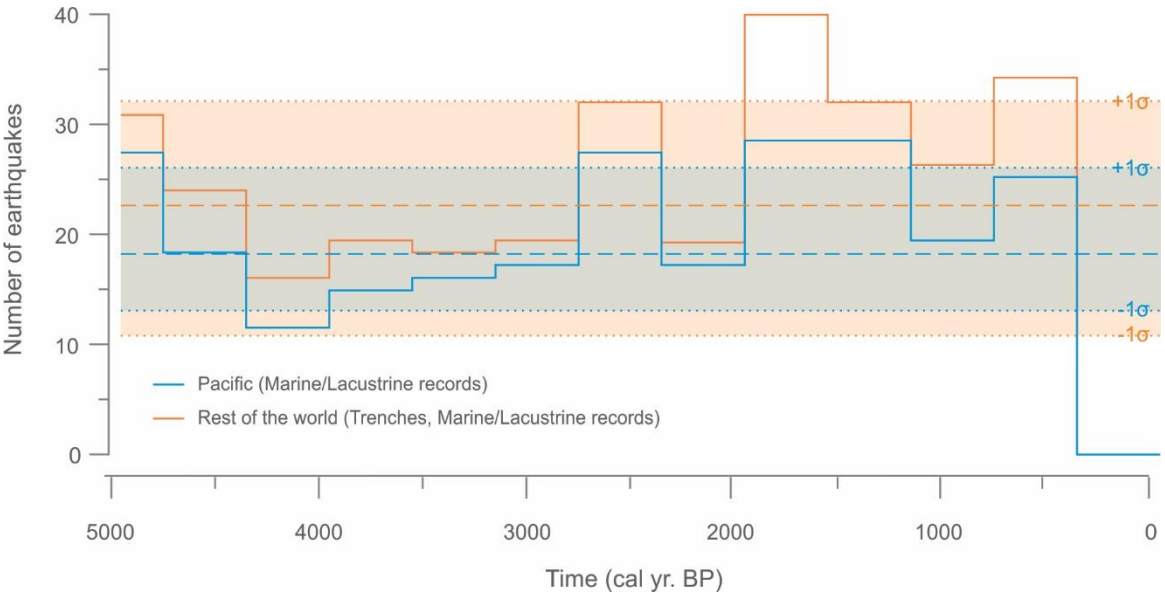

Figure 5.4. Discriminated comparison of catalogues for different regions of the world. The blue and orange lines show counts of earthquakes for a catalogue combining mixed marine/lacustrine records from the Pacific and the rest of the world, respectively (trenches, marine and lacustrine), grouped into 400-year time bins. The dashed colored lines are the means of each catalogue, whereas the dotted colored lines illustrate the 1σ (66%) confidence level of the means.

5.4 Holocene paleo-seismicity clustering

In order to determine whether the temporal distribution of seismic events in our merged catalogue follows a periodic or random pattern, we analyzed the Schuster spectrum of the catalogue (Fig. 5.5) following the methodology used by Ader and Avouac (2013). The method is based on the Schuster test (Schuster, 1897), initially developed to assess the tidal modulation of earthquakes: to verify the potential periodicity at a time period T, the k^{th} earthquake in the catalog occurring at time t_k is represented as a unit step in the direction defined by the phase angle $\theta_k = 2\pi t_k/T$. Following N steps, with N the number of earthquakes present in the catalog, the distance to the origin is expressed by:

$$D^2 = \left(\sum_{k=1}^{N} \cos\theta_k\right)^2 + \left(\sum_{k=1}^{N} \sin\theta_k\right)^2$$

Hypothesizing a random and uniform distribution of earthquakes, the probability of encountering a distance D is $p = e^{-D^2/N}$. If $p < \alpha$ the uniform event-distribution hypothesis is rejected at a confidence level $(1-\alpha)$. According to Ader and Avouac (2013), such a condition is necessary but not sufficient to establish periodicity at a period T, because non-uniformity detected by the Schuster test can be induced by a brief and intense seismic outburst occurring at any time (Bragato, 2017). It is recommended (Ader and Avouac, 2013) to consider the whole Schuster spectrum (i.e. p-values computed for a range of time periods): significant sinusoidal periodicity refers to a restricted maximum in the spectrum. Stricter limits are imposed for the probability p in order to guarantee a specified confidence level: Periodicity is confirmed above the $(1-\alpha)$ confidence level if $p < \alpha T/T_{tot}$ (T_{tot} representing the whole observation period) instead of $p < \alpha$, as required by the original test.

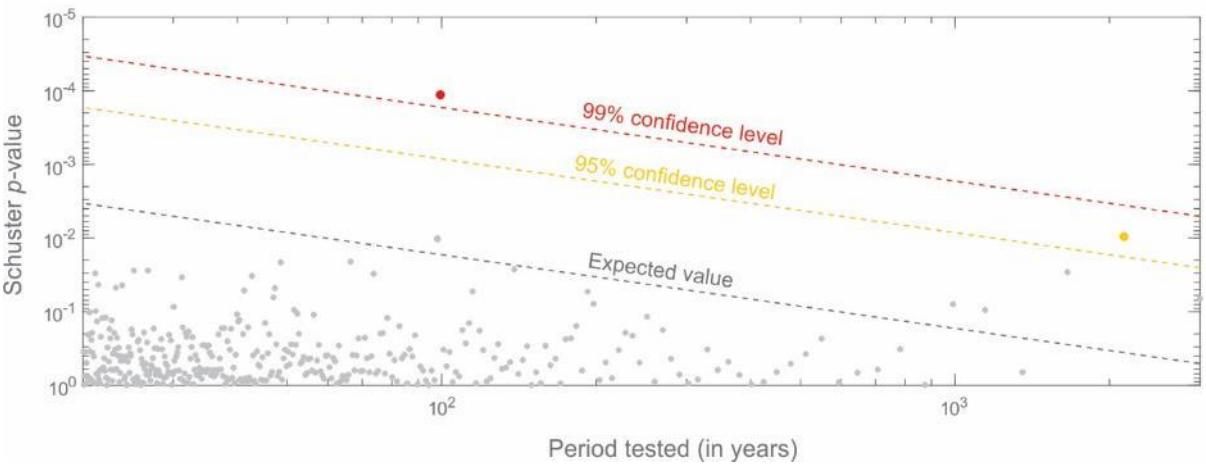

Figure 5.5. Schuster spectrum for the global catalogue in the time range 5000 cal. yr. BP – 1992 AD. Red dashed line is the 99% confidence level. Yellow dashed line is the 95% confidence level and the grey dashed line is the expected value

We computed the Schuster spectrum using the Matlab script of Ader and Avouac (2013) for the global catalogue in the time range 5000 cal yr BP – 1992 AD, exploring periods of oscillation between 20 and 3000 years (Fig. 5.5). The spectrum highlights two marked periodicities at 100 years, which is significant at the 99% confidence level, and at 2000 years, significant at the 95% confidence level. According to the Schuster test, we can discard the null hypothesis that this is a result of a random process at the 99% confidence level for the 100 yr periodicity and at 95% confidence for the 2000 yr periodicity. Nevertheless, a limit of the Schuster-spectrum approach is that increasing the number of periods T for which the Schuster test is performed makes it easier to obtain a low p-value in at least one test by chance (Bragato, 2017).

5.5 Discussion

5.5.1 Correlation with other natural periodic phenomena

In the light of the apparently significant periodicities of 100 and 2000 years in the global earthquake catalogue, we looked for natural processes having the same periodicity. The apparent global synchronicity in the catalogues suggests that the periodicities reflect climatic rather than tectonic forcing.

Bond et al. (2001) demonstrated solar influence on North-Atlantic climate throughout the Holocene, through the control of solar flux on surface winds and surface-ocean hydrography in the sub-polar North Atlantic. They found a close correlation between changes in production rates of cosmogenic nuclides (^{14}C and ^{10}Be) and temporal changes outlined by proxies of ice debris (IRD) measured in Greenland marine sediment cores, from the centennial (100-200 years) to the millennial (1470 ± 500 years). Atmospheric circulation over Greenland changed abruptly around the same time (Bond et al., 2001).

Supported by observations throughout the Holocene and in multiple locations, Obrochta et al. (2012) advanced a complex cycle model, including a combination of cycles of about 1000 and 2000 years rather than a cycle of ~1500±500 years. Since our paleo-seismic catalogue is global (Figs. 5.1 to 5.3) and as Bond et al. (2001) study is limited to the Northern Hemisphere, conceptually, it can't explain the periodicity that we see in our catalogue. Because of that, we searched for climate signals that are not limited to one hemisphere in an attempt to unravel the potential drivers of the temporal paleo-seismic clustering through the Mid-Holocene. We also justify this decision as the periodicity of a 100-year period could be misleading but would reflect an analytical bias due to under-sampling. Most of the climatic variability over the Mid and Late-Holocene is registered on land as neoglaciations, or periods of glacial advance that are smaller in extent than full-scale glaciations (e.g. Wanner et al., 2011; Solomina et al., 2015). We compared our merged catalogue with proxies reflecting the different neoglacial stages (Fig. 6; Schaefer et al., 2009 and reference therein) from the Northern and Southern Hemispheres, as well as to a global reconstruction of glacial advances (Wanner et al., 2011; Solomina et al., 2015) and of total solar irradiance (Steinhilber et al., 2009).

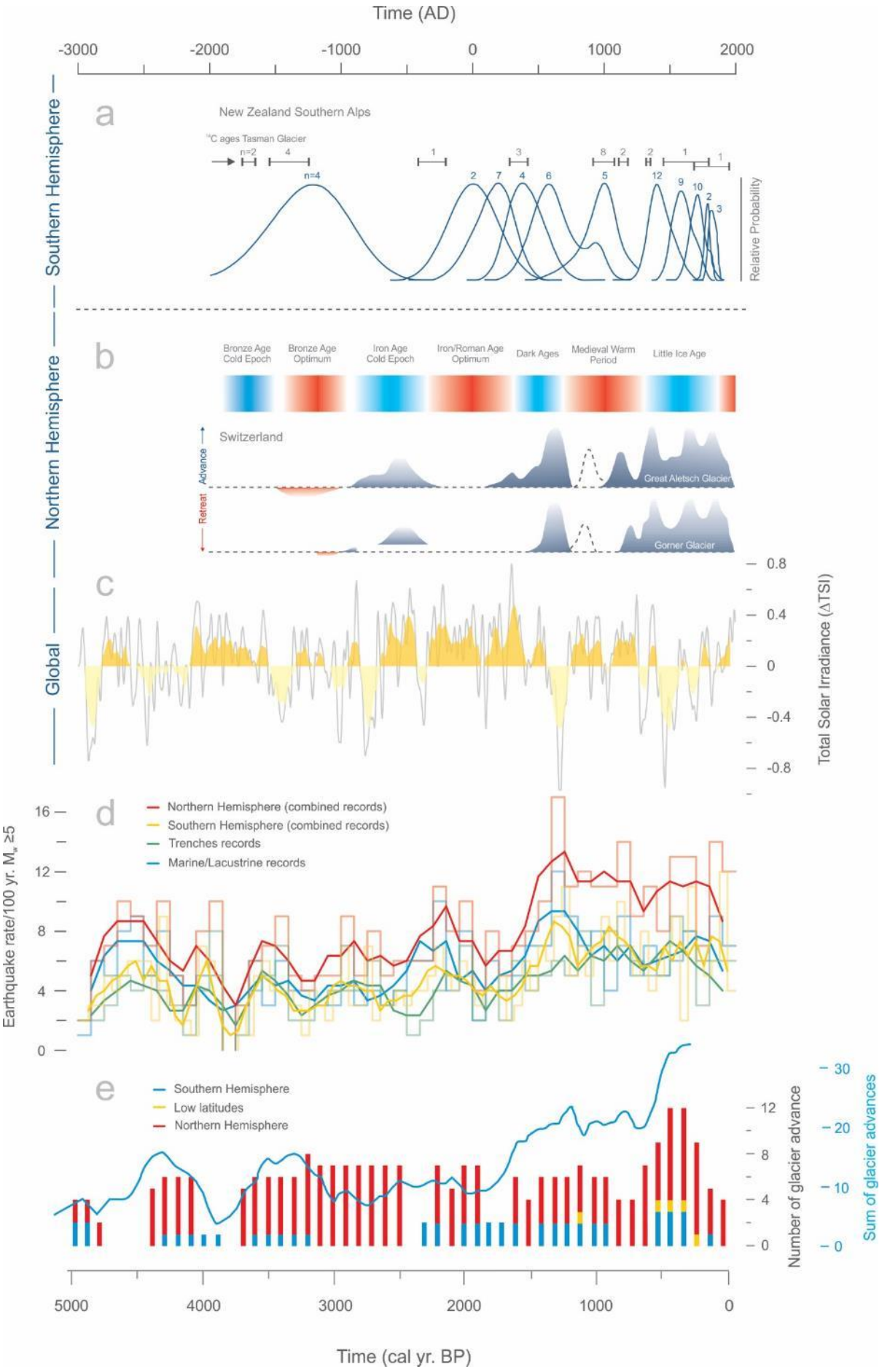
Time (AD)
-3000
-2000
-1000
0
1000
2000
Southern Hemisphere
Northern Hemisphere
Global
a
New Zealand Southern Alps
14C ages Tasman Glacier
n=2
4
n=4
1
3
8
2
2
1
1
2
7
4
6
5
12
9
10
2
3
Relative Probability
b
Bronze Age Cold Epoch
Bronze Age Optimum
Iron Age Cold Epoch
Iron/Roman Age Optimum
Dark Ages
Medieval Warm Period
Little Ice Age
Switzerland
Advance
Retreat
Great Aletsch Glacier
Gorner Glacier
c
0.8
0.4
0
-0.4
-0.8
Total Solar Irradiance (ΔTSI)
d
Northern Hemisphere (combined records)
Southern Hemisphere (combined records)
Trenches records
Marine/Lacustrine records
16
12
8
4
0
Earthquake rate/100 yr. Mw ≥5
e
Southern Hemisphere
Low latitudes
Northern Hemisphere
12
8
4
0
Number of glacier advance
30
20
10
0
Sum of glacier advances
5000
4000
3000
2000
1000
0
Time (cal yr. BP)

Figure 5.6. Comparison of the number of earthquakes in a 100-year window with different climatic proxies from the Southern and Northern Hemispheres. (**a**) Southern Hemisphere; timing of Holocene glacier fluctuations near Mount Cook, New Zealand Southern Alps, together with published ^{14}C ages on soils buried by Mount Cook glacier expansion events over the past 4000 years (Schaefer et al., 2009). The probability plots at the bottom are summary curves of individual ^{10}Be boulder ages from Mueller Glacier moraines, except for the 1650-AD moraine (Tasman Glacier) and 1370- and 1020-AD moraines (Hooker Glacier). (**b**) Northern Hemisphere; general timeline of climatic fluctuations, note the lack of precision on the definition of durations. Below the timeline, the fluctuations of two index glaciers in the Swiss Alps, the Great Aletsch Glacier and the Gorner Glacier, reconstructed from historical accounts and tree-ring and radiocarbon data from fossil wood (Holzhauser et al., 2005), are shown. (**c**) Global; total solar irradiance reconstruction (W m^{-2}; Steinhilberet et al., 2009). (**d**) Earthquake counts within a 100-year window for the global paleo-earthquake database and the associated running average curves. In red, Northern Hemisphere combined sub-catalogue; yellow, Southern Hemisphere combined sub-catalogue; green, trenches sub-catalogue; blue, tsunami deposits and marine/lacustrine sediment cores sub-catalogue. (**e**) Reconstruction of global glacier advances. Bars show the number of glacier advances from Solomina et al. (2015). The blue curve is the sum of glacier advances from Wanner et al. (2011).

Neither reconstructions of glacier advances and cold periods for the Northern and Southern Hemisphere, nor the global reconstruction of solar irradiance show significant correlation with the seismic rate fluctuations (Fig. 5.5 a to c). However, a correlation seems to emerge between the global sum of glacial advances against our seismicity rate. It appears that the temporal clustering of the catalogue coincides with the variation in the sum of glacier advances (Fig. 5.5 d to e). The four clusters identified in the global seismic catalogue above (5000 to ~4200 cal yr BP, ~3900 to ~3500 cal yr BP, ~2700 to ~2300 cal yr BP and ~1800 to ~400 cal yr BP) all seem to correspond to periods of maximum glacier extent, except for ~3900 to ~3500 cal yr BP (Fig. 5.5).

5.5.2 Ice sheets, crustal deformation and seismicity

Temporal clustering of paleo-seismicity is not a new finding; McCalpin and Nishenko (1996) already provided evidence for temporal clustering of Holocene seismicity for the Wasatch fault zone in Utah (USA). The hypotheses as to the source of this clustering and the underlying drivers took time to be established. It is known that earthquakes cluster at decadal to multidecadal time-scales, commonly when a large earthquake triggers a number of aftershocks of variable magnitude that can trigger other earthquakes, giving rise to a local earthquake avalanche (Helmstetter and Sornette, 2002). However, potential clustering mechanisms at the centennial to millennial scales remain unclear. Nicol et al. (2009) emphasized that in some cases, a perceived increase in earthquake occurrence or seismic rate during the Holocene may simply result from a sampling bias towards faults with higher Holocene slip rates. Nevertheless, if several faults and thrusts exhibit synchronous increases in their slip or earthquake-occurrence rates, for which the timing can be correlated with major climate transitions, an external driving force from changing loads on the crust should be considered (Nicol et al., 2009).

Hetzel and Hampel (2005) developed finite-element models to investigate the slip-rate variations on normal faults during glacial-interglacial changes in surface loads for the Wasatch region, observed initially by McCalpin and Nishenko (1996). They proposed that changes in ice-cap volume and thereby the load acting on the lithosphere significantly alter its stress field by producing a momentary signal in conjunction with the tectonic stress fiel background (Fig.

5.7; Hampel et al., 2009). Such stress field variations affect, in turn, the deformation of the earth's crust and in particular the slip behavior of existing faults (Hetzel and Hampel, 2005; Hampel et al., 2009).

Their results show normal faults and thrust faults located below the ice cap/glacier experience a decrease in their slip rate for any value of dip during ice-cap growth and a significant increase during ice-cap retreat (Fig. 5.7). On the other hand, faults on the border of the ice cap/glacier that are loaded on their footwall or hanging wall exhibit a mirror pattern, marked by an increase of slip rate during ice loading and a decrease during retreat (Fig. 5.8; Hampel et al., 2009).

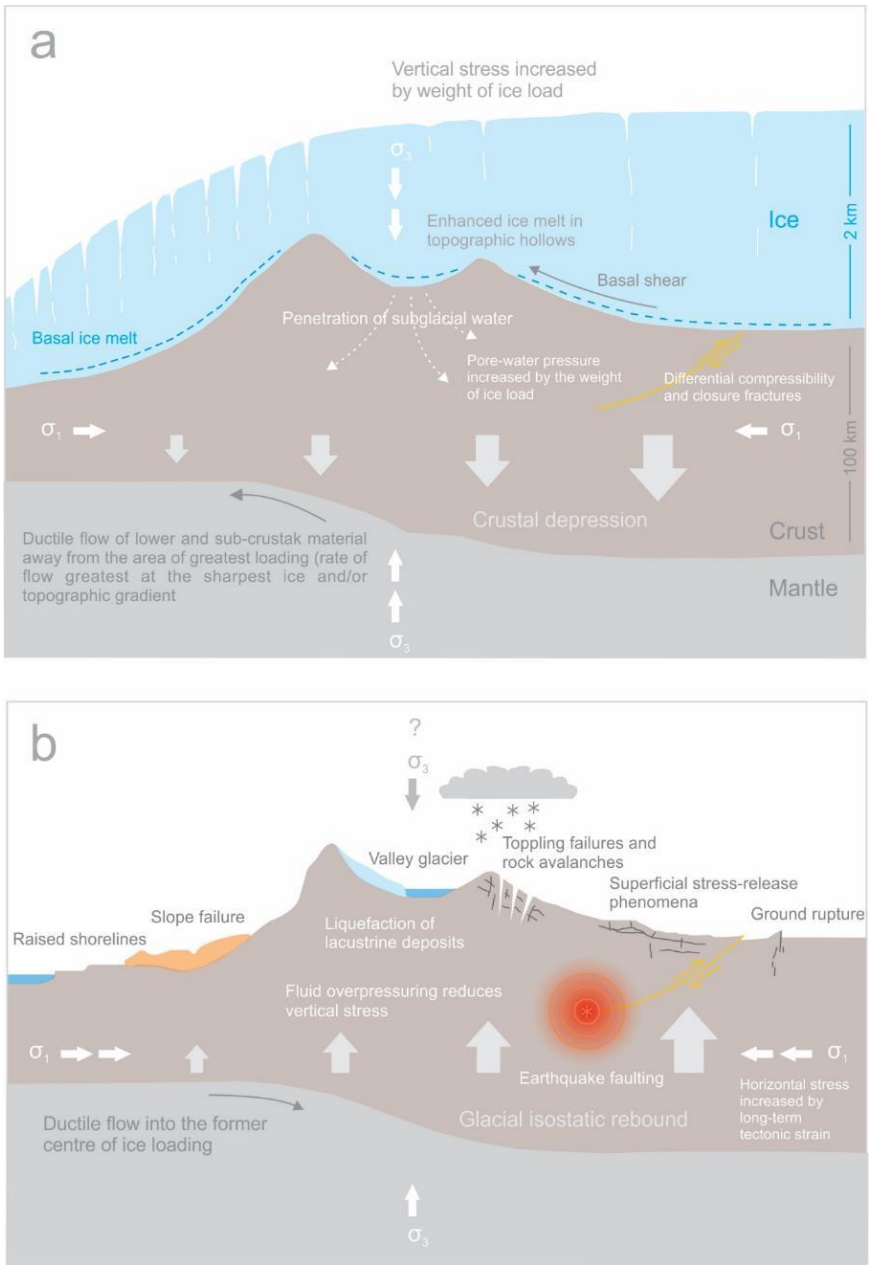

Figure 5.7. Sketch representation of glacial loading and unloading on the lithosphere in a region with a compressive stress regime. (**a**) Glacial loading through an extended ice cap. (**b**) Unloading. Note the considerable vertical exaggeration difference between the crustal thickness (~100 km) and the ice-sheet thickness (~ 3km). Modified from Stewart et al. (2000)

However, these models were developed for the behavior of faults during post-Last Glacial Maximum (LGM) deglaciation and they cannot be readily applied to our study since glacial advances related to neoglaciations never had the magnitude and extent of those of the LGM. Nevertheless, one of the results of these models provides a potential climatic driver for the apparent synchronicity between glacier advances during neoglaciations and the global increase in seismicity. If we consider that most of the faults are located adjacent rather than in regions where the crust is loaded by glaciers, the Hampel et al. (2009) models predict an increase in seismicity during glacial advances (Fig. 5.8).

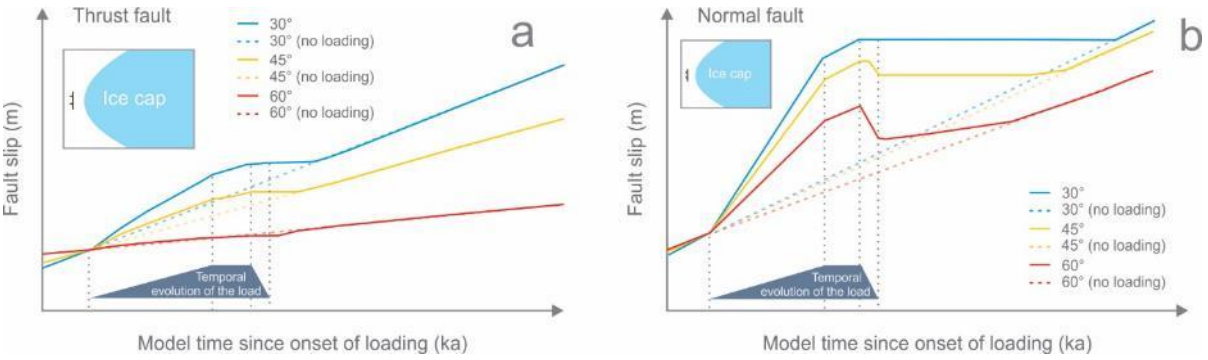

Figure 5.8. Hampel et al.'s (2009) model result when thrust and normal faults are located outside the ice cap, for fault dips of 30°, 45° and 60°. Evolution of the slip as a function of the time elapsed since the initiation of the load for (**a**) a thrust fault and (**b**) a normal fault. Solid lines are slip curves extracted from the experiment with subsequent loading and unloading. The dashed lines illustrate the evolution of the slip of the unloaded experiments. The time evolution of the load is indicated by the grey blue polygon under the slip curves. Modified from Hampel et al. (2009).

Given the relatively low load variations during neoglacial advances (low ice mass differences), it is worth investigating if the changes in seismicity during the Mid and Late Holocene may be due to changes in climatic parameters that caused the glaciers to advance (e.g., increase in precipitation), rather than glacier variations themselves. Another potential driver could be related to high-frequency and low-amplitude climatic variations. Contemporary changes in water storage and associated surface loading produce elastic deformation of the lithosphere (Argus et al., 2014; Amos et al., 2014; Borsa et al., 2014; Johnson et al., 2018). A recent study by Johnson et al. (2018) in California highlighted that seasonal water storage impacts and modulates the stress field and therefore the seismicity. In California, snow accumulation in the Sierra Nevada, the surface of the waterbodies, and groundwater are driven by a high-frequency annual cycle of wet and dry periods.

This seasonality in water loading impacts the lithosphere, as shown by vertical and horizontal surface displacements reflecting the elastic response under hydrospheric loads (Fu et al., 2012; Chanard et al., 2014). Such high-frequency small-scale phenomena have been linked to modulation of large-scale regional seismic activity (Bettinelli et al., 2008; Bollinger et al., 2007; Heki et al., 2003; Pollitz et al., 2013). Heki (2001) emphasized a seasonal modulation of the interseismic strain buildup driven by snow loads in Japan. Bollinger et al. (2007) and Bettineli (2008) reported seismicity rates that were elevated by 30% to 60% during the winter months compared to the summer months in Nepal. Ader et al. (2013) demonstrated seasonal variations

of seismicity, with an increase of seismicity in the winter as high as 40% in the Nepal Himalaya. In the same range of frequency, it has been shown that regional seismicity may also be affected by annual changes in atmospheric pressure (Gao et al., 2000), surface temperature (Ben-Zion et al., 2013), snow accumulation (Heki et al., 2003) and crustal pore pressure (Hainzl et al., 2013; Godard and Burbank, 2011). These studies illustrate that high-frequency and low-amplitude climatic processes are capable of directly affecting the stress field of the lithosphere through loading and unloading, generating an elastic response of the latter.

It has also been pointed out that the coefficient of friction of faults could also be modulated by climatic processes through changes in pore-fluid pressure (Chéry and Vernant, 2006; Godard and Burbank, 2011). Considering the possibility that a change in precipitation rate and phase (snow versus rain) may have affected pore-fluid water would allow a more enhanced and dynamic response in the seismic activity, as the slip rate is directly affected.

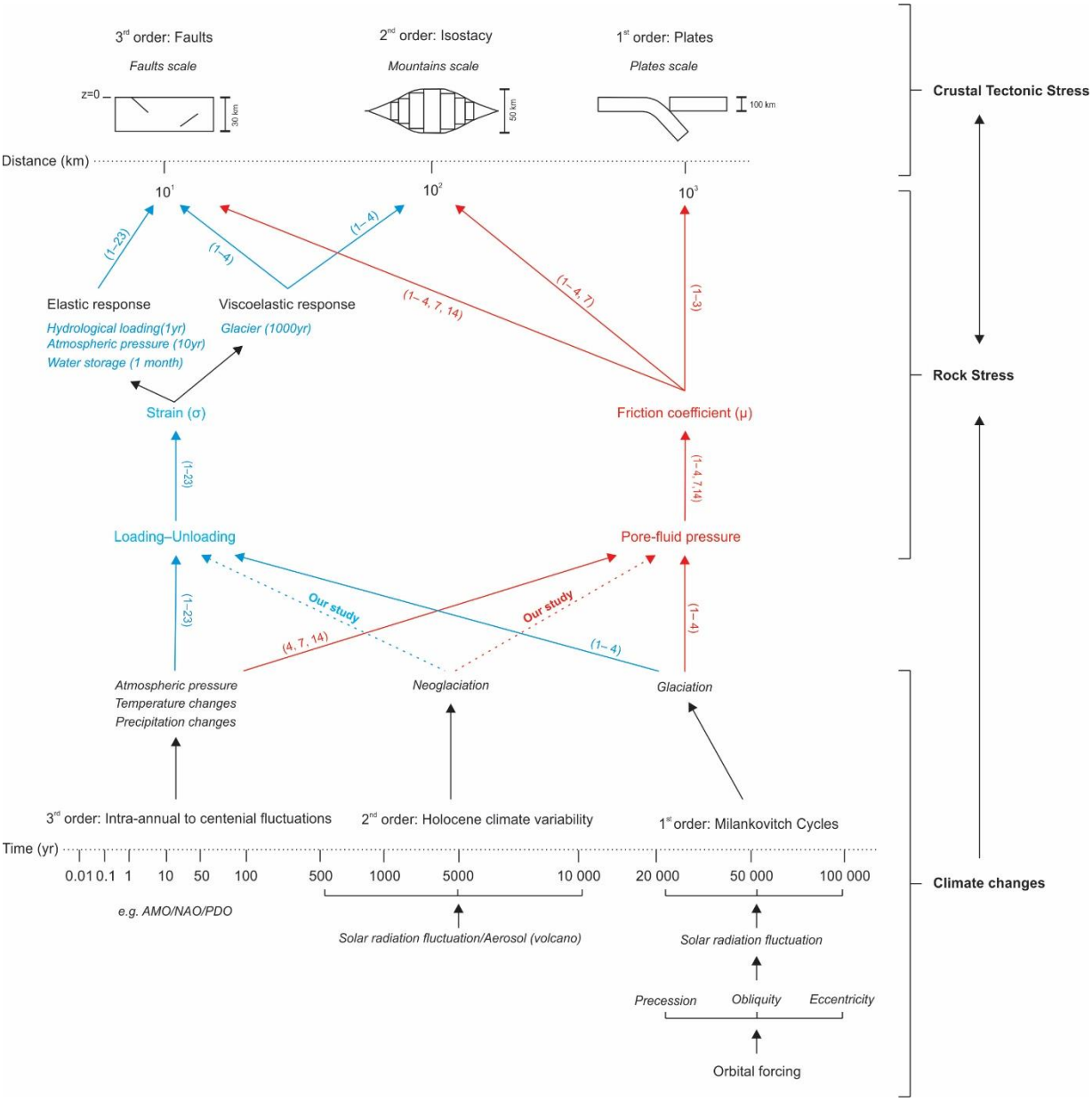

Figure 5.10. Summary of the climatic phenomena affecting the strain (σ) and the friction coefficient (μ) at different temporal and spatial scales. Reference numbers within the summary: ref. 1, Stewart et al., 2000; ref. 2, Hetzel and Hampel, 2005; ref. 3, Hampel et al., 2009; ref. 4, Goddard and Burbank, 2011; ref. 5, Gao et al., 2000; ref. 6, Heki et al., 2003; ref. 7, Chéry and Vernant, 2006; ref. 8, Bollinger et al., 2007; ref. 9, Bettineli et al., 2008; ref. 10, Fu et al., 2012; ref. 11, Pollitz et al., 2013; ref. 12, Ader et al., 2013; ref. 13, Ben-Zion et al., 2013; ref. 14, Hainzl et al., 2013; ref. 15, Argus et al., 2014; ref. 16, Amos et al., 2014; ref. 18, Borsa et al., 2014; ref. 19, Chanard et al., 2014; ref. 20, Scafetta et al., 2015; ref. 21, Bragato et al., 2017; ref. 22, Craig et al., 2017; ref. 23, Johnson et al., 2018. (Crustal Tectonic Stress inset modified after Zang and Stephansson,2010)

As illustrated by Johnson et al (2018), small changes in static stress conditions can influence the nucleation and occurrence of earthquakes. Such stress changes can promote or inhibit nucleation. In doing so, earthquakes will occur more often during slip-encouraging loading conditions.

5.6 Conclusions and perspectives

In view of those preliminary results, we can draw a number conclusions. What emerges from this exploratory study is first that our merged catalogue covering 7000 years of global seismicity presents clustering. The seismic dynamics within the merged catalogue appear to be driven by nonrandom processes with significant periodicities of 100 (99% confidence) and 2000 years (95% confidence).

By looking at global climate processes it appears that the seismic clusters are synchronous with the variation of the sum of glacial advances through the Mid and Late Holocene. Prior models of crustal loading and unloading can explain this common trend between an increase in glacial advance and a rise in the number of earthquakes. Nonetheless, we are in favor of a more complex model (Fig. 5.10). Given the complexity of lithospheric, atmospheric and surface-process interactions, a number of factors may have contributed to the increase in the number of earthquakes during crustal loading by glaciers. Considering the magnitude of glacial advances during neoglaciations, the associated load is too low to have a sufficient impact on the lithospheric stress field. We thus propose the modulation of seismicity during the Holocene by periods of synchronization of high-frequency/low-amplitude climatic variability with high-amplitude/low-frequency variability (Fig. 5.10; e.g. Milankovitch cycles). Indeed, the effects of glaciations on the lithosphere and its stress field are still present today. By combining high-frequency climatic phenomena affecting both the stress field, by loading and unloading the lithosphere, and the friction coefficient, by changes in pore-fluid pressure, it would be possible to explain this Mid-Holocene earthquake clustering.

To conclude with a future perspective, the evidence of seismicity modulation that appears synchronous to climate changes during the Mid and Late-Holocene raises questions for the current global climate change and its impact on the lithospheric stress field and earthquake occurrence.

Chapter 6

Conclusions and Perspectives

6.1 Conclusions

Seismic hazard assessment on regional to global scales is based on many conceptual hypotheses, including models for the temporal distribution of earthquakes and for the factors modulating seismicity over time, which have led for instance to the seismic-gap hypothesis. The fate of the population of seismically active areas, who continuously face the threat of the next devastating earthquake, is directly affected by those scientific concepts and hypotheses.
In this work, I have investigated one of the world's most populated and seismically active regions, the Himalayan arc, focusing on the economically precarious and remote western districts of Nepal. I have developed a new approach in this Himalayan context by using lacustrine sediments to generate a new and continuous paleo-seismological record through the Mid Holocene. Three lakes have been targeted; Lake Rara (Mugu district), Lake Phoksundo (Dolpo district) and Lake Dhumba (Mustang district), but I have only been able to produce a reliable age-depth model for Lake Rara due to the lack of organic matter for radiocarbon dating in the other lakes. This study has therefore focused on Lake Rara. By using a multi-proxy approach, I have been able to reconstruct the seismic activity of the last ~700 years through identification of earthquake-triggered turbidites in short (40 cm) sediment cores. I have mainly used Titanium concentrations, together with grain-size profiles and CT radiographs, as turbidite indicators, as well as bulk organic geochemistry to identify the origin of the reworked sediments. Likewise, I used Ti concentrations to identify turbidites in a 6000-year sediment core from Lake Rara obtained through collaboration with Japanese colleagues. As grain-size had not been measured along the long core and no samples were available for analysis, I used the Ti concentration as a turbidite proxy and generated the longest continuous Himalayan seismic time series currently available. Alongside the paleoseismicity studies over the Holocene, I have attempted to contribute some new perspectives on the impact of glaciations on the landscape of western Nepal, as well as on their potential extent through the Last Glacial Maximum. The retreat of the glaciers allowed the development of lakes and thereby permitted to record the significant seismic activity of western Nepal, thereby providing a link between my studies on glaciation and landscape evolution on the one hand and the paleoseismicity studies on the other.

Having established these new short (~700 yr) and long (~6000 yr) paleoseismic records provided me the analytical and conceptual tools to apprehend some of the main paleoseismological and seismological issues on a Himalayan to a global scale and leads me to draw the following main conclusions:

On the seismic-gap hypothesis, from a regional to a continental scale. Western Nepal lies within the "central Himalayan seismic gap", one of the prominent seismic gaps recognised along the Himalayan arc . The last major earthquake in this region is the Ms ~8.2 1505 AD earthquake, dating back to 500 years ago. Since then, no earthquakes have been recorded either in the available historical archives or in the geological record. In contrast, the short sediment cores from Lake Rara contain eight earthquake-triggered turbidites in the last ~700 years. Three of them, including the 1505 AD event, were also present in instrumental (1916 AD), historical (1505 AD), or geological (12^{th}-14^{th} century AD) records, and six of them post-date the 1505 AD event. Analysis and modelling of seismic shaking intensities indicate that the earthquakes triggering these turbidites must have had magnitudes $M_w \geq 6.5$. This new lake-based seismic record indicates that seismic activity in western Nepal is similar to that in central Nepal. Therefore, these new data lead me to question the seismic-gap hypothesis and suggest that it is biased by a lack of historical documents and geological records. I have outlined two issues that may have led to hypothesizing the presence of a seismic gap in western Nepal.

First, access to the historical narrative in western Nepal has been and remains complicated by various factors. Whether a major natural disaster marks a turning point in the history of a society is a striking question in the context of western Nepal, given the complexity of its clan and kingdom history, spirituality, linguistic and social structure (e.g., for a review Ramble, 1998, 1999). Most of the available texts relating to earthquakes in western Nepal were protected and preserved by the former British Raj of India. In contrast, for earthquakes that occurred in western Nepal but were not recorded in India, the most important sources that potentially relate natural phenomena are the village records (bem-chag). These were written using Tibetan and Devanagari script but include local orthographical and dialectical features (e.g. Ramble, 1998, 1999; Helman-Wazny and Ramble, 2017). The local oral tradition and folklore also constitute an important source of accounts, including details that are not found in the written sources (e.g. Ramble, 1998, 1999; Helman-Wazny and Ramble, 2017). However, the majority of these sources remain partially or very inaccessible to foreign researchers, leading to a significant lack of historical accounts of past seismic activity in western Nepal.

Second, our modelling of shaking intensity showed significant uncertainties due to the lack of locally calibrated Intensity Prediction Equations (IPE). The uncertainty in local shaking intensity propagates into the estimated magnitude of seismic events responsible for triggering the observed turbidites. The large discrepancy between the modelled and observed isoseismals for past earthquakes in western Nepal stems from the difficulty of producing reliable intensity maps. The past seismic activity of western Nepal and surrounding areas has been almost exclusively analysed in terms of macro-seismic effects to assess intensities. Therefore, it is important to have an idea of the similarities and differences in environmental and construction conditions with western regions, against which the intensity scales have been calibrated (Ambraseys and Jackson, 2003).

Vulnerability of dwellings impacted by earthquakes in the Himalayan region varies considerably from one region to another and over time (e.g. Bukhari et al., 2017). Most traditional buildings in the western and central Himalaya can be divided into two systems of

paraseismic architecture (for review: Langenbach, 2015 and 2016). The first system, referred to as "taq" in Kashmiri and "bhatar" in Pashtun, consists of thick load-bearing masonry or stone piers with thinner masonry/stone walls in between (Fig. 6.1). These separate sections of masonry/stone walls and piers are then laced together with timber that forms ring beams around the exterior walls. This timber lacing is configured as ladders laid horizontally in the wall, increasing their resistance to earthquakes (Langenbach, 2010, 2013, 2015, 2016). Similar architecture is present in some valleys in Nepal. Following the October 2005 Kashmir earthquake (M_w 7.6), Rai and Murty (2006) highlighted that *"the timber studs resist progressive destruction of the wall and prevent propagation of diagonal shear crack and out-of-plane failure"*, and suggested that *"there is an urgent need to revive these traditional masonry practices, which have proven their ability to resist earthquake load."*

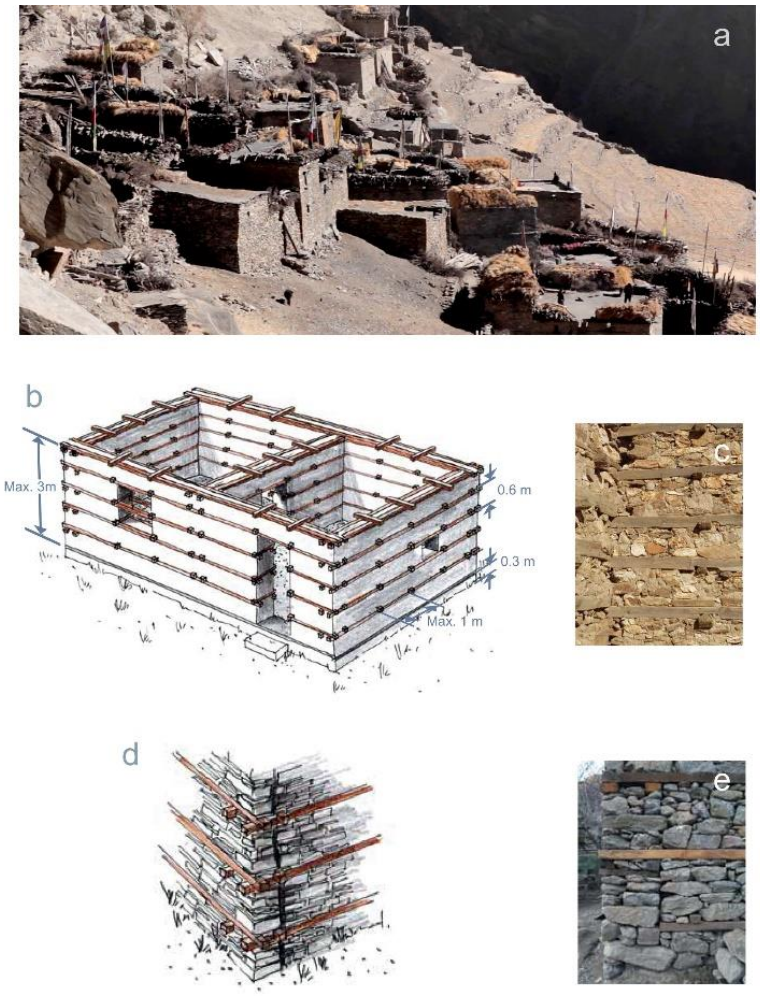

Figure 6.1. Himalayan earthquake-resistant vernacular architecture. (**a**). Illustration of western Nepal "bhatar style" buildings in Mukot, Dolpo, Nepal. (**b**) and (**d**) are sketches illustrating the main features of the bhatar house architecture. (**d**). Illustration of the space between the walls allowing the building to resist to shear strength. (**c**) and (**e**) are photos exemplifying the building elements depicted in (**b**) and (**d**) (modified after NWFP, 2007).

Himalayan earthquake time-distribution models. Through statistical analysis on the long paleoseismic time series covering 6000 years, we have developed a model of temporal earthquake distribution behaviour over the Mid- to Late Holocene. Up to now, models used to describe the time distribution of earthquakes in the central Himalaya were periodic to quasi-periodic given the poor resolution on past earthquake activity. The long core from Lake Rara constitutes the longest and most continuous paleoseismic record at the scale of the Himalaya; we have statistically characterized the time distribution of the 50 events contained by this catalogue. To first order, the results show that time intervals between large ($M_w \geq 7$) earthquakes are described by a Poissonian distribution. Second-order events have been identified as fluctuations around the Poisson distribution, appear to be correlated and grouped within clusters. These patterns have been calibrated against the 50 largest instrumental events from the USGS catalogue (covering 1974-2018) at the scale of the entire Himalayan arc. Like the regional long-term record, this orogen-scale short-term record is also inconsistent with a periodic to quasi-periodic earthquake time distribution. Those important results constitute a paradigm shift, in that they imply that the occurrence of major to moderate events is as uncertain as that of smaller events at any period, drastically increasing the Himalayan seismic hazard. From a global and conceptual perspective, this analysis suggests that seismological and paleoseismological records show the same level of complexity, even though they have very different temporal and spatial resolutions. The inferred Poisson distribution of major-earthquake recurrence times further supports and strengthens the above conclusion that the seismic-gap hypothesis is no longer appropriate for western Nepal and most likely at the scale of the Himalaya. Indeed, by definition, the seismic-gap hypothesis in its modern form depends on a periodic to quasi-periodic earthquake-recurrence model (e.g., Nishenko and Sykes, 1993; Kagan and Jackson, 1995).

Global seismic modulation through climate changes. When comparing the time distribution of the seismic records from western Nepal against paleoseismic records around the world, I noticed the same variation of seismic rates throughout the Mid to Late Holocene. Seismic clustering through the Holocene has already been proposed regionally but never at a global scale. I therefore synthesised a global paleoseismic database based on strict criteria and used this to analyse the time distribution of global seismicity over the last 5000 years. The analysis suggests that a non-random process, with two marked periodicities at ~100 and ~2000 years, drives the signal but, given the possibility of under-sampling artefacts, these results should be interpreted with caution. I have attempted to correlate the observed seismic-rate variations with known climatic proxies. Previous studies have shown the impact of glaciations on the crustal stress field, and thereby the seismic activity, by loading and unloading of the crust. As one of the most significant characteristics of Holocene climate variability is the recurrent advance of glaciers during periods of neoglaciation, I used a global reconstruction of glacial advances as a proxy of climate changes. When comparing the global seismicity against neoglacial advances over the Mid and Late Holocene, similar fluctuations appear. However, given the mechanics of stress-field modulation by glaciers and ice caps, it appears that the Holocene glacial advances by themselves do not suffice to explain the inferred seismic-rate variations. In order to better grasp the complexity of the coupling between climate changes and seismic-rate variations through the Mid- to Late Holocene, I compiled recent studies of climatic modulation of seismic

activity at different timescales. By looking at low-frequency/high-amplitude climatic phenomena (e.g., glaciation) as well as high-frequency/low-amplitude phenomena (e.g., monsoonal variations), I propose that the seismic clustering is due to periods of synchronization of both high- and low-frequency climatic processes. Both processes affect the crustal stress field through changes in the load and/or the friction coefficient (through changes in the pore-fluid pressure), and thereby potentially the slip rate of faults. While it is known that glaciation and water storage can modulate the crustal stress field, the possible modulation of seismic rate by Holocene climate variability implies that the current global climate change could impact the crustal stress field and, thereby, earthquake occurrence.

These results show the complexity of earthquake time distributions from a regional (i.e., western Nepal) to a sub-continental (i.e. Himalayan arc) and global scale. I therefore suggest that, whereas models describing seismic time distributions have long been conceptually opposed depending on the time scale that they focused on (short for seismology versus long for paleoseismology), the seismic periodicity tends toward randomness on all timescales. This hypothesis has a strong impact on seismic hazard assessment in both the Himalaya and elsewhere. It also implies that the seismic-gap hypothesis is most likely no longer relevant at both Himalayan and global scales. Finally, the analysis of a global paleoseismic archive opens the discussion on possible impacts of climate changes on the Earth's stress field and associated seismicity, modulated through changes in surface loads and pore-fluid pressure.

6.2 Perspectives

The above conclusions, while still partly speculative, have far-reaching implications. I therefore conclude this thesis by proposing potential future work allowing to test and further develop these conclusions at both a Himalayan and a global scale.

To further resolve the question of the validity of the seismic-gap hypothesis and thereby the best model to describe time distributions of seismic events, the approach developed here could be extended to other known seismic gaps along the Himalayan arc. This would require several long sediment cores having at least the same time coverage (~6000 years) from adequate lakes along the Himalayan arc, i.e. those with the sensitivity to record regional seismic activity. Based on such cores we should be able, provided they record sufficient numbers of earthquakes, to run similar statistical analyses and compare the different time-distribution behaviours. By building a Himalayan-wide lake record, we will also be able to reduce the uncertainty on the earthquake-intensity threshold to trigger a turbidite as well as decreasing the uncertainties involved with generating intensity maps. A preliminary lake study is already underway in Bhutan, where a group headed by Romain Le Roux-Mallouf has cored a lake in the summer of 2017 building on the experience and approach I acquired at Lake Rara.

To continue the study of seismic modulation by Holocene climate variability, we would need to expand the global paleoseismic record. Wavelet analysis by frequency filtering could be used to extract the characteristic timescales of different kinds of climatic processes. Furthermore, mechanical (visco-elastic) models of the crust, combining pore-fluid pressure and load variation

at regional to continental scales through time would allow quantifying the potential modulation of seismicity by climatic variations.

Finally, as this work has implications for seismic risk assessment, I feel it is crucial to develop a more holistic approach including anthropologists, architects and civil/geotechnical engineers, as well as local community stakeholders to rethink earthquake preparedness policies. Amongst the many key issues to be addressed are re-establishing a "seismic culture" (e.g., Degg and Homan, 2005; Halvorson and Hamilton, 2007) through increasing attention to this constant threat, rethinking governmental building regulations, etc.

References

Adams, J. W., D. (1994). Near-term probability of the future Cascadia megaquake. U. G. Survey, US Geological Survey: 94-568.

Ader, T., J. P. Avouac, J. Liu-Zeng, H. Lyon-Caen, L. Bollinger, J. Galetzka, J. Genrich, M. Thomas, K. Chanard, S. N. Sapkota, S. Rajaure, P. Shrestha, L. Ding and M. Flouzat (2012). "Convergence rate across the Nepal Himalaya and interseismic coupling on the Main Himalayan Thrust: Implications for seismic hazard." Journal of Geophysical Research-Solid Earth 117.

Ader, T. J. and J. P. Avouac (2013). "Detecting periodicities and declustering in earthquake catalogs using the Schuster spectrum, application to Himalayan seismicity." Earth and Planetary Science Letters 377: 97-105.

Ader, T. J., N. Lapusta, J. P. Avouac and J. P. Ampuero (2014). "Response of rate-and-state seismogenic faults to harmonic shear-stress perturbations." Geophysical Journal International 198(1): 385-413.

Ali, S. N., R. H. Biswas, A. D. Shukla and N. Juyal (2013). "Chronology and climatic implications of Late Quaternary glaciations in the Goriganga valley, central Himalaya, India." Quaternary Science Reviews 73: 59-76.

Allen, T. I., D. J. Wald and C. B. Worden (2012). "Intensity attenuation for active crustal regions." Journal of Seismology 16(3): 409-433.

Ambraseys, N. and D. Jackson (2003). "A note on early earthquakes in northern India and southern Tibet." Current Science 84(4): 570-582.

Ambraseys, N. N. and J. Douglas (2004). "Magnitude calibration of north Indian earthquakes." Geophysical Journal International 159(1): 165-206.

Amos, C. B., P. Audet, W. C. Hammond, R. Burgmann, I. A. Johanson and G. Blewitt (2014). "Uplift and seismicity driven by groundwater depletion in central California." Nature 509(7501): 483-+.

Anderson, J. G. and J. N. Brune (1999). "Methodology for using precarious rocks in Nevada to test seismic hazard models." Bulletin of the Seismological Society of America 89(2): 456-467.

Andrews, J. T. (1975). Glacial Systems: An Approach to Glaciers and their Environments. . North Scituate, Massachusetts, Duxbury Press

Argus, D. F., Y. N. Fu and F. W. Landerer (2014). "Seasonal variation in total water storage in California inferred from GPS observations of vertical land motion." Geophysical Research Letters 41(6): 1971-1980.

Arnaud, F., V. Lignier, M. Revel, M. Desmet, C. Beck, M. Pourchet, F. Charlet, A. Trentesaux and N. Tribovillard (2002). "Flood and earthquake disturbance of Pb-210 geochronology (Lake Anterne, NW Alps)." Terra Nova 14(4): 225-232.

Arnold, M., S. Merchel, D. L. Bourles, R. Braucher, L. Benedetti, R. C. Finkel, G. Aumaitre, A. Gottdang and M. Klein (2010). "The French accelerator mass spectrometry facility ASTER: Improved performance and developments." Nuclear Instruments and

Methods in Physics Research Section B-Beam Interactions with Materials and Atoms 268(11-12): 1954-1959.

Arora, S. and J. N. Malik (2017). "Overestimation of the earthquake hazard along the Himalaya: constraints in bracketing of medieval earthquakes from paleoseismic studies." Geoscience Letters 4(1): 19.

Ashley, G. M. (2002). Glaciolacustrine environments. Modern and Past Glacial Environments. J. Menzies. Oxford, Butterworth-Heinemann: 335-359.

Atkinson, G. M. and D. J. Wald (2007). ""Did you feel it"? Intensity data: A surprisingly good measure of earthquake ground motion." Seismological Research Letters 78(3): 362-368.

Avouac, J. P. (2003). Mountain building, erosion, and the seismic cycle in the Nepal Himalaya. Advances in Geophysics, Vol 46. R. Dmowska. 46: 1-80.

Bakun, W. H. and C. M. Wentworth (1997). "Estimating earthquake location and magnitude from seismic intensity data." Bulletin of the Seismological Society of America 87(6): 1502-1521.

Balco, G., J. Briner, R. C. Finkel, J. A. Rayburn, J. C. Ridge and J. M. Schaefer (2009). "Regional beryllium-10 production rate calibration for late-glacial northeastern North America." Quaternary Geochronology 4(2): 93-107.

Bali, R., S. N. Ali, K. K. Agarwal, S. K. Rastogi, K. Krishna and P. Srivastava (2013). "Chronology of late Quaternary glaciation in the Pindar valley, Alaknanda basin, Central Himalaya (India)." Journal of Asian Earth Sciences 66: 224-233.

Ballantyne, C. K. (2002). "Paraglacial geomorphology." Quaternary Science Reviews 21(18-19): 1935-2017.

Barros, A. P. and D. P. Lettenmaier (1994). "Dynamic modeling of orographically induced precipitation." Reviews of Geophysics 32(3): 265-284.

Beeler, N. M. and D. A. Lockner (2003). "Why earthquakes correlate weakly with the solid Earth tides: Effects of periodic stress on the rate and probability of earthquake occurrence." Journal of Geophysical Research-Solid Earth 108(B8).

Benn, D. I. and D. J. A. Evans (1998). Glaciers and Glaciation. New Work, John Wiley and Sons, Inc.

Benn, D. I. and L. A. Owen (1998). "The role of the Indian summer monsoon and the mid-latitude westerlies in Himalayan glaciation: review and speculative discussion." Journal of the Geological Society 155: 353-363.

Benn, D. I. and L. A. Owen (2002). "Himalayan glacial sedimentary environments: a framework for reconstructing and dating the former extent of glaciers in high mountains." Quaternary International 97-8: 3-25.

Ben-Zion, Y. and A. A. Allam (2013). "Seasonal thermoelastic strain and postseismic effects in Parkfield borehole dilatometers." Earth and Planetary Science Letters 379: 120-126.

Berryman, K. R., U. A. Cochran, K. J. Clark, G. P. Biasi, R. M. Langridge and P. Villamor (2012). "Major Earthquakes Occur Regularly on an Isolated Plate Boundary Fault." Science 336(6089): 1690-1693.

Bertrand, S., F. Charlet, E. Chapron, N. Fagel and M. De Batist (2008). "Reconstruction of the Holocene seismotectonic activity of the Southern Andes from seismites recorded in

Lago Icalma, Chile, 39 degrees S." Palaeogeography Palaeoclimatology Palaeoecology 259(2-3): 301-322.

Bertrand, S., K. A. Hughen, J. Sepulveda and S. Pantoja (2012). "Geochemistry of surface sediments from the fjords of Northern Chilean Patagonia (44-47 degrees S): Spatial variability and implications for paleoclimate reconstructions." Geochimica Et Cosmochimica Acta 76: 125-146.

Bettinelli, P., J. P. Avouac, M. Flouzat, L. Bollinger, G. Ramillien, S. Rajaure and S. Sapkota (2008). "Seasonal variations of seismicity and geodetic strain in the Himalaya induced by surface hydrology." Earth and Planetary Science Letters 266(3-4): 332-344.

Bilham, R. (1995). "Location and magnitude of the 1833 Nepal earthquake and its relation to the rupture zones contiguous great Himalayan earthquakes." Current Science 69(2): 101-128.

Bilham, R. (2004). "Earthquakes in India and the Himalaya: tectonics, geodesy and history." Annals of Geophysics 47(2-3): 839-858.

Bilham, R., V. K. Gaur and P. Molnar (2001). "Earthquakes - Himalayan seismic hazard." Science 293(5534): 1442-1444.

Bilham, R. and K. Wallace (2005). "Future Mw>8 earthquakes in the Himalaya: implications from the 26 Dec 2004 Mw=9.0 earthquake on India's eastern plate margin." Geological Survey of Indian Special Publication 85: 1-14.

Bisht, P., S. N. Ali, A. D. Shukla, S. Negi, Y. P. Sundriyal, M. G. Yadava and N. Juyal (2015). "Chronology of late Quaternary glaciation and landform evolution in the upper Dhauliganga valley, (Trans Himalaya), Uttarakhand, India." Quaternary Science Reviews 129: 147-162.

Blaauw, M. and J. A. Christen (2011). "Flexible Paleoclimate Age-Depth Models Using an Autoregressive Gamma Process." Bayesian Analysis 6(3): 457-474.

Blott, S. J. and K. Pye (2001). "GRADISTAT: A grain size distribution and statistics package for the analysis of unconsolidated sediments." Earth Surface Processes and Landforms 26(11): 1237-1248.

Bolch, T., A. Kulkarni, A. Kaab, C. Huggel, F. Paul, J. G. Cogley, H. Frey, J. S. Kargel, K. Fujita, M. Scheel, S. Bajracharya and M. Stoffel (2012). "The State and Fate of Himalayan Glaciers." Science 336(6079): 310-314.

Bollinger, L., F. Perrier, J. P. Avouac, S. Sapkota, U. Gautam and D. R. Tiwari (2007). "Seasonal modulation of seismicity in the Himalaya of Nepal." Geophysical Research Letters 34(8).

Bollinger, L., S. N. Sapkota, P. Tapponnier, Y. Klinger, M. Rizza, J. Van der Woerd, D. R. Tiwari, R. Pandey, A. Bitri and S. B. de Berc (2014). "Estimating the return times of great Himalayan earthquakes in eastern Nepal: Evidence from the Patu and Bardibas strands of the Main Frontal Thrust." Journal of Geophysical Research-Solid Earth 119(9): 7123-7163.

Bollinger, L., P. Tapponnier, S. N. Sapkota and Y. Klinger (2016). "Slip deficit in central Nepal: omen for a repeat of the 1344 AD earthquake?" Earth Planets and Space 68.

Bond, G., B. Kromer, J. Beer, R. Muscheler, M. N. Evans, W. Showers, S. Hoffmann, R. Lotti-Bond, I. Hajdas and G. Bonani (2001). "Persistent solar influence on north Atlantic climate during the Holocene." Science 294(5549): 2130-2136.

Bookhagen, B. and D. W. Burbank (2006). "Topography, relief, and TRMM-derived rainfall variations along the Himalaya." Geophysical Research Letters 33(8).

Bookhagen, B. and D. W. Burbank (2010). "Toward a complete Himalayan hydrological budget: Spatiotemporal distribution of snowmelt and rainfall and their impact on river discharge." Journal of Geophysical Research-Earth Surface 115.

Bookhagen, B., R. C. Thiede and M. R. Strecker (2005). "Late Quaternary intensified monsoon phases control landscape evolution in the northwest Himalaya." Geology 33(2): 149-152.

Boos, W. R. and Z. M. Kuang (2010). "Dominant control of the South Asian monsoon by orographic insulation versus plateau heating." Nature 463(7278): 218-U102.

Borsa, A. A., D. C. Agnew and D. R. Cayan (2014). "Ongoing drought-induced uplift in the western United States." Science 345(6204): 1587-1590.

Bothe, O., K. Fraedrich and X. H. Zhu (2011). "Large-scale circulations and Tibetan Plateau summer drought and wetness in a high-resolution climate model." International Journal of Climatology 31(6): 832-846.

Bragato, P. L. (2017). "Periodicity of Strong Seismicity in Italy: Schuster Spectrum Analysis Extended to the Destructive Earthquakes of 2016." Pure and Applied Geophysics 174(10): 3725-3735.

Braucher, R., V. Guillou, D. L. Bourles, M. Arnold, G. Aumaitre, K. Keddadouche, E. Nottoli and A. Team (2015). "Preparation of ASTER in-house Be-10/Be-9 standard solutions." Nuclear Instruments and Methods in Physics Research Section B-Beam Interactions with Materials and Atoms 361: 335-340.

Briner, J. P., N. E. Young, B. M. Goehring and J. M. Schaefer (2012). "Constraining Holocene 10Be production rates in Greenland." Journal of Quaternary Science 27(1): 2-6.

Brown, E. T., J. M. Edmond, G. M. Raisbeck, F. Yiou, M. D. Kurz and E. J. Brook (1991). "Examination of surface exposure ages of Antarctic moraines using insitu produced 10Be and 26Al." Geochimica Et Cosmochimica Acta 55(8): 2269-2283.

Bukhari, K. Y., M.

Dar, M. A. (2017). "Seismic Vulnerability of Century Old Buildings of Srinagar City, Kashmir Himalaya, India - A Case Study " i-manager's Journal on Civil Engineering 7: 45-51.

Carosi, R., C. Montomoli, D. Rubatto and D. Visona (2006). Normal-sense shear zones in the core of the Higher Himalayan Crystallines (Bhutan Himalaya): evidence for extrusion? Channel Flow, Ductile Extrusion and Exhumation in Continental Collision Zones. R. D. Law, M. P. Searle and L. Godin. 268: 425-+.

Carosi, R., C. Montomoli and D. Visona (2002). "Is there any detachment in the Lower Dolpo (western Nepal)?" Comptes Rendus Geoscience 334(12): 933-940.

Carosi, R., C. Montomoli and D. Visona (2007). "A structural transect in the Lower Dolpo: Insights on the tectonic evolution of Western Nepal." Journal of Asian Earth Sciences 29(2-3): 407-423.

Carrivick, J. L. and F. S. Tweed (2013). "Proglacial lakes: character, behaviour and geological importance." Quaternary Science Reviews 78: 34-52.

Carver, G. A., A. S. Jayko, D. W. Valentine and W. H. Li (1994). "Coastal uplift associated with the 1992 Cape Mendocino earthquake, northern California." Geology 22(3): 195-198.

Cattin, R. and J. P. Avouac (2000). "Modeling mountain building and the seismic cycle in the Himalaya of Nepal." Journal of Geophysical Research-Solid Earth 105(B6): 13389-13407.

Chanard, K., J. P. Avouac, G. Ramillien and J. Genrich (2014). "Modeling deformation induced by seasonal variations of continental water in the Himalaya region: Sensitivity to Earth elastic structure." Journal of Geophysical Research-Solid Earth 119(6): 5097-5113.

Chery, J. and P. Vernant (2006). "Lithospheric elasticity promotes episodic fault activity." Earth and Planetary Science Letters 243(1-2): 211-217.

Chmeleff, J., F. von Blanckenburg, K. Kossert and D. Jakob (2010). "Determination of the Be-10 half-life by multicollector ICP-MS and liquid scintillation counting." Nuclear Instruments and Methods in Physics Research Section B-Beam Interactions with Materials and Atoms 268(2): 192-199.

Corbi, F., F. Funiciello, M. Moroni, Y. van Dinther, P. M. Mai, L. A. Dalguer and C. Faccenna (2013). "The seismic cycle at subduction thrusts: 1. Insights from laboratory models." Journal of Geophysical Research-Solid Earth 118(4): 1483-1501.

Costa, J. E. and R. L. Schuster (1988). "The formation and failure of natural dams." Geological Society of America Bulletin 100(7): 1054-1068.

Cox, T. F. and T. Lewis (1976). "Conditioned distance ratio method for analyzing spatial patterns." Biometrika 63(3): 483-491.

Craig, T. J., K. Chanard and E. Calais (2017). "Hydrologically-driven crustal stresses and seismicity in the New Madrid Seismic Zone." Nature Communications 8.

Cuven, S., P. Francus and S. F. Lamoureux (2010). "Estimation of grain size variability with micro X-ray fluorescence in laminated lacustrine sediments, Cape Bounty, Canadian High Arctic." Journal of Paleolimnology 44(3): 803-817.

Cua, G., Wald, D.J., Allen, T.I., Garcia, D., Worden, C.B., Gerstenberger, M., Lin, K. and Marano, K. (2010) ""Best practices" for using macroseismic intensity and ground motion intensity conversion equations for hazard and loss models in GEM1". GEM Technical Report 2010-4, GEM Foundation, Pavia, Italy.

Dahl, S. O., J. Bakke, O. Lie and A. Nesje (2003). "Reconstruction of former glacier equilibrium-line altitudes based on proglacial sites: an evaluation of approaches and selection of sites." Quaternary Science Reviews 22(2-4): 275-287.

de Arcangelis, L., C. Godano, J. R. Grasso and E. Lippiello (2016). "Statistical physics approach to earthquake occurrence and forecasting." Physics Reports-Review Section of Physics Letters 628: 1-91.

DeCelles, P. G., G. E. Gehrels, J. Quade, T. P. Ojha, P. A. Kapp and B. N. Upreti (1998). "Neogene foreland basin deposits, erosional unroofing, and the kinematic history of the Himalayan fold-thrust belt, western Nepal." Geological Society of America Bulletin 110(1): 2-21.

DeCelles, P. G., D. M. Robinson, J. Quade, T. P. Ojha, C. N. Garzione, P. Copeland and B. N. Upreti (2001). "Stratigraphy, structure, and tectonic evolution of the Himalayan fold-thrust belt in western Nepal." Tectonics 20(4): 487-509.

Degg, M. and J. Homan (2005). "Earthquake vulnerability in the Middle East." Geography 90: 54-66.

Deng, Q. D., P. Z. Zhang, X. W. Xu, X. P. Yang, S. Z. Peng and X. Y. Feng (1996). "Paleoseismology of the northern piedmont of Tianshan Mountains, northwestern China." Journal of Geophysical Research-Solid Earth 101(B3): 5895-5920.

Derbyshire, E. (1987). "A history of the glacial stratigraphy in China." Quaternary Science Reviews 6: 301-314.

Dortch, J. M., L. A. Owen and M. W. Caffee (2013). "Timing and climatic drivers for glaciation across semi-arid western Himalayan-Tibetan orogen." Quaternary Science Reviews 78: 188-208.

Drew, F. (1873). "Alluvial and lacustrine deposits and glacial records of the upper Indus basin; part 1, alluvial deposits." The Quarterly journal of the Geological Society of London 29: 449-471.

Dyurgerov, M., M. F. Meier and D. B. Bahr (2009). "A new index of glacier area change: a tool for glacier monitoring." Journal of Glaciology 55(192): 710-716.

Dziewonski, A. M., T. A. Chou and J. H. Woodhouse (1981). "Determination of earthquake source parameters from waveform data for studies of global and regional seismicity." Journal of Geophysical Research 86(NB4): 2825-2852.

Eakins, J. D. and R. T. Morrison (1978). "New procedure for determination of Pb-210 in lake and marine sediments." International Journal of Applied Radiation and Isotopes 29(9-10): 531-536.

Ekstrom, G., M. Nettles and A. M. Dziewonski (2012). "The global CMT project 2004-2010: Centroid-moment tensors for 13,017 earthquakes." Physics of the Earth and Planetary Interiors 200: 1-9.

Eugster, P., D. Scherler, R. C. Thiede, A. T. Codilean and M. R. Strecker (2016). "Rapid Last Glacial Maximum deglaciation in the Indian Himalaya coeval with midlatitude glaciers: New insights from Be-10-dating of ice-polished bedrock surfaces in the Chandra Valley, NW Himalaya." Geophysical Research Letters 43(4): 1589-1597.

Feldl, N. and R. Bilham (2006). "Great Himalayan earthquakes and the Tibetan plateau." Nature 444(7116): 165-170.

Fenton, C. R., R. L. Hermanns, L. H. Blikra, P. W. Kubik, C. Bryant, S. Niedermann, A. Meixner and M. M. Goethals (2011). "Regional Be-10 production rate calibration for the past 12 ka deduced from the radiocarbon-dated Grotlandsura and Russenes rock avalanches at 69 degrees N, Norway." Quaternary Geochronology 6(5): 437-452.

Finkel, R. C., L. A. Owen, P. L. Barnard and M. W. Caffee (2003). "Beryllium-10 dating of Mount Everest moraines indicates a strong monsoon influence and glacial synchroneity throughout the Himalaya." Geology 31(6): 561-564.

Folk, R. L. W., W. C. (1957). "Brazos River bar: A study in the significance of the grain size parameters." Journal of Sedimentary Research 27: 3-26.

Fort, M. (2004). Quaternary glaciation in the Nepal Himalaya. Developments in Quaternary Sciences. J. Ehlers and P. L. Gibbard, Elsevier. 2: 261-278. Fort, M., Rimal, L. N., Bourles, D., Guillou, V., Balescu, S., Huot, S. and L. Lamothe (2013). "The paraglacial, giant landslide dam of Phoksundo Lake (Dolpo District, Western Nepal Himalaya). (In preparation).

Frenzel, B. (1950). "Die Vegetations- und Landschaftszonen Nordeurasiens während der letzten Eiszeit und während der PostglazialenWarmezeit." Abhandlungen der Mathematisch-Naturwissenschaftlichen Klasse 13: 937-1099.

Frueh, W. T. and S. T. Lancaster (2014). "Correction of deposit ages for inherited ages of charcoal: implications for sediment dynamics inferred from random sampling of deposits on headwater valley floors." Quaternary Science Reviews 88: 110-124.

Fu, Y. N. and J. T. Freymueller (2012). "Seasonal and long-term vertical deformation in the Nepal Himalaya constrained by GPS and GRACE measurements." Journal of Geophysical Research-Solid Earth 117.

Fuchs, G. (1977). "The Geology of the Karnali and Dolpo Regions, Western Nepal." Jahrbuch der Geologischen Bundesanstalt 120: 165-217.

Fuchs, G. and W. Frank (1970). The Geology of West Nepal between the Rivers Kali Gandaki and Thulo Bheri. Vienna, Jahrbuch der Geologischen Bundesanstalt.

Gabet, E. J., D. W. Burbank, B. Pratt-Sitaula, J. Putkonen and B. Bookhagen (2008). "Modem erosion rates in the High Himalayas of Nepal." Earth and Planetary Science Letters 267(3-4): 482-494.

Gao, S. S., P. G. Silver, A. T. Linde and I. S. Sacks (2000). "Annual modulation of triggered seismicity following the 1992 Landers earthquake in California." Nature 406(6795): 500-504.

Gardner, J. K. and L. Knopoff (1974). "Sequence of earthquakes in southern California, with aftershocks removed, Poissonian." Bulletin of the Seismological Society of America 64(15): 1363-1367.

Ghazoui, Z., Bertrand, S., Vanneste, K., Yokoyama, Y., Nomade, J., Gajurel, A.P., and P. A. van der Beek (2018). “Large post-1505 AD earthquakes in western Nepal revealed by a new lake sediment record.” Nature Communications (in review).

Ghosh, G. K. and A. K. Mahajan (2013). "Intensity attenuation relation at Chamba-Garhwal area in north-west Himalaya with epicentral distance and magnitude." Journal of Earth System Science 122(1): 107-122.

Godard, V., D. L. Bourles, F. Spinabella, D. W. Burbank, B. Bookhagen, G. B. Fisher, A. Moulin and L. Leanni (2014). "Dominance of tectonics over climate in Himalayan denudation." Geology 42(3): 243-246.

Godard, V. and D. W. Burbank (2011). "Mechanical analysis of controls on strain partitioning in the Himalayas of central Nepal." Journal of Geophysical Research-Solid Earth 116.

Goehring, B. M., O. S. Lohne, J. Mangerud, J. I. Svendsen, R. Gyllencreutz, J. Schaefer and R. Finkel (2012). "Late glacial and holocene 10Be production rates for western Norway." Journal of Quaternary Science 27(1): 89-96.

Goldfinger, C., Y. Ikeda, R. S. Yeats and J. J. Ren (2013). "Superquakes and Supercycles." Seismological Research Letters 84(1): 24-32.

Gomez, B., A. Corral, A. R. Orpin, M. J. Page, H. Pouderoux and P. Upton (2015). "Lake Tutira paleoseismic record confirms random, moderate to major and/or great Hawke's Bay (New Zealand) earthquakes." Geology 43(2): 103-106.

Grove, J. M. (2004). Little Ice ages: Ancient and modern. London, Routledge.

Grujic, D., I. Coutand, B. Bookhagen, S. Bonnet, A. Blythe and C. Duncan (2006). "Climatic forcing of erosion, landscape, and tectonics in the Bhutan Himalayas." Geology 34(10): 801-804.

Hainzl, S., Y. Ben-Zion, C. Cattania and J. Wassermann (2013). "Testing atmospheric and tidal earthquake triggering at Mt. Hochstaufen, Germany." Journal of Geophysical Research-Solid Earth 118(10): 5442-5452.

Halvorson, S. J. and J. P. Hamilton (2007). "Vulnerability and the erosion of seismic culture in mountainous Central Asia." Mountain Research and Development 27(4): 322-330.

Hampel, A., R. Hetzel and G. Maniatis (2010). "Response of faults to climate-driven changes in ice and water volumes on Earth's surface." Philosophical Transactions of the Royal Society a-Mathematical Physical and Engineering Sciences 368(1919): 2501-2517.

Hampel, A., R. Hetzel, G. Maniatis and T. Karow (2009). "Three-dimensional numerical modeling of slip rate variations on normal and thrust fault arrays during ice cap growth and melting." Journal of Geophysical Research-Solid Earth 114.

Harper, J. T. and N. F. Humphrey (2003). "High altitude Himalayan climate inferred from glacial ice flux." Geophysical Research Letters 30(14).

Harvey, J. E., D. W. Burbank and B. Bookhagen (2015). "Along-strike changes in Himalayan thrust geometry: Topographic and tectonic discontinuities in western Nepal." Lithosphere 7(5): 511-518.

Hayes, G. P., R. W. Briggs, W. D. Barnhart, W. L. Yeck, D. E. McNamara, D. J. Wald, J. L. Nealy, H. M. Benz, R. D. Gold, K. S. Jaiswal, K. Marano, P. S. Earle, M. G. Hearne, G. M. Smoczyk, L. A. Wald and S. V. Samsonov (2015). "Rapid Characterization of the 2015 M-w 7.8 Gorkha, Nepal, Earthquake Sequence and Its Seismotectonic Context." Seismological Research Letters 86(6): 1557-1567.

Heki, K. (2003). "Snow load and seasonal variation of earthquake occurrence in Japan." Earth and Planetary Science Letters 207(1-4): 159-164.

Helman-Wazny, A. and C. Ramble (2017). "Tibetan documents in the archives of the Tantric Lamas of Tshognam in Mustang, Nepal: An interdisciplinary case study." Revue D Etudes Tibetaines(39): 266-341.

Helmstetter, A. (2003). "Is earthquake triggering driven by small earthquakes?" Physical Review Letters 91(5).

Helmstetter, A. and D. Sornette (2002). "Subcritical and supercritical regimes in epidemic models of earthquake aftershocks." Journal of Geophysical Research-Solid Earth 107(B10).

Herman, F., P. Copeland, J. P. Avouac, L. Bollinger, G. Maheo, P. Le Fort, S. Rai, D. Foster, A. Pecher, K. Stuwe and P. Henry (2010). "Exhumation, crustal deformation, and thermal structure of the Nepal Himalaya derived from the inversion of thermochronological and thermobarometric data and modeling of the topography." Journal of Geophysical Research-Solid Earth 115.

Herrendorfer, R., Y. van Dinther, T. Gerya and L. A. Dalguer (2015). "Earthquake supercycle in subduction zones controlled by the width of the seismogenic zone." Nature Geoscience 8(6): 471-U473.

Hetzel, R. and A. Hampel (2005). "Slip rate variations on normal faults during glacial-interglacial changes in surface loads." Nature 435(7038): 81-84.

Hewitt, K. (2009). "Catastrophic rock slope failures and late Quaternary developments in the Nanga Parbat-Haramosh Massif, Upper Indus basin, northern Pakistan." Quaternary Science Reviews 28(11-12): 1055-1069.

Hodges, K. V. (2000). "Tectonics of the Himalaya and southern Tibet from two perspectives." Geological Society of America Bulletin 112(3): 324-350.

Howarth, J. D., S. J. Fitzsimons, R. J. Norris and G. E. Jacobsen (2014). "Lake sediments record high intensity shaking that provides insight into the location and rupture length of large earthquakes on the Alpine Fault, New Zealand." Earth and Planetary Science Letters 403: 340-351.

Holzhauser, H., M. Magny and H. J. Zumbuühl (2005). "Glacier and lake-level variations in west-central Europe over the last 3500 years." The Holocene 15(6): 789-801.

Hu, G., C. L. Yi, J. F. Zhang, J. H. Liu and T. Jiang (2015). "Luminescence dating of glacial deposits near the eastern Himalayan syntaxis using different grain-size fractions." Quaternary Science Reviews 124: 124-144.

Hubbard, J., R. Almeida, A. Foster, S. N. Sapkota, P. Burgi and P. Tapponnier (2016). "Structural segmentation controlled the 2015 M-w 7.8 Gorkha earthquake rupture in Nepal." Geology 44(8): 639-642.

Iturrizaga, L. (2003). "Distribution and genesis of lateroglacial valleys in the Karakoram Mountains (Pakistan)." Zeitschrift Fur Geomorphologie 47: 51-74.

Jackson, D. (2002). The great Western-Himalayan earthquake of 1505: A rupture of the Central Himalayan Gap? Tibet, Past and Present: Tibetan Studies I. H. Blezer. 2: 147-159.

Johnson, C. W., Y. N. Fu and R. Burgmann (2017). "Seasonal water storage, stress modulation, and California seismicity." Science 356(6343): 1161-1164.

Johnson, P. G. (1984). "Paraglacial conditions of instability and mass movement - A discussion." Zeitschrift Fur Geomorphologie 28(2): 235-250.

Jouanne, F., J. L. Mugnier, S. N. Sapkota, P. Bascou and A. Pecher (2017). "Estimation of coupling along the Main Himalayan Thrust in the central Himalaya." Journal of Asian Earth Sciences 133: 62-71.

Kagan, Y. Y. (2013). Earthquakes: models, statistics, testable forecasts. New York, John Wiley and Sons, Inc.

Kagan, Y. Y., P. Bird and D. D. Jackson (2010). "Earthquake Patterns in Diverse Tectonic Zones of the Globe." Pure and Applied Geophysics 167(6-7): 721-741.

Kagan, Y. Y. and D. D. Jackson (1995). "New seismic gap hypothesis - 5 years after." Journal of Geophysical Research-Solid Earth 100(B3): 3943-3959.

Kak, A. C. S., M. (1988). Principles of computerized tomographic imaging, IEEE Press.

Kaser, G. O., H. (2002). Tropical Glaciers, Cambridge University Press.

Kelly, P. M. and C. B. Sear (1984). "Climatic impact of explosive volcanic eruptions." Nature 311(5988): 740-743.

Kelson, K. I., G. D. Simpson, R. B. VanArsdale, C. C. Haraden and W. R. Lettis (1996). "Multiple late Holocene earthquakes along the Reelfoot fault, central New Madrid seismic zone." Journal of Geophysical Research-Solid Earth 101(B3): 6151-6170.

Kenner, S. J. and M. Simons (2005). "Temporal clustering of major earthquakes along individual faults due to post-seismic reloading." Geophysical Journal International 160(1): 179-194.

Kirkbride, M. P. and S. Winkler (2012). "Correlation of Late Quaternary moraines: impact of climate variability, glacier response, and chronological resolution." Quaternary Science Reviews 46: 1-29.

Klute, F. (1930). "Verschiebung der Klimagebiete der letzten Eiszeit." Petermanns Mitt 209: 166-182.

Kohl, C. P. and K. Nishiizumi (1992). "Chemical isolation of quartz for measurement of insitu produced cosmogenic nuclides." Geochimica Et Cosmochimica Acta 56(9): 3583-3587.

Korschinek, G., A. Bergmaier, T. Faestermann, U. C. Gerstmann, K. Knie, G. Rugel, A. Wallner, I. Dillmann, G. Dollinger, C. L. von Gostomski, K. Kossert, M. Maiti, M. Poutivtsev and A. Remmert (2010). "A new value for the half-life of Be-10 by Heavy-Ion Elastic Recoil Detection and liquid scintillation counting." Nuclear Instruments and Methods in Physics Research Section B-Beam Interactions with Materials and Atoms 268(2): 187-191.

Korup, O., D. R. Montgomery and K. Hewitt (2010). "Glacier and landslide feedbacks to topographic relief in the Himalayan syntaxes." Proceedings of the National Academy of Sciences of the United States of America 107(12): 5317-5322.

Kremer, K., S. B. Wirth, A. Reusch, D. Fah, B. Bellwald, F. S. Anselmetti, S. Girardclos and M. Strasser (2017). "Lake-sediment based paleoseismology: Limitations and perspectives from the Swiss Alps." Quaternary Science Reviews 168: 1-18.

Kuhle, M. (1985). "Ein Subtropisches Inlandeis Als Eiszeitauslöser, Südtibet Un Mt. Everest Expedition 1984." Nachrichten aus der Universität Gottingen: 1-17.

Kuhle, M. (1985). "Permafrost and periglacial indicators on the Tibetan plateau from the Himalaya mountains in the south to the Quilian Shan in the north (28-40 degrees N)." Zeitschrift Fur Geomorphologie 29(2): 183-192.

Kuhle, M. (1995). "Glacial isostatic uplift of Tibet as a consequence of a former ice sheet." GeoJournal 37: 431-449.

Kull, C., S. Imhof, M. Grosjean, R. Zech and H. Veit (2008). "Late Pleistocene glaciation in the Central Andes: Temperature versus humidity control - A case study from the eastern Bolivian Andes (17 degrees S) and regional synthesis." Global and Planetary Change 60(1-2): 148-164.

Kumahara, Y. and R. Jayangondaperumal (2013). "Paleoseismic evidence of a surface rupture along the northwestern Himalayan Frontal Thrust (HFT)." Geomorphology 180: 47-56.

Kumar, S., S. G. Wesnousky, R. Jayangondaperumal, T. Nakata, Y. Kumahara and V. Singh (2010). "Paleoseismological evidence of surface faulting along the northeastern Himalayan front, India: Timing, size, and spatial extent of great earthquakes." Journal of Geophysical Research-Solid Earth 115.

Kumar, S., S. G. Wesnousky, T. K. Rockwell, R. W. Briggs, V. C. Thakur and R. Jayangondaperumal (2006). "Paleoseismic evidence of great surface rupture earthquakes along the Indian Himalaya." Journal of Geophysical Research-Solid Earth 111(B3).

Kumar, V., M. Mehta, A. Mishra and A. Trivedi (2017). "Temporal fluctuations and frontal area change of Bangni and Dunagiri glaciers from 1962 to 2013, Dhauliganga Basin, central Himalaya, India." Geomorphology 284: 88-98.

Langenbach, R. (2010). Better than steel? The use of timber for large and tall buildings from ancient times until the present.

Langenbach, R. (2013). The great counterintuitive: Re-evaluating historic and contemporary building construction for earthquake collapse prevention.

Langenbach, R. (2015). The earthquake resistant vernacular architecture in the Himalayas. Seismic retrofitting: Learning from vernacular architecture. London, Correia, Lourenço and Varum: 83-92.

Langenbach, R. (2016). What we learn from vernacular construction. Nonconvetional and Vernacular Construction Materials, Woodhead Publishing: 3-26.

Lave, J., D. Yule, S. Sapkota, K. Basant, C. Madden, M. Attal and R. Pandey (2005). "Evidence for a great medieval earthquake (approximate to 1100 AD) in the Central Himalayas, Nepal." Science 307(5713): 1302-1305.

Le Fort, P. (1975). "Himalayas, the collided range: Present knowledge of the continental arc." American Journal of Science 275a: 1-44.

Le Roux-Mallouf, R., M. Ferry, J. F. Ritz, T. Berthet, R. Cattin and D. Drukpa (2016). "First paleoseismic evidence for great surface-rupturing earthquakes in the Bhutan Himalayas." Journal of Geophysical Research-Solid Earth 121(10): 7271-7283.

Lemarchand, N. and J. R. Grasso (2007). "Interactions between earthquakes and volcano activity." Geophysical Research Letters 34(24).

Lifton, N. (2016). "Implications of two Holocene time-dependent geomagnetic models for comogenic nuclide production rate scaling." Earth and Planetary Science Letters 433: 257-268.

Lifton, N., T. Sato and T. J. Dunai (2014). "Scaling in situ cosmogenic nuclide production rates using analytical approximations to atmospheric cosmic-ray fluxes." Earth and Planetary Science Letters 386: 149-160.

Linde, A. T. and I. S. Sacks (1998). "Triggering of volcanic eruptions." Nature 395(6705): 888-890.

Loibl, D., F. Lehmkuhl and J. Griessinger (2014). "Reconstructing glacier retreat since the Little Ice Age in SE Tibet by glacier mapping and equilibrium line altitude calculation." Geomorphology 214: 22-39.

Louis, H. (1955). "Schneegrenze und Schneegrenzbestimmung." Geographisches Taschenbuch 55: 414-418.

Lu, Z., H. Yi and L. X. Wen (2018). "Loading-Induced Earth's Stress Change Over Time." Journal of Geophysical Research-Solid Earth 123(5): 4285-4306.

Main, I. (1996). "Statistical physics, seismogenesis, and seismic hazard." Reviews of Geophysics 34(4): 433-462.

Mann, M. E., R. S. Bradley and M. K. Hughes (1998). "Global-scale temperature patterns and climate forcing over the past six centuries." Nature 392(6678): 779-787.

Martin, L. C. P., P. H. Blard, G. Balco, J. Lave, R. Delunel, N. Lifton and V. Laurent (2017). "The CREp program and the ICE-D production rate calibration database: A fully

parameterizable and updated online tool to compute cosmic ray exposure ages." Quaternary Geochronology 38: 25-49.

Marzocchi, W. and L. Zaccarelli (2006). "A quantitative model for the time-size distribution of eruptions." Journal of Geophysical Research-Solid Earth 111(B4).

Mathieu, G. G., P. E. Biscaye, R. A. Lupton and D. E. Hammond (1988). "System for measurement of Rn-222 at low levels in natural waters." Health Physics 55(6): 989-992.

McCalpin, J. P. (1993). "Neotectonics of the northeastern Basin and Range margin, western USA." Zeitschrift Fur Geomorphologie 94: 137-157.

McCalpin, J. P. and V. S. Khromovskikh (1995). "Holocene paleoseismicity of the Tunka Fault, Baikal rift, Russia." Tectonics 14(3): 594-605.

McCalpin, J. P. and S. P. Nishenko (1996). "Holocene paleoseismicity, temporal clustering, and probabilities of future large (M>7) earthquakes on the Wasatch fault zone, Utah." Journal of Geophysical Research-Solid Earth 101(B3): 6233-6253.

McGregor, H. V., L. Dupont, J. B. W. Stuut and H. Kuhlmann (2009). "Vegetation change, goats, and religion: a 2000-year history of land use in southern Morocco." Quaternary Science Reviews 28(15-16): 1434-1448.

Mehta, M., D. P. Dobhal, B. Pratap, Z. Majeed, A. K. Gupta and P. Srivastava (2014). "Late Quaternary glacial advances in the Tons River Valley, Garhwal Himalaya, India and regional synchronicity." Holocene 24(10): 1336-1350.

Merchel, S. and U. Herpers (1999). "An update on radiochemical separation techniques for the determination of long-lived radionuclides via accelerator mass spectrometry." Radiochimica Acta 84(4): 215-219.

Merritts, D. J. (1996). "The Mendocino triple junction: Active faults, episodic coastal emergence, and rapid uplift." Journal of Geophysical Research-Solid Earth 101(B3): 6051-6070.

Meyers, P. A. and J. L. Teranes (2001). “Sediment organic matter.” In: Last, W. M. and Smol, J. P. (eds) “Tracking Environmental Changes Using Lake Sediment, Vol. 2: Physical and Geochemical Methods”. Dordrecht: Kluwer Academic, 239–270.

Moernaut, J., M. Van Daele, K. Fontijn, K. Heirman, P. Kempf, M. Pino, G. Valdebenito, R. Urrutia, M. Strasser and M. De Batist (2018). "Larger earthquakes recur more periodically: New insights in the megathrust earthquake cycle from lacustrine turbidite records in south-central Chile." Earth and Planetary Science Letters 481: 9-19.

Moernaut, J., M. Van Daele, K. Heirman, K. Fontijn, M. Strasser, M. Pino, R. Urrutia and M. De Batist (2014). "Lacustrine turbidites as a tool for quantitative earthquake reconstruction: New evidence for a variable rupture mode in south central Chile." Journal of Geophysical Research-Solid Earth 119(3): 1607-1633.

Moernaut, J., M. Van Daele, M. Strasser, M. A. Clare, K. Heirman, M. Viel, J. Cardenas, R. Kilian, B. L. de Guevara, M. Pino, R. Urrutia and M. De Batist (2017). "Lacustrine turbidites produced by surficial slope sediment remobilization: A mechanism for continuous and sensitive turbidite paleoseismic records." Marine Geology 384: 159-176.

Molnar, P., W. R. Boos and D. S. Battisti (2010). Orographic Controls on Climate and Paleoclimate of Asia: Thermal and Mechanical Roles for the Tibetan Plateau. Annual

Review of Earth and Planetary Sciences, Vol 38. R. Jeanloz and K. H. Freeman. 38: 77-102.

Monecke, K., F. S. Anselmetti, A. Becker, M. Sturm and D. Giardini (2004). "The record of historic earthquakes in lake sediments of Central Switzerland." Tectonophysics 394(1-2): 21-40.

Monelli, D., M. Pagani, G. Weatherill, L. Danciu and J. Garcia (2014). "Modeling Distributed Seismicity for Probabilistic Seismic-Hazard Analysis: Implementation and Insights with the OpenQuake Engine." Bulletin of the Seismological Society of America 104(4): 1636-1649.

Mugnier, J. L., A. Gajurel, P. Huyghe, R. Jayangondaperumal, F. Jouanne and B. Upreti (2013). "Structural interpretation of the great earthquakes of the last millennium in the central Himalaya." Earth-Science Reviews 127: 30-47.

Murari, M. K., L. A. Owen, J. M. Dortch, M. W. Caffee, C. Dietsch, M. Fuchs, W. C. Haneberg, M. C. Sharma and A. Townsend-Small (2014). "Timing and climatic drivers for glaciation across monsoon-influenced regions of the Himalayan-Tibetan orogen." Quaternary Science Reviews 88: 159-182.

Murphy, M. A., M. H. Taylor, J. Gosse, C. R. P. Silver, D. M. Whipp and C. Beaumont (2014). "Limit of strain partitioning in the Himalaya marked by large earthquakes in western Nepal." Nature Geoscience 7(1): 38-42.

Nakamura, A., Y. Yokoyama, H. Maemoku, H. Yagi, M. Okamura, H. Matsuoka, N. Miyake, T. Osada, H. Teramura, D. P. Adhikari, V. Dangol, Y. Miyairi, S. Obrochta and H. Matsuzaki (2012). "Late Holocene Asian monsoon variations recorded in Lake Rara sediment, western Nepal." Journal of Quaternary Science 27(2): 125-128.

Nakata, T. (1989). Active faults of the Himalaya of India and Nepal. Tectonics of the western Himalayas. J. L. L. Malinconico and R. J. Lillie, Geological Society of America.

Nicol, A., J. Walsh, V. Mouslopoulou and P. Villamor (2009). "Earthquake histories and Holocene acceleration of fault displacement rates." Geology 37(10): 911-914.

Nishenko, S. P. and L. R. Sykes (1993). "Seismic gap hypothesis - 10 years after - comment." Journal of Geophysical Research-Solid Earth 98(B6): 9909-9916.

NWFP, UN Habitat (2007). “Bhatar construction, timber reinforced masonry: An illustrated guide for craftsmen”. https://unhabitat.org

Obrochta, S. P., H. Miyahara, Y. Yokoyama and T. J. Crowley (2012). "A re-examination of evidence for the North Atlantic "1500-year cycle" at Site 609." Quaternary Science Reviews 55: 23-33.

Okada, A. (1980). "Quaternary faulting along the Median tectonic line of southwest Japan." Memoirs of the Geological Society of Japan 18: 79-108.

Okada, A. I., Y. (1991). "Active faults and Neotectonics in Japan." Quaternary Research 30(2): 161-174.

Okada, H. (1989). "Anatomy of trench-slope bassins - examples from the Nankai Trough." Palaeogeography Palaeoclimatology Palaeoecology 71(1-2): 3-13.

Okino, T. and Y. Satoh (1986). "Morphology, physics, chemistry and biology of Lake Rara in west Nepal." Hydrobiologia 140(2): 125-133.

Ota, Y. and J. Chappell (1996). "Late Quaternary coseismic uplift events on the Huon Peninsula, Papua New Guinea, deduced from coral terrace data." Journal of Geophysical Research-Solid Earth 101(B3): 6071-6082.

Owen, L. A. (2009). "Latest Pleistocene and Holocene glacier fluctuations in the Himalaya and Tibet." Quaternary Science Reviews 28(21-22): 2150-2164.

Owen, L. A. and D. I. Benn (2005). "Equilibrium-line altitudes of the Last Glacial Maximum for the Himalaya and Tibet: an assessment and evaluation of results." Quaternary International 138: 55-78.

Owen, L. A., M. W. Caffee, K. R. Bovard, R. C. Finkel and M. C. Sharma (2006). "Terrestrial cosmogenic nuclide surface exposure dating of the oldest glacial successions in the Himalayan orogen: Ladakh Range, northern India." Geological Society of America Bulletin 118(3-4): 383-392.

Owen, L. A., M. W. Caffee, R. C. Finkel and Y. B. Seong (2008). "Quaternary glaciation of the Himalayan-Tibetan orogen." Journal of Quaternary Science 23(6-7): 513-531.

Owen, L. A. and J. M. Dortch (2014). "Nature and timing of Quaternary glaciation in the Himalayan-Tibetan orogen." Quaternary Science Reviews 88: 14-54.

Owen, L. A., R. C. Finkel, P. L. Barnard, H. Z. Ma, K. Asahi, M. W. Caffee and E. Derbyshire (2005). "Climatic and topographic controls on the style and timing of Late Quaternary glaciation throughout Tibet and the Himalaya defined by Be-10 cosmogenic radionuclide surface exposure dating." Quaternary Science Reviews 24(12-13): 1391-1411.

Owen, L. A., R. C. Finkel, M. Haizhou and P. L. Barnard (2006). "Late Quaternary landscape evolution in the Kunlun Mountains and Qaidam Basin, Northern Tibet: A framework for examining the links between glaciation, lake level changes and alluvial fan formation." Quaternary International 154: 73-86.

Owen, L. A., R. C. Finkel, M. Haizhou, J. Q. Spencer, E. Derbyshire, P. L. Barnard and M. W. Caffee (2003). "Timing and style of Late Quaternary glaciation in northeastern Tibet." Geological Society of America Bulletin 115(11): 1356-1364.

Owen, L. A., C. L. Yi, R. C. Finkel and N. K. Davis (2010). "Quaternary glaciation of Gurla Mandhata (Naimon'anyi)." Quaternary Science Reviews 29(15-16): 1817-1830.

Pagani, M. M., D.,Weatherill, G., Danciu, L., Crowley, H., Silva, V., Henshaw, P., Butler, L., Nastasi, M. L. S., Panzeri, M.,Vigano, D. (2014). "OpenQuake Engine: An Open Hazard (and Risk) Software for the Global Earthquake Model." Seismological Research Letters 85(3): 692-702.

Pandey, M. R. M., O. (1988). "The distribution of intensity of the Bihar-Nepal earthquake of the 15 January 1934 and bounds on the extent of the rupture zone." Jourrnal of Nepal Geological Society 5: 22-44.

Pantosti, D., G. Daddezio and F. R. Cinti (1996). "Paleoseismicity of the Ovindoli-Pezza fault, central Apennines, Italy: A history including a large, previously unrecorded earthquake in the Middle Ages (860-1300 AD)." Journal of Geophysical Research-Solid Earth 101(B3): 5937-5959.

Patton, J. R., C. Goldfinger, A. E. Morey, K. Ikehara, C. Romsos, J. Stoner, Y. Djadjadihardja, Udrekh, A. Sri, E. Z. Gaffar and A. Vizcaino (2015). "A 6600 year earthquake history

in the region of the 2004 Sumatra-Andaman subduction zone earthquake." Geosphere 11(6): 2067-2129.

Penck, A. B., E. (1909). Die Alpen im Eiszeitalter. Vienna, Tauchnitz.

Pezzopane, S. K., J. W. Whitney and T. E. Dawson (1996). Models of earthquake reccurence and preliminary paleoearthquake magnitudes at Yucca Mountain. Seismotectonic framework and characterization of faulting at Yucca Mountain, Nevada. J. W. Whitney Nevada, Milestone 3GSH100M Denver, CO, US Geological Survey: 5-5000.

Pierce, I. and S. G. Wesnousky (2016). "On a flawed conclusion that the 1255AD earthquake ruptured 800km of the Himalayan Frontal Thrust east of Kathmandu." Geophysical Research Letters 43(17): 9026-9029.

Plaker, G. and C. M. Rubin (1994). Paleoseismic evidence for “yo-yo” tectonics above the eastern Aleutian subduction zone: coseismic uplift alternating with even larger interseismic submergence. U. G. Survey, US Geological Survey: 155-157.

Pollitz, F. F., A. Wech, H. Kao and R. Burgmann (2013). "Annual modulation of non-volcanic tremor in northern Cascadia." Journal of Geophysical Research-Solid Earth 118(5): 2445-2459.

Pouderoux, H., J. N. Proust and G. Lamarche (2014). "Submarine paleoseismology of the northern Hikurangi subduction margin of New Zealand as deduced from Turbidite record since 16 ka." Quaternary Science Reviews 84: 116-131.

Pratt-Sitaula, B., D. W. Burbank, A. M. Heimsath, N. F. Humphrey, M. Oskin and J. Putkonen (2011). "Topographic control of asynchronous glacial advances: A case study from Annapurna, Nepal." Geophysical Research Letters 38.

Putkonen, J., J. Connolly and T. Orloff (2008). "Landscape evolution degrades the geologic signature of past glaciations." Geomorphology 97(1-2): 208-217.

Putkonen, J. and T. Swanson (2003). "Accuracy of cosmogenic ages for moraines." Quaternary Research 59(2): 255-261.

Qiao, B. J. and C. L. Yi (2017). "Reconstruction of Little Ice Age glacier area and equilibrium line attitudes in the central and western Himalaya." Quaternary International 444: 65-75.

Rai, D. C. and C. V. R. Murty (2006). "Effects of the 2005 Muzaffarabad (Kashmir) earthquake on built environment." Current Science 90(8): 1066-1070.

Rajendran, C. P., B. John and K. Rajendran (2015). "Medieval pulse of great earthquakes in the central Himalaya: Viewing past activities on the frontal thrust." Journal of Geophysical Research-Solid Earth 120(3): 1623-1641.

Ramble, C. (1998). The classification of territorial divinities in Pagan and Buddhist rituals of South Mustang.

Ramble, C. (1999). "Selves in time and place: Identities, experience, and history in Nepal." Journal of Asian Studies 58(3): 879-881.

Reimer, P. J., E. Bard, A. Bayliss, J. W. Beck, P. G. Blackwell, C. B. Ramsey, C. E. Buck, H. Cheng, R. L. Edwards, M. Friedrich, P. M. Grootes, T. P. Guilderson, H. Haflidason, I. Hajdas, C. Hatte, T. J. Heaton, D. L. Hoffmann, A. G. Hogg, K. A. Hughen, K. F. Kaiser, B. Kromer, S. W. Manning, M. Niu, R. W. Reimer, D. A. Richards, E. M. Scott, J. R. Southon, R. A. Staff, C. S. M. Turney and J. van der Plicht (2013). "Intcal13

and Marine13 radiocarbon curves 0-50,000 years cal BP." Radiocarbon 55(4): 1869-1887.

Robert, X., P. van der Beek, J. Braun, C. Perry, M. Dubille and J. L. Mugnier (2009). "Assessing Quaternary reactivation of the Main Central thrust zone (central Nepal Himalaya): New thermochronologic data and numerical modeling." Geology 37(8): 731-734.

Rubin, C. M., B. P. Horton, K. Sieh, J. E. Pilarczyk, P. Daly, N. Ismail and A. C. Parnell (2017). "Highly variable recurrence of tsunamis in the 7,400 years before the 2004 Indian Ocean tsunami." Nature Communications 8: 12.

Rupper, S. and G. Roe (2008). "Glacier Changes and Regional Climate: A Mass and Energy Balance Approach." Journal of Climate 21(20): 5384-5401.

Rupper, S., G. Roe and A. Gillespie (2009). "Spatial patterns of Holocene glacier advance and retreat in Central Asia." Quaternary Research 72(3): 337-346.

Saichev, A. and D. Sornette (2007). "Power law distributions of seismic rates." Tectonophysics 431(1-4): 7-13.

Saichev, A. and D. Sornette (2007). "Theory of earthquake recurrence times." Journal of Geophysical Research-Solid Earth 112(B4).

Sanchez, L. and R. Shcherbakov (2012). "Temporal scaling of volcanic eruptions." Journal of Volcanology and Geothermal Research 247: 115-121.

Sapkota, S. N., L. Bollinger, Y. Klinger, P. Tapponnier, Y. Gaudemer and D. Tiwari (2013). "Primary surface ruptures of the great Himalayan earthquakes in 1934 and 1255 (vol 6, pg 71, 2013)." Nature Geoscience 6(2): 152-152.

Satake, K. and B. F. Atwater (2007). Long-term perspectives on giant earthquakes and tsunamis at subduction zones. Annual Review of Earth and Planetary Sciences. 35: 349-374.

Scafetta, N. and A. Mazzarella (2015). "Spectral coherence between climate oscillations and the M ≥7 earthquake historical worldwide record." Natural Hazards 76(3): 1807-1829.

Schaefer, J. M., G. H. Denton, M. R. Kaplan, A. Putnam, R. C. Finkel, D. J. A. Barrell, B. G. Andersen, R. Schwartz, A. Mackintosh, T. Chinn and C. Schluchter (2009). "High-Frequency Holocene Glacier Fluctuations in New Zealand Differ from the Northern Signature." Science 324(5927): 622-625.

Schafer, J. M., S. Tschudi, Z. Z. Zhao, X. H. Wu, S. Ivy-Ochs, R. Wieler, H. Baur, P. W. Kubik and C. Schluchter (2002). "The limited influence of glaciations in Tibet on global climate over the past 170 000 yr." Earth and Planetary Science Letters 194(3-4): 287-297.

Scharer, K. M., G. P. Biasi, R. J. Weldon and T. E. Fumal (2010). "Quasi-periodic recurrence of large earthquakes on the southern San Andreas fault." Geology 38(6): 555-558.

Scherler, D., B. Bookhagen and M. R. Strecker (2011). "Spatially variable response of Himalayan glaciers to climate change affected by debris cover." Nature Geoscience 4(3): 156-159.

Scherler, D., B. Bookhagen and M. R. Strecker (2014). "Tectonic control on Be-10-derived erosion rates in the Garhwal Himalaya, India." Journal of Geophysical Research-Earth Surface 119(2): 83-105.

Schiffman, C., B. S. Bali, W. Szeliga and R. Bilham (2013). "Seismic slip deficit in the Kashmir Himalaya from GPS observations." Geophysical Research Letters 40(21): 5642-5645.

Schnellmann, M., F. S. Anselmetti, D. Giardini, J. A. McKenzie and S. N. Ward (2002). "Prehistoric earthquake history revealed by lacustrine slump deposits." Geology 30(12): 1131-1134.

Schuster, A. (1897). "On lunar and solar periodicities of earthquakes." Proceedings of the Royal Society of London 61: 455-465.

Seong, Y. B., L. A. Owen, M. P. Bishop, A. Bush, P. Clendon, L. Copland, R. Finkel, U. Kamp and J. F. Shroder (2007). "Quaternary glacial history of the central karakoram." Quaternary Science Reviews 26(25-28): 3384-3405.

Shakesby, R. A. and J. A. Matthews (1996). "Glacial activity and paraglacial landsliding in the Devensian Lateglacial: Evidence from Craig Cerrig-gleisiad and Fan Dringarth, Fforest Fawr (Brecon Beacons), South Wales." Geological Journal 31(2): 143-157.

Shaw, R. B. (1871). Visits to High Tartary, Yarkard and Kashgar. Hong Kong, Oxford University Press.

Shi, Y., B. Zheng and S. Li (1992). "Last glaciation and maximum glaciation in the Qinghai-Xizang (Tibet) Plateau: A controversy to M. Kuhle's ice sheet hypothesis." Chinese Geographical Science 2(4): 293-311.

Shukla, T., M. Mehta, M. K. Jaiswal, P. Srivastava, D. P. Dobhal, H. C. Nainwal and A. K. Singh (2018). "Late Quaternary glaciation history of monsoon-dominated Dingad basin, central Himalaya, India." Quaternary Science Reviews 181: 43-64.

Silver, C. R. P., M. A. Murphy, M. H. Taylor, J. Gosse and T. Baltz (2015). "Neotectonics of the Western Nepal Fault System: Implications for Himalayan strain partitioning." Tectonics 34(12): 2494-2513.

Small, D. and D. Fabel (2015). "A Lateglacial Be-10 production rate from glacial lake shorelines in Scotland." Journal of Quaternary Science 30(6): 509-513.

Solomina, O. N., R. S. Bradley, D. A. Hodgson, S. Ivy-Ochs, V. Jomelli, A. N. Mackintosh, A. Nesje, L. A. Owen, H. Wanner, G. C. Wiles and N. E. Young (2015). "Holocene glacier fluctuations." Quaternary Science Reviews 111: 9-34.

Srivastava, H. N., B. K. Bansal and M. Verma (2013). "Largest earthquake in Himalaya: An appraisal." Journal of the Geological Society of India 82(1): 15-22.

Srivastava, P., R. Agnihotri, D. Sharma, N. Meena, M. P. Sundriyal, A. Saxena, R. Bhushan, R. Sawlani, U. S. Banerji, C. Sharma, P. Bisht, N. Rana and R. Jayangondaperumal (2017). "8000-year monsoonal record from Himalaya revealing reinforcement of tropical and global climate systems since mid-Holocene." Scientific Reports 7.

Steinhilber, F., J. Beer and C. Frohlich (2009). "Total solar irradiance during the Holocene." Geophysical Research Letters 36.

Stevens, V. L. and J. P. Avouac (2015). "Interseismic coupling on the main Himalayan thrust." Geophysical Research Letters 42(14): 5828-5837.

Stevens, V. L. and J. P. Avouac (2016). "Millenary M-w > 9.0 earthquakes required by geodetic strain in the Himalaya." Geophysical Research Letters 43(3): 1118-1123.

Stevens, V. L. and J. P. Avouac (2017). "Determination of M-max from Background Seismicity and Moment Conservation." Bulletin of the Seismological Society of America 107(6): 2578-2596.

Stewart, I. S., J. Sauber and J. Rose (2000). "Glacio-seismotectonics: ice sheets, crustal deformation and seismicity." Quaternary Science Reviews 19(14-15): 1367-1389.

Storchak, D. A., D. Di Giacomo, I. Bondar, E. R. Engdahl, J. Harris, W. H. K. Lee, A. Villasenor and P. Bormann (2013). "Public Release of the ISC-GEM Global Instrumental Earthquake Catalogue (1900-2009)." Seismological Research Letters 84(5): 810-815.

Strasser, M., F. S. Anselmetti, D. Fah, D. Giardini and M. Schnellmann (2006). "Magnitudes and source areas of large prehistoric northern Alpine earthquakes revealed by slope failures in lakes." Geology 34(12): 1005-1008.

Strecker, M. R., R. N. Alonso, B. Bookhagen, B. Carrapa, G. E. Hilley, E. R. Sobel and M. H. Trauth (2007). Tectonics and climate of the southern central Andes. Annual Review of Earth and Planetary Sciences. 35: 747-787.

Stroeven, A. P., J. Heyman, D. Fabel, S. Bjorck, M. W. Caffee, O. Fredin and J. M. Harbor (2015). "A new Scandinavian reference Be-10 production rate." Quaternary Geochronology 29: 104-115.

Sykes, L. R. and W. Menke (2006). "Repeat times of large earthquakes: Implications for earthquake mechanics and long-term prediction." Bulletin of the Seismological Society of America 96(5): 1569-1596.

Szeliga, W., S. Hough, S. Martin and R. Bilham (2010). "Intensity, Magnitude, Location, and Attenuation in India for Felt Earthquakes since 1762." Bulletin of the Seismological Society of America 100(2): 570-584.

Tahir, M. and J. R. Grasso (2014). "Aftershock Patterns of M-s > 7 Earthquakes in the India-Asia Collision Belt: Anomalous Results from the Muzaffarabad Earthquake Sequence, Kashmir, 2005." Bulletin of the Seismological Society of America 104(1): 1-23.

Tahir, M., J. R. Grasso and D. Amorese (2012). "The largest aftershock: How strong, how far away, how delayed?" Geophysical Research Letters 39.

Taylor, M. and A. Yin (2009). "Active structures of the Himalayan-Tibetan orogen and their relationships to earthquake distribution, contemporary strain field, and Cenozoic volcanism." Geosphere 5(3): 199-214.

Thiede, R. C., J. R. Arrowsmith, B. Bookhagen, M. O. McWilliams, E. R. Sobel and M. R. Strecker (2005). "From tectonically to erosionally controlled development of the Himalayan orogen." Geology 33(8): 689-692.

Traversa, P. and J. R. Grasso (2009). "Brittle Creep Damage as the Seismic Signature of Dyke Propagations within Basaltic Volcanoes." Bulletin of the Seismological Society of America 99(3): 2035-2043.

Uppala, S. M., P. W. Kallberg, A. J. Simmons, U. Andrae, V. D. Bechtold, M. Fiorino, J. K. Gibson, J. Haseler, A. Hernandez, G. A. Kelly, X. Li, K. Onogi, S. Saarinen, N. Sokka, R. P. Allan, E. Andersson, K. Arpe, M. A. Balmaseda, A. C. M. Beljaars, L. Van De Berg, J. Bidlot, N. Bormann, S. Caires, F. Chevallier, A. Dethof, M. Dragosavac, M. Fisher, M. Fuentes, S. Hagemann, E. Holm, B. J. Hoskins, L. Isaksen, P. Janssen, R. Jenne, A. P. McNally, J. F. Mahfouf, J. J. Morcrette, N. A. Rayner, R. W. Saunders, P. Simon, A. Sterl, K. E. Trenberth, A. Untch, D. Vasiljevic, P. Viterbo and J. Woollen (2005). "The ERA-40 re-analysis." Quarterly Journal of the Royal Meteorological Society 131(612): 2961-3012.

Upreti, B. N. (1999). "An overview of the stratigraphy and tectonics of the Nepal Himalaya." Journal of Asian Earth Sciences 17(5-6): 577-606.

van Dam, T., J. Wahr, P. C. D. Milly, A. B. Shmakin, G. Blewitt, D. Lavallee and K. M. Larson (2001). "Crustal displacements due to continental water loading." Geophysical Research Letters 28(4): 651-654.

van der Beek, P., C. Litty, M. Baudin, J. Mercier, X. Robert and E. Hardwick (2016). "Contrasting tectonically driven exhumation and incision patterns, western versus central Nepal Himalaya." Geology 44(4): 327-330.

Verardo, D. J., P. N. Froelich and A. McIntyre (1990). "Determination of organic carbon and nitrogen in marine sediments using the Carlo Erba NA-1500 Analyser." Deep-Sea Research 37: 157-165.

von Blanckenburg, F., R. K. O'Nions, N. S. Belshaw, A. Gibb and J. R. Hein (1996). "Global distribution of beryllium isotopes in deep ocean water as derived from Fe-Mn crusts." Earth and Planetary Science Letters 141(1-4): 213-226.

von Wissmann, H. (1959). "Die heutige Vergletscherung und Schneegrenze in Hochasien mit Hinweisen auf die Vergletscherung der letzten Eiszeit." Abhandlungen der Mathematisch-Naturwissenschaftlichen 14: 121-123.

Wanner, H., O. Solomina, M. Grosjean, S. P. Ritz and M. Jetel (2011). "Structure and origin of Holocene cold events." Quaternary Science Reviews 30(21-22): 3109-3123.

Weidinger, J. T. I., H. J. (2000). "Landslide dams of Tal, Latamrang, Ghatta Khola, Ringmo and Dharbang in the Neapl Himalayas and related hazards." Journal of the Nepal Geological Society 22: 371-380.

Weidinger, J.T. (2011) Stability and Life Span of Landslide Dams in the Himalayas (India, Nepal) and the Qin Ling Mountains (China). In: Evans, S.G., Hermanns, R.L., Strom, A. and Scarascia-Mugnozza, G., Eds., Natural and Artificial Rockslide Dams, Springer, Berlin, 243-277. http://dx.doi.org/10.1007/978-3-642-04764-0_8

Wesnousky, S. G., Y. Kumahara, D. Chamlagain, I. K. Pierce, A. Karki and D. Gautam (2017). "Geological observations on large earthquakes along the Himalayan frontal fault near Kathmandu, Nepal." Earth and Planetary Science Letters 457: 366-375.

Wesnousky, S. G., Y. Kumahara, D. Chamlagain, I. K. Pierce, T. Reedy, S. J. Angster and B. Giri (2017). "Large paleoearthquake timing and displacement near Damak in eastern Nepal on the Himalayan Frontal Thrust." Geophysical Research Letters 44(16): 8219-8226.

Wesnousky, S. G., Y. Kumahara, T. Nakata, D. Chamlagain and P. Neupane (2018). "New Observations Disagree With Previous Interpretations of Surface Rupture Along the Himalayan Frontal Thrust During the Great 1934 Bihar-Nepal Earthquake." Geophysical Research Letters 45(6): 2652-2658.

Whipple, K. X. (2009). "The influence of climate on the tectonic evolution of mountain belts." Nature Geoscience 2(2): 97-104.

Wilhelm, B., J. Nomade, C. Crouzet, C. Litty, P. Sabatier, S. Belle, Y. Rolland, M. Revel, F. Courboulex, F. Arnaud and F. S. Anselmetti (2016). "Quantified sensitivity of small lake sediments to record historic earthquakes: Implications for paleoseismology." Journal of Geophysical Research-Earth Surface 121(1): 2-16.

Willett, S. D. (1999). "Orogeny and orography: The effects of erosion on the structure of mountain belts." Journal of Geophysical Research-Solid Earth 104(B12): 28957-28981.

Wobus, C., A. Heimsath, K. Whipple and K. Hodges (2005). "Active out-of-sequence thrust faulting in the central Nepalese Himalaya." Nature 434(7036): 1008-1011.

Wu, S. C., C. A. Cornell and S. R. Winterstein (1995). "A hybrid reccurence model and its implication on seismic hazard results." Bulletin of the Seismological Society of America 85(1): 1-16. Yagi, H. (1977). "Origin of the Phoksundo Tal (Lake), Dolpa district, western Nepal". Journal of the Nepal Geological Society 15: 1-7.

Yokoyama, Y., M. Koizumi, H. Matsuzaki, Y. Miyairi and N. Ohkouchi (2010). "Developing ultra small-scale radiocarbon sample measurement at the University of Tokyo." Radiocarbon 52(2): 310-318.

Yokoyama, Y., Y. Miyairi, H. Matsuzaki and F. Tsunomori (2007). "Relation between acid dissolution time in the vacuum test tube and time required for graphitization for AMS target preparation." Nuclear Instruments and Methods in Physics Research Section B-Beam Interactions with Materials and Atoms 259(1): 330-334.

Young, N. E., J. M. Schaefer, J. P. Briner and B. M. Goehring (2013). "A Be-10 production-rate calibration for the Arctic." Journal of Quaternary Science 28(5): 515-526.

Yule, D., Dawson, S., Lavé, J., Sapkota, S. and D. Tiwari (2006). “Possible evidence for surface rupture of the Main Frontal Thrust during the great 1505 Himalayan earthquake, far-western Nepal.” American Geophysical Union Fall Meeting Abstracts #S33C–05.

Zang, A. and O. Stephansson (2010). Global stress. Stress Field of the Earth's Crust. Dordrecht, Springer Science + Business Media: 253-265.

Zech, R., I. Rohringer, P. Sosin, H. Kabgov, S. Merchel, S. Akhmadaliev and W. Zech (2013). "Late Pleistocene glaciations in the Gissar Range, Tajikistan, based on Be-10 surface exposure dating." Palaeogeography Palaeoclimatology Palaeoecology 369: 253-261.

Zech, R., M. Zech, P. W. Kubik, K. Kharki and W. Zech (2009). "Deglaciation and landscape history around Annapurna, Nepal, based on Be-10 surface exposure dating." Quaternary Science Reviews 28(11-12): 1106-1118.

Appendix A

Apatite Fision-Track results from a Dolpo transect (western Nepal)

This appendix provides an overview of the first field expedition in western Nepal (October─December 2013). The purpose of this mission was to collect river sediment samples in order to study the link between erosion, climate and tectonics based on Apatite fision-track (AFT) thermochronology and cosmogenic nuclide (^{10}Be) measurements on detrital apatite grains.

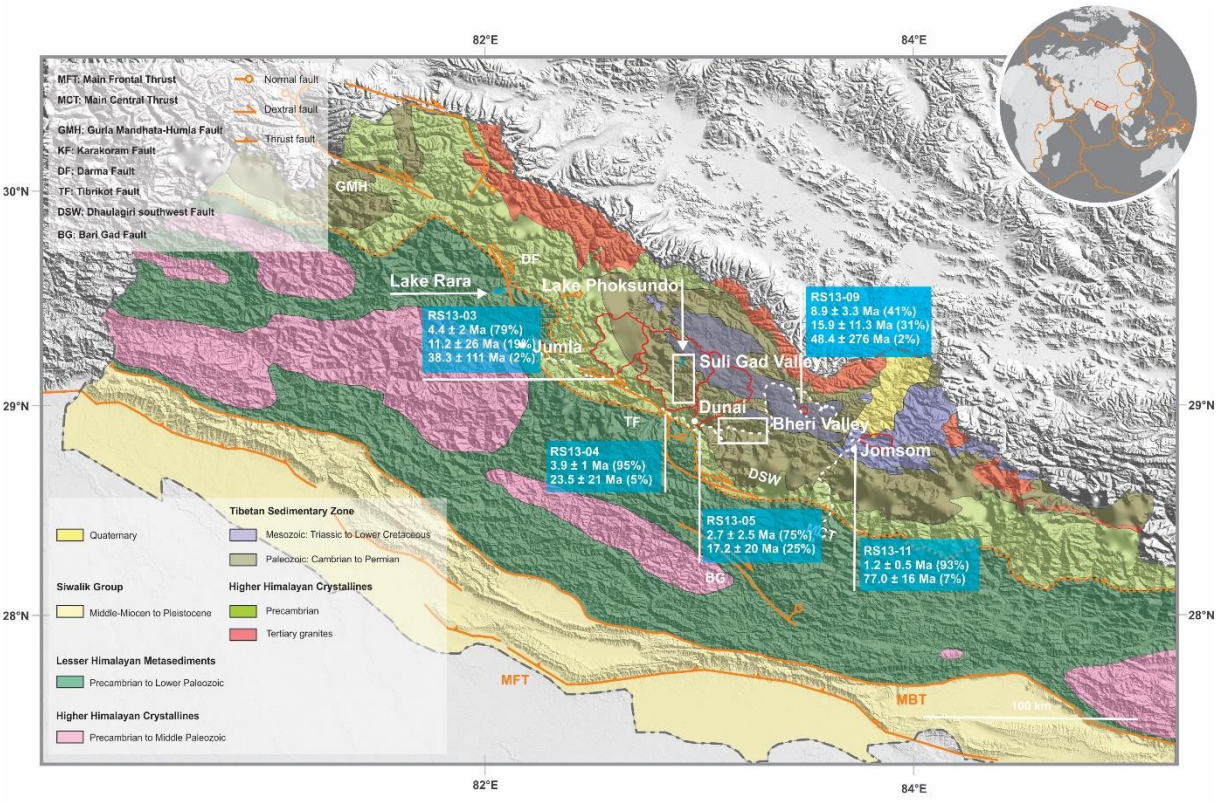

Figure A1. Simplified geological map of western Nepal (modified after Upretti, 1999). The blue boxes contain the different ages obtained from AFT measurements on river samples. The red curves illustrate the watersheds where the samples were collected. The white dotted curve illustrates the sampling journey. Active faults are shown in continuous orange lines and inactive major thrusts in dashed lines.

Appendix B

Short sediment core results from lakes Rara, Phoksundo and Dhumba (western Nepal)

This appendix provides an overview of the second expedition in western Nepal (October–December 2014). The purpose of this mission was to collect lacustrine sediment cores in order to study the regional paleoseismicity. In this appendix, we present the results obtained on the most representative core of each lake (Rara, Phoksundo and Dhumba). The location of the other cores is presented on the lake bathymetric maps, and the cores are illustrated using photographs and radiographs.

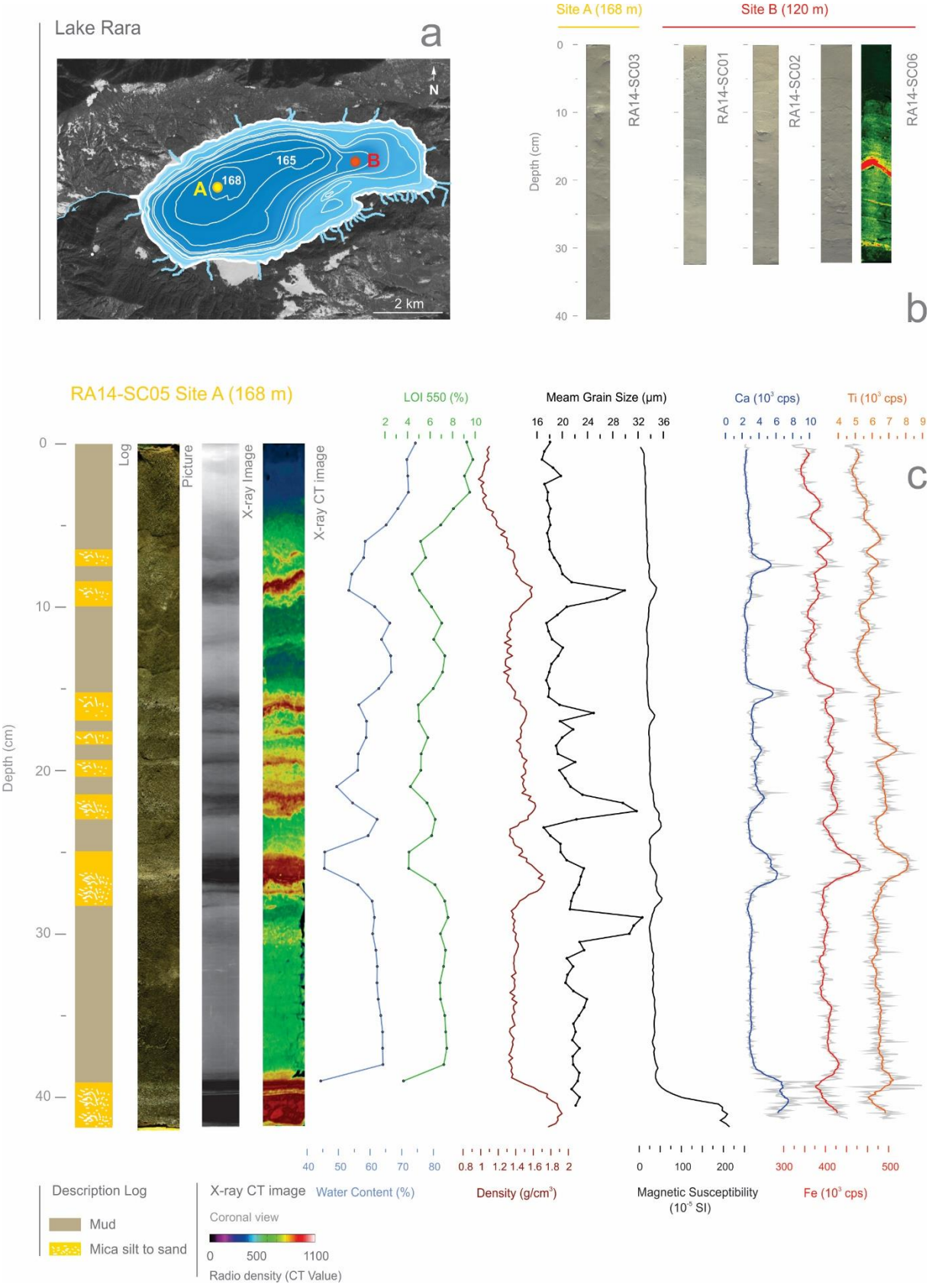

Figure B1. Summary of short sediment core results from Lake Rara. (**a**) Coring site location. (**b**) Photogaphs and X-ray CT scan image for all sediment cores. (**c**) Summary of the main results obtained on RA14-SC05 from site A at a depth of 168 m.

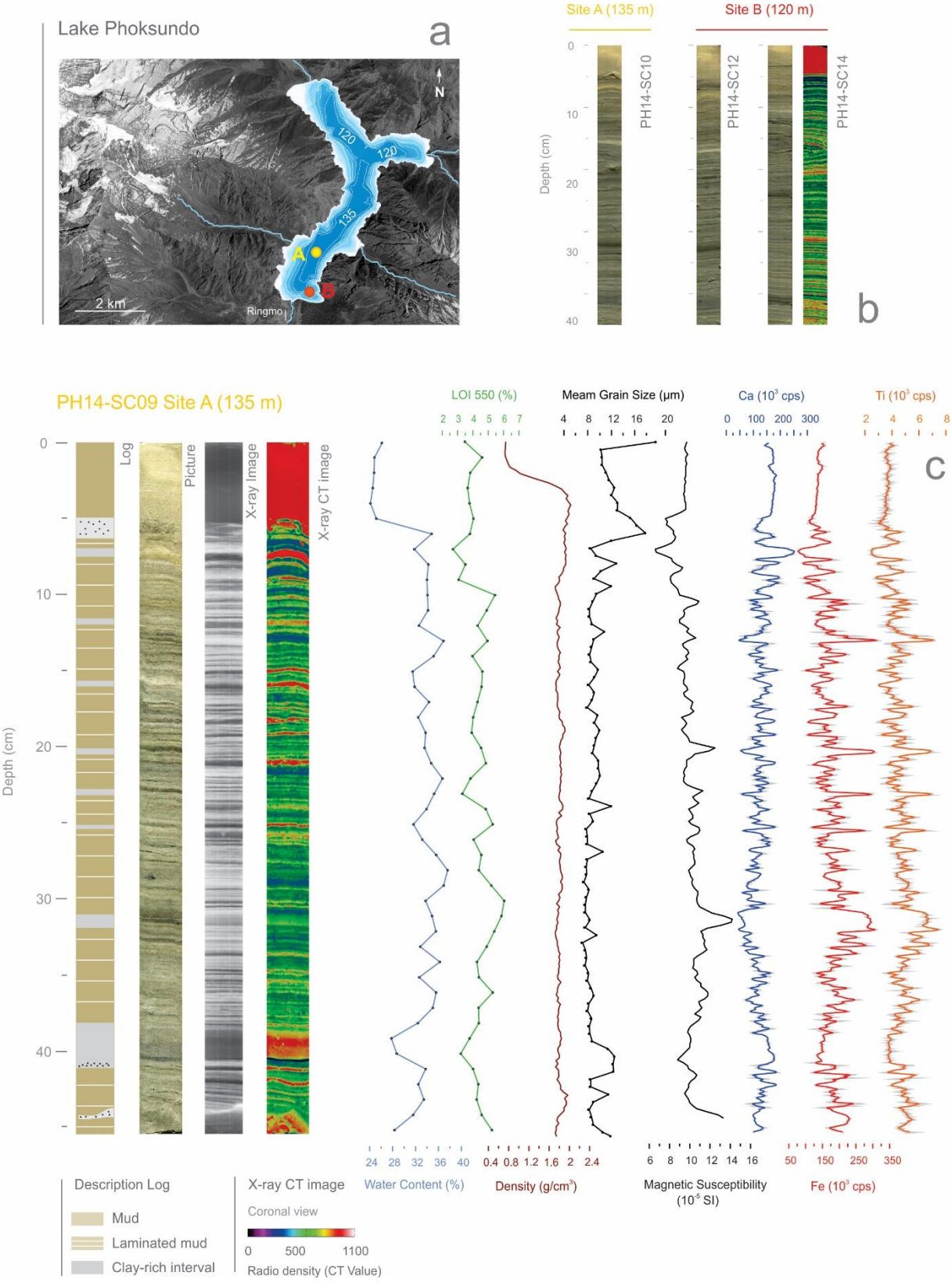

Figure B2. Summary of short sediment core results from Lake Phoksundo. (**a**) Coring site location. (**b**) Photographs and X-ray CT scan image for all sediment cores. (**c**) Summary of the main results obtained on PH14-SC09 from site A at a depth of 135 m.

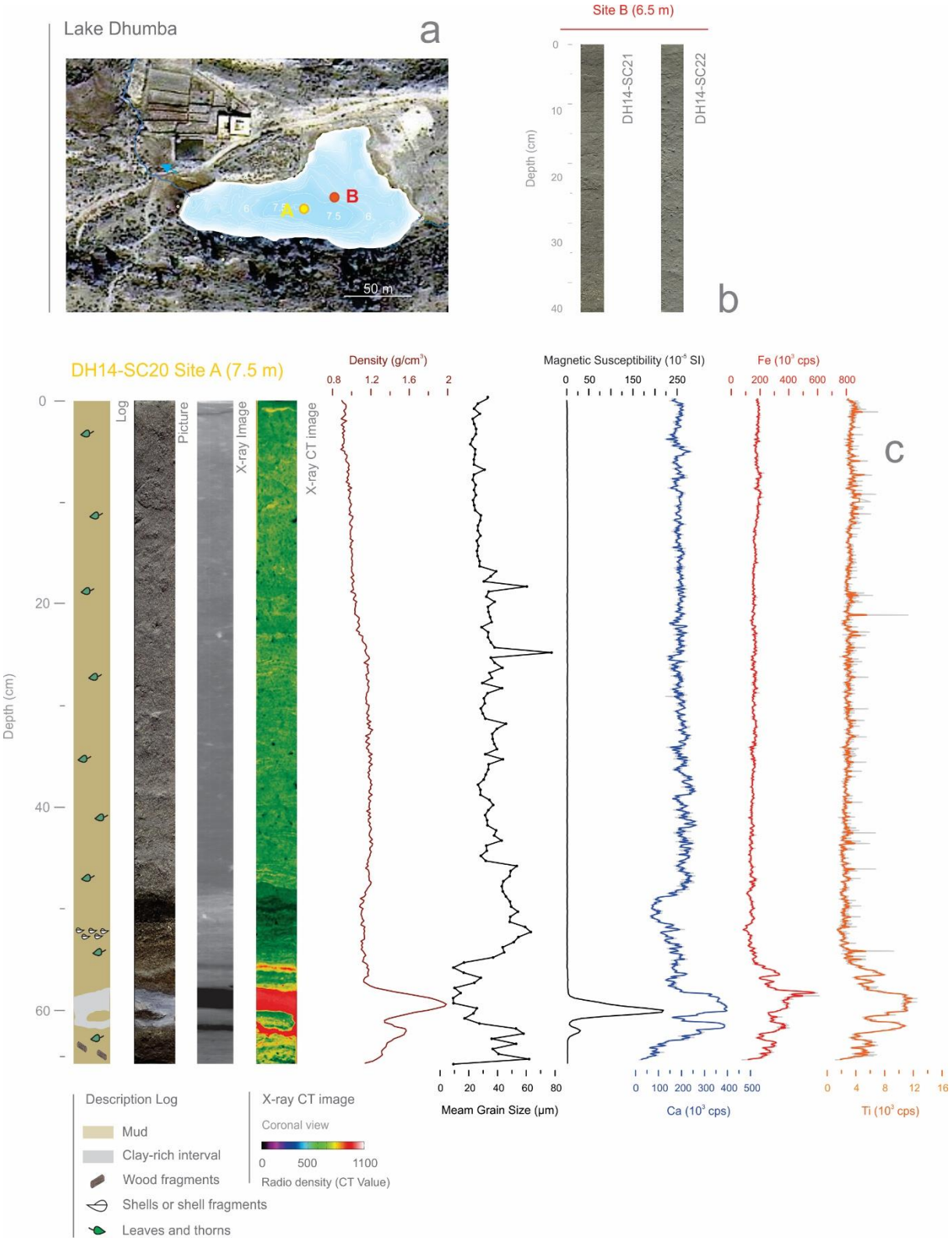

Figure B3. Summary of short sediment core results from Lake Dhumba. (**a**) Coring site location. (**b**) Photographs of all sediment cores. (**c**) Summary of the main results of DH14-SC20 from site A at a depth of 7.5 m.

Acknowledgements

First of all, I would like to thank in particular the members of the reading committee, Flavio Anselmetti and Rodolphe Cattin, as well as the members of the jury, Marc De Batist, Monique Fort and Jean-Robert Grasso, for their willingness to spend the time to read and evaluate this thesis.

I would also like to extend my sincere gratitude to my thesis supervisor Peter van der Beek who, despite the many changes of directions and difficulties throughout the project, continued to support me and showed great confidence. This great confidence and freedom allowed me to accomplish exceptional fieldwork as well as to explore different fields of study ranging from thermochronology to seismology. I will always be grateful for your willingness to help, listen and share your expertise at any time and without hesitation. I regret that we did not get the opportunity to work together on the field and share that special life experience; thank you Peter! Furthermore, a big thank you goes to Sebastien Bertrand who has joined this thesis project along the way. Just like Peter, you served as lighthouse through this thesis. I would particularly like to thank you for your support both as co-director of this thesis and as a friend. We have known each other for several years now since our first meeting in Bremerhaven, through the Patagonian fjords until the concretization of this thesis, I will never stop cherishing the times we shared.

A sincere thank you goes to the Marie Curie action without their financial support this splendid project would not have seen the light of day. In this context, I would like to thank in particular all the members of the ITECC project from PI's to my ITECC friends. We shared strong and exceptional moments from our meetings to the field school in Nepal; thank you! A very special place is dedicated to you, Gwladys. I still can't find the words to express the pain of your absence. Our projects suddenly stopped on a summer day. We had planned to go at the Mont Blanc summit together with Natalie to celebrate the end of our thesis, glass of champagne in our hands. We will touch the sky with your memory carrying us.

Big thanks goes to Jean-Robert Grasso for all our discussions and conceptual exploration. I have greatly enjoyed working with you and I sincerely thank you for your patience and listening. You introduced me to the world of seismology when I never imagined I would be able to explore it. I remember with a smile, trying to understand your first explanations, again « un tout grand merci »!

I would like to thank in particular the people who assisted me at ISTerre (University of Grenoble) and the RCMG (University of Ghent) in terms of laboratory work, advice and support. I would like to express my sincere gratitude to Prof. Stephen Louwye from the Department of Geology (University of Ghent)) for his dedication and patience in managing the last moment of my joint-PhD application. I would like to sincerely thank Marc De Batist for welcoming me so warmly to the RCMG.

A big thank you goes to Ananta Prasad Gajurel for his support, dedication, without him, the field would not have been possible, and the samples would still be at the DHL office in Kathmandu.

Gael and Francois, we met among the fjords, lakes and rivers of Patagonia. We shared laughter, sweat, and the discomfort of a saltwater-flooded tent. This thesis I partly owe it to you, thank you again!

In terms of experience and strong friendship, I would like to sincerely thank Arnaud, Guillaume, Jerôme, Lorenzo and Rham for the exceptional fieldwork we spent together recovering mud from the bottom of the lakes. There are few people with whom you can share the promiscuity and discomfort of a tent for several months and you are among them. I can never thank you enough for these very special moments shared together and for the invaluable pleasure of sharing these moments with close friends. I owe many thanks to a number of people from inside as well as outside of ISTerre and the RCMG. I would like to express my deepest gratitude to all who contributed to the nice atmosphere and who took time to talk, laugh and discuss with me (Benjamin, Cecile, Cyril, Corentin, David, Elke, Elien, Evelien, Filip, Flor Koen, Inka, John, Jasper, Maarten, Nore, Rachel, Stan, Shan, Tim, Tom, Thomas and Willem).

Je voudrais remercier du fond de mon cœur ma petite équipe d'ISTerre Jérôme, Julien, Stéphane, Laurent, Swann, Romain, Cyril et Xavier. Vous avez rendu les jours gris un peu moins gris et le ciel bleu un peu plus azur. Je me dois d'écrire quelques lignes spécialement dédicacé à mon principale hébergeur et ami, Jérôme Nomade. Tu es apparu dans ma vie et dans cette thèse tel une bourrasque d'un vent chaud et réconfortant. Je n'aurai de cesse de te remercier pour ta générosité et ton accueil. Nous avons partagé des moments fort que cela soit sur le terrain à négocier l'accès au lac Rara en passant par nos discussions sur ton canapé entre coupé des venues d'Alex, Clément, Marina et Marie. En parlant de générosité de cœur ; Alex, Marina, Clément et Marie je ne le répéterai jamais assez mais merci. Merci de m'avoir accueil les bras ouverts, les moments passés en votre compagnie ont posé les bases d'une très belle amitié.

Véro et Pierrick, je prends ce moment pour vous remercier encore et encore de votre amitié. Vous m'avez permis de trouver un refuge, une échappatoire en venant vous retrouver que cela soit au Tour et au Faysse. Je connais peu de personne aussi généreuse en amitié. Nos discussions et soirées au refuge m'ont permis de prendre la distance nécessaire sur mon travail afin d'y revenir avec plus d'entrain. Vous avez été là dans les moments plus difficiles et les plus heureux et j'ai toujours pu compter sur votre épaule, encore un tout grand merci !

En parlant de chaine de montagne et de géologie je voudrais tout particulièrement remercier Philippe, Serge, Guy et Pierrick. Vous m'avez pris sous votre épaule et m'avez donné l'autonomie de parcourir nos plus beaux sommets alpins. Plus qu'une passion, vous m'avez fait découvrir et initié à un mode de vie au rythme des glaciers et des éléments. Je ne vous remercierai jamais assez de votre amitié et de votre soutien au cours de cette thèse.

Among the people who had the opportunity to share my daily life, I would like to thank in particular my colleagues and office friends Loïc and Dawei. I promise you that I will stay in your heart and let you manage for the allocation of my office chair. Eric and Natalie, what a disappointment to have shared so little time together at the office. For a while, you were able to work alongside with the pile of papers that materialized my presence. Natalie, I remember with nostalgia and happiness our first days in Grenoble between administration and barbecue.

Encore un tout grand merci à Arthur et Xavier. Vous m'avez accompagné pour réaliser ce projet de documentaire lors de ma première expédition. Ce fut des moments extrêmement fort humainement, je ne vous remercierai jamais assez.

De manière générale je voudrais remercier du fond de mon cœur l'ensemble de mes amis. Je suis extrêmement chanceux de vous avoir et de bénéficier d'un tel soutien de votre part. Je ne saurai pas par où commencer pour vous remercier, alors je vous dis tout simplement merci !

Anecdotally, I would like to thank in particular the taxi driver in Santiago de Chile for waiting until I could send my application to the ITECC project. I would like to thank Matt and Motte for teaching me how to ride a motorcycle to collect the last samples in the Kali Gandaki Valley.

Finally, I would like to express my deepest gratitude to my mother, Véronique Schaus. She always wanted the best for me, showed great interest in my studies, took the time to listen to my problems, and suffered with me during difficult times. It goes without saying that without her unfailing support, this thesis would not have been a reality and I would not have been the person I am.